ornl

NUREG/CR-4256
ORNL/TM-9574

OAK RIDGE
NATIONAL
LABORATORY

MARTIN MARIETTA

Measurement of Response Time and Detection of Degradation in Pressure Sensor/Sensing Line Systems

M. E. Buchanan
L. F. Miller
J. A. Thie
T. W. Kerlin
G. E. Ragan
J. March-Leuba

Prepared for the
U.S. Nuclear Regulatory Commission
Office of Nuclear Regulatory Research
Under Interagency Agreement DOE 40-550-75

8512270230 850930
PDR NUREG
CR-4256 R PDR

OPERATED BY
MARTIN MARIETTA ENERGY SYSTEMS, INC.
FOR THE UNITED STATES
DEPARTMENT OF ENERGY

NOTICE

This report was prepared as an account of work sponsored by an agency of the United States Government. Neither the United States Government nor any agency thereof, or any of their employees, makes any warranty, expressed or implied, or assumes any legal liability or responsibility for any third party's use, or the results of such use, of any information, apparatus product or process disclosed in this report, or represents that its use by such third party would not infringe privately owned rights.

Available from

Superintendent of Documents
U.S. Government Printing Office
Post Office Box 37082
Washington, D.C. 20013-7982

and

National Technical Information Service
Springfield, VA 22161

NUREG/CR-4256
ORNL/TM-9574
Distribution Category R1

Instrumentation and Controls Division

MEASUREMENT OF RESPONSE TIME AND DETECTION OF DEGRADATION IN PRESSURE SENSOR/SENSING LINE SYSTEMS

M. E. Buchanan
L. F. Miller*
J. A. Thie†
T. W. Kerlin*
G. E. Ragan*
J. March-Leuba*

*The University of Tennessee, Knoxville, Tennessee 37916
†Analysis & Measurement Services, Inc., Knoxville, Tennessee 37919

Manuscript Completed: August 1985
Date of Issue: September 1985

Prepared for the
U.S. Nuclear Regulatory Commission
Office of Nuclear Regulatory Research
Washington, DC 20555
Under Interagency Agreement DOE 40-550-75

NRC FIN No. B0481

Prepared by the
OAK RIDGE NATIONAL LABORATORY
Oak Ridge, Tennessee 37831
operated by
MARTIN MARIETTA ENERGY SYSTEMS, INC.
for the
U.S. DEPARTMENT OF ENERGY
under Contract No. DE-AC05-840R21400

TABLE OF CONTENTS

LIST OF FIGURES

ABSTRACT

A team evaluated several methods for remote measurement of the response time and detection of degradation (blockage or air in lines) of pressure sensor/sensing line systems typical of nuclear power plants. A method was developed for obtaining the response time of force-balance pressure transmitters by briefly interrupting the power supply to the transmitter. The data thus generated are then analyzed in conjunction with a model to predict transmitter response to an actual pressure perturbation. The research team also evaluated a pressure perturbation method for determining the asymptotic delay time of a pressure-sensing line and found that this method yields accurate results for essentially unblocked sensing lines. However, these pressure perturbation tests are not recommended for use in nuclear power plants because they are difficult to implement on-line. A third method for remote measurement applied noise analysis methods that yielded accurate estimates of asymptotic delay times for blockage or air in sensing lines. Even though noise analysis methods worked well in the laboratory, it is recommended that further evaluation be performed in operating nuclear plants.

1. INTRODUCTION

Remote in situ methods to detect degradation in the response time of nuclear plant pressure sensor/sensing line systems were evaluated at the request of the Instrumentation and Control Branch of the U.S. Nuclear Regulatory Commission (NRC) Office of Nuclear Regulatory Research.

Pressure sensor/sensing line systems include the pressure sensor, sensing line, associated snubbers, valves, and signal-conditioning equipment. Pressure measurement systems are used in nuclear plant protection systems to trip the reactor and to initiate engineered safety features in a specified time period. Current in situ methods for response time testing of pressure sensors are difficult to accomplish and are performed inside containment; thus, testing is limited to periods when the plant is shutdown. Furthermore, the industry currently has no remote method to verify the response time of pressure-sensing lines. Therefore, the availability of a remote in situ method for response time testing would enable confirmation of satisfactory operability of pressure sensors and of associated sensing lines when desired rather than only at plant shutdown.

Oak Ridge National Laboratory (ORNL) and the University of Tennessee, Knoxville (UTK) surveyed industry experience with pressure-sensing systems and identified several instances where sensing lines were blocked by freezing, boric acid, or valves that were inadvertently closed. Electronic failures were the most frequent type of pressure sensor failure.

The current method to verify response time requires that the transmitter be isolated from the sensing line and that a pressure ramp be input to the transmitter to test its operability and response time. This ramp test does not address the sensing line problems and can be performed only during plant shutdown.

Some of the methods evaluated in this work, if adopted by the nuclear industry, have the potential for overcoming the limitations of current practices. The methods evaluated for remote in situ testing are (1) a transient pressure reduction method (referred to as the TPR method) that involves introducing a small pressure variation into the sensing line by opening a remotely operated solenoid valve and thus permitting fluid to flow into a small isolated chamber; (2) interruption of the ac power to the power supply of force-balance pressure transmitters for remote verification of sensor response time [referred to as the power interrupt (PI) method]; and (3) analysis of the frequency spectrum of naturally occurring pressure fluctuations (referred to as noise analysis) to continuously monitor the complete pressure sensing system (line, sensor, electronics, etc.) for degradation that may affect the system response time.

These three methods were evaluated in the laboratory at pressures up to 2000 psi and in the Forced Convection Test Facility (FCTF) at ORNL which simulates flow, temperature, and pressure conditions of a commercial pressurized water reactor (PWR). A detailed description of the test

procedures is given in Appendix A of this report. The ability of the various methods to detect degradation in pressure-sensing systems was evaluated by introducing blockages and air into sensing lines and by degrading the response of the pressure sensor. A nuclear-qualified force-balance pressure sensor together with a representative pressure-sensing system (sensing line, valves, etc.) was used to evaluate the methods. Laboratory-grade, fast-response pressure sensors were used as reference transmitters to verify the response time of the representative system. A theoretical model (described in Appendix B) describing the dynamic response of the sensing system was developed and used to aid in the evaluation of the test results.

2. PRESSURE-SENSING SYSTEM TESTING METHODS

2.1 BACKGROUND

Transient testing of systems or instruments usually employs one of three common test inputs: a step, a ramp, or a sinusoid. The step is the most common, but the ramp has been adopted for most testing on pressure sensors for nuclear plant safety systems. This is because design basis accidents result in pressure transients that approximate ramps.

For sensors operating in the linear range, there are simple relations between responses to step input and to a ramp input. For example, consider a first-order system:

$$G(s) = \frac{1}{\tau s+1} . \qquad (2.1)$$

The step response is given by:

$$y(t) = 1-e^{-t/\tau} . \qquad (2.2)$$

This is shown graphically in Fig. 2.1. The time constant, τ, may be obtained by determining the time required for a test transient to span 63.2% of its total change.

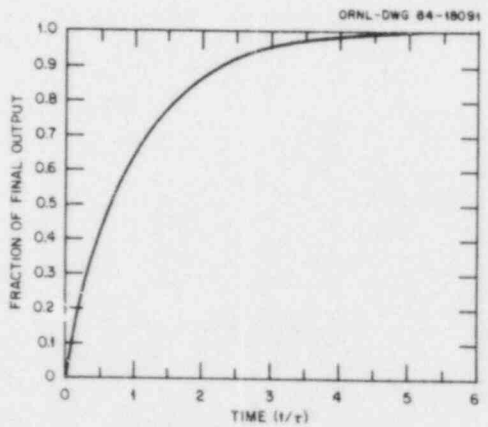

Fig. 2.1. Step response of a first-order system.

The ramp response for a ramp, ct is:

$$y(t) = c\ (t - \tau) + c\tau e^{-t/\tau} . \qquad (2.3)$$

This response is shown graphically in Fig. 2.2 where the quantity of interest is the ramp time delay (τ). For first-order systems, the ramp time delay and the time constant are equal.

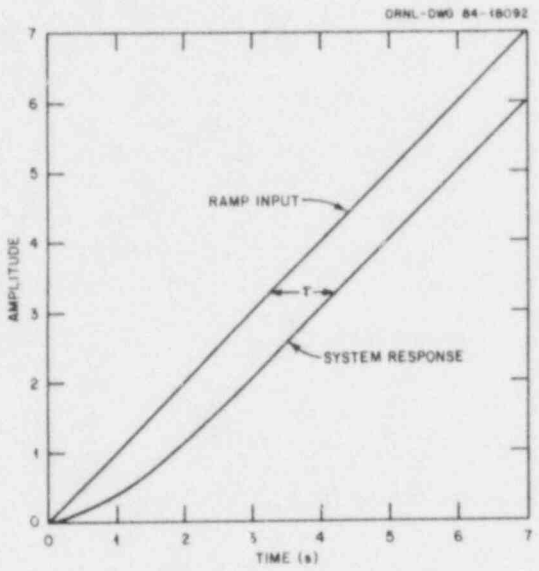

Fig. 2.2. Ramp response of a first-order system.

It can be shown that for a general, n^{th} order system with no zeros in its transfer function, the following is true:

$$\text{ramp time delay} = \tau_1 + \tau_2 + \ldots \tau_n \qquad (2.4)$$

where τ_i = modal time constant. (The time constant for the i^{th} term, or mode, in the solution.)

A system with one input and one output may be depicted as shown in Fig. 2.3.

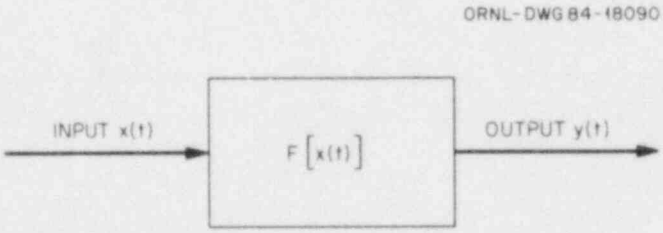

Fig. 2.3. Block diagram illustration of an input/output system.

Assuming that the gain is unity or that proper scaling has been done, τ can be measured after a suitable lapse of time as shown in Fig. 2.4. The gain and asymptotic ramp delay time are both dependent on the system, but both are independent of the ramp rate (for any asymptotically stable, linear system). The term "asymptotic ramp delay time" will be denoted by the symbol τ.

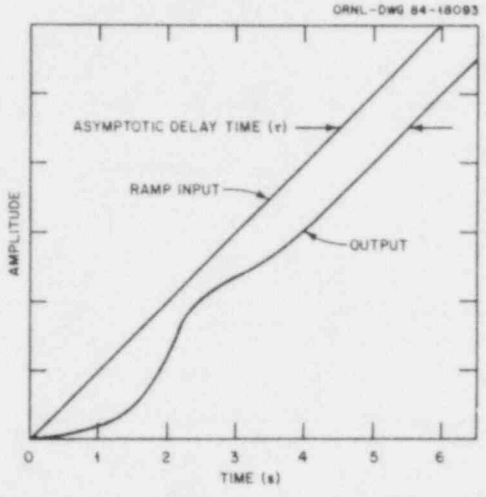

Fig. 2.4. Illustration of asymptotic ramp delay time.

Although the input of ramp pressure signals to pressure transmitters (Ramp testing) is the method currently used to measure response time of pressure sensors it can be performed only during plant shutdown. Furthermore, ramp testing only determines the response time of the transmitters and cannot determine when the sensing lines are blocked.

2.2 NOISE ANALYSIS METHODOLOGY

2.2.1 Principles of the Test

Noise in a reactor process signal can be defined as normally occurring fluctuations on the signal around its average value. Noise is caused by a multitude of phenomena; and, due to its stochasticity, the value of the signal at a particular time is unpredictable. Therefore, the noise has to be described by average values such as power spectral densities (PSDs) or correlation functions. The basis for using a noise analysis technique for pressure sensor/sensing line time-delay measurements is that pressure perturbations in the primary system are seen (or detected) through the sensing line and sensor transfer functions. If changes occur in any of these transfer functions, they may be reflected in the output noise PSD. Noise analysis can be used to identify changes in signal characteristics and to determine time delay when the pressure measurement system is operating in a linear mode (nonlinear behavior such as experienced in some pressure sensors may render this method inappropriate for quantitative measurements).

In general, two types of delays can be observed in dynamic systems: (a) a pure time delay, which is characterized by a linear phase versus the frequency relationship between input and output, and (b) an asymptotic time delay introduced by the poles of the transfer function. This second type affects both the gain and the phase of such a transfer function, whereas the first type affects only the phase. Degradations

of the sensing line or pressure sensor will result in time delays of the second type. Therefore, this is the type of delay that we will address in this section. The expected effect on pressure noise of these degradations will be presented here along with some proposed methods for detecting and quantifying them. The application of these methods to laboratory data will be presented in Sect. 3.1.

2.2.2 Effect of Sensing Line Degradation on Pressure Noise

As previously discussed, the noise in the primary system pressure is seen at the sensor location through the sensing line transfer function. Degradations of the line will affect its transfer function and, consequently, the output noise PSD.

A typical sensing line transfer function (from the Forced Convection Test Facility loop, described in Appendix A) is presented in Fig. 2.5. This transfer function has been obtained by simultaneously analyzing the

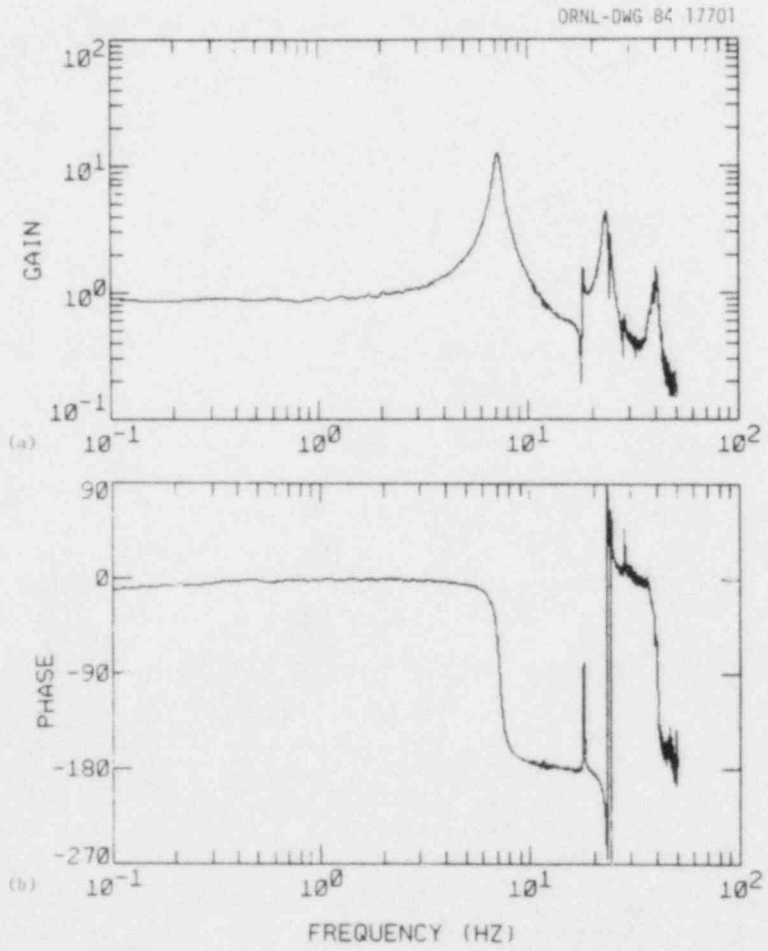

Fig. 2.5. Typical sensing-line transfer function: (a) gain (adimensional) and (b) phase (degrees).

responses from two high-frequency Validyne pressure sensors located at the inlet and sensing end of the line. The characteristics which can be observed (see Appendix B) are (a) the Helmholtz resonance located at 7 Hz, (b) the half-wave standing wave resonance at about 23 Hz, and (c) the full-wave standing wave resonance in the vicinity of 41 Hz. Theory predicts that if the line friction increases or if voids appear in the line, these resonances will widen (become less pronounced) because of the increased damping, and their frequency will be reduced. This effect is seen clearly in Fig. 2.6, which shows the sensing line transfer function for several positions of a needle valve located at the sensing line inlet. Note that the resonances widen as the valve is closed and that the resonances have completely disappeared when the inlet valve is turned to one quarter turn open.

In mathematical terms, the original resonances are formed by two complex conjugate poles with a particular damping coefficient. As the valve is being closed, the damping coefficient, which determines the time delay,

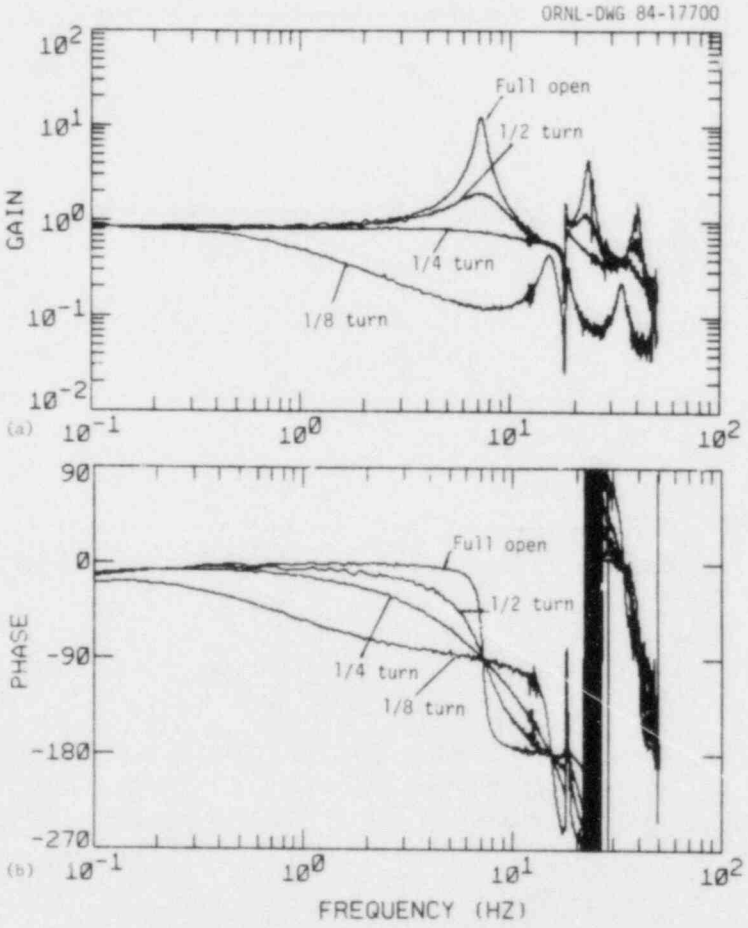

Fig. 2.6. Sensing line transfer function changes as a valve located near the sensing line inlet is closed: (a) gain (adimensional) and (b) phase (degrees).

increases. When the damping is made greater than one, the poles become real. Further increase of the damping causes one of them to move toward lower frequencies, and the other toward higher frequencies. This will appear as a downward break in the magnitude of the transfer function. The low-frequency pole, which is clearly distinguishable in the one-eighth turn case (Fig. 2.6), is the one causing the most significant time delay.

The effect of voids in the sensing line is mainly to reduce the frequency of oscillation and to increase the damping coefficient (see Appendix B). Both effects increase the time delay of the sensing line. Figure 2.7 presents an example of the effect of voids on the magnitude of the sensing line transfer function. The reduction in frequency and the increase in damping are apparent, but this reduction is not as dramatic as with the case of increased line friction due to blockages. This observation implies that voids in the line probably do not pose as significant a problem with respect to time delay as do blockages.

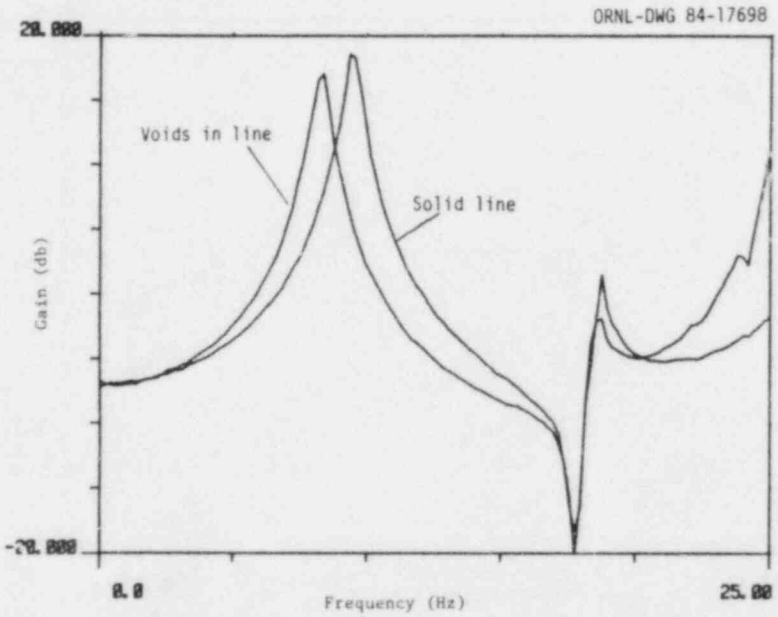

Fig. 2.7. Effect of voids on sensing line transfer function.

In order to monitor the performance of the sensing line, the damping of the Helmholtz resonance must be determined. If the resonance is not apparent, the time delay is determined from the position of the low-frequency pole.

2.2.3 Effect of Sensor Degradation on Pressure Noise

This study is concerned primarily with a failure in which the sensor dynamic characteristics have degraded to the point of introducing a noticeable damping, which produces large time delays, following step or

ramp inputs. This degradation will be evidenced in the transfer function of the sensor as a pole at low frequency.

A typical transfer function of a nuclear-qualified pressure sensor (Foxboro Model NE11GM) is shown in Fig. 2.8. This transfer function was obtained by simultaneously measuring the pressure noise with the Foxboro sensor and a fast-response Validyne pressure sensor located near it. Two main features are evident: (a) a resonance in the vicinity of 16 Hz and (b) a break frequency corresponding to a real pole at about 1 Hz. Phase lags of -90 and -180° are associated with the real and complex poles. The real pole contributes the largest amount to the sensing time delay, which can be estimated from the position of this pole as $\tau = 1/\omega = 0.159$ s.

A degradation of the sensor will cause the low-frequency pole to move toward lower frequencies and, thus, increase the time delay.

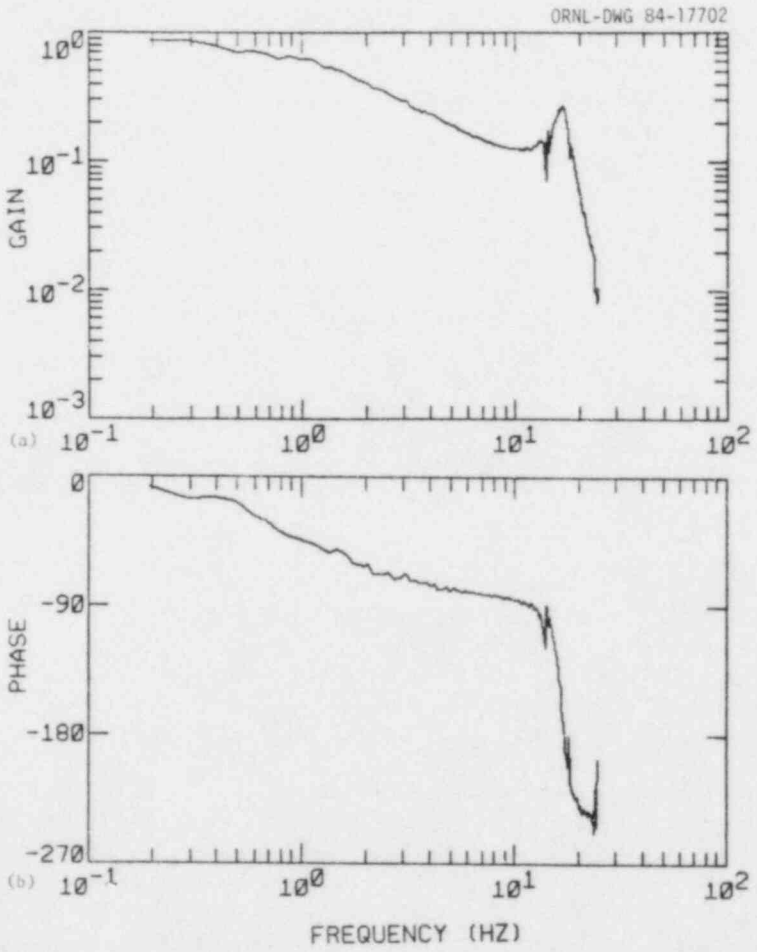

Fig. 2.8. Typical transfer function of a Foxboro (Model NE11GM) nuclear-qualified sensor: (a) gain (adimensional) and (b) phase (degrees).

2.2.4 Time Delay Estimation from Noise Measurements

We have seen in the previous sections that severe degradations of the sensing line or sensor will show up in the output pressure noise through the appearance of low-frequency poles. Therefore, in order to detect severe line or sensor degradations, one must look for signs related to the existence of low-frequency poles. Several techniques can be used for this purpose; their accuracy and applicability depend on available instrumentation. Some of these techniques are presented in this section which fall into two broad categories: (a) transfer-function measurements, which require the existence of at least two sensors, and (b) output-noise measurements, which rely exclusively on the existing instrumentation.

2.2.4.1 Transfer-Function Measurements

Two sensors are needed for transfer-function measurements. If the sensors are available, transfer functions, like the ones presented in Figs. 2.5 and 2.8, can be computed by simultaneously measuring the pressure noise with both sensors. The time delay introduced by these transfer functions can be determined very accurately from a fit in terms of poles and zeros. The delay can be calculated from the formulas $\tau = 2\zeta/\omega$ in the case of complex poles or $\tau = 1/\omega$ for real poles, where ω is the natural frequency of the pole in rad/s and ζ is the damping coefficient. An approximate value of the delay can alternatively be obtained as the inverse of the frequency at which the transfer function phase becomes $-45°$.

Depending on the location of the second sensor, different transfer functions are measured; thus, different time delays are estimated. If an extra sensor is installed at the sensing line inlet (as was the case for Fig. 2.5), then both the sensing line and pressure sensor time delays can be measured. If the sensor is installed at the sensing end of the line (a more accessible place), then only the pressure sensor transfer function can be measured.

Therefore, by using a transfer-function measurement, both the sensing line and pressure sensor time delays can be determined very accurately. However, this method is only applicable if a second sensor is installed on the sensing line.

2.2.4.2 Output Noise Measurement

If only one sensor is available at the end of the sensing line, the time delay measurement cannot be as accurate as with a transfer-function measurement, but it is still possible. For instance, Fig. 2.9 shows the PSDs of the pressure noise corresponding to the same conditions as Fig. 2.6 as seen by a high-frequency-response Validyne sensor and a nuclear-qualified Foxboro sensor respectively. In this figure, the Helmholtz resonance at 7 Hz is observable in the full-open position, and the disappearance of the resonance is apparent as the inlet valve is being closed. The Validyne sensor, which has a much wider bandwidth

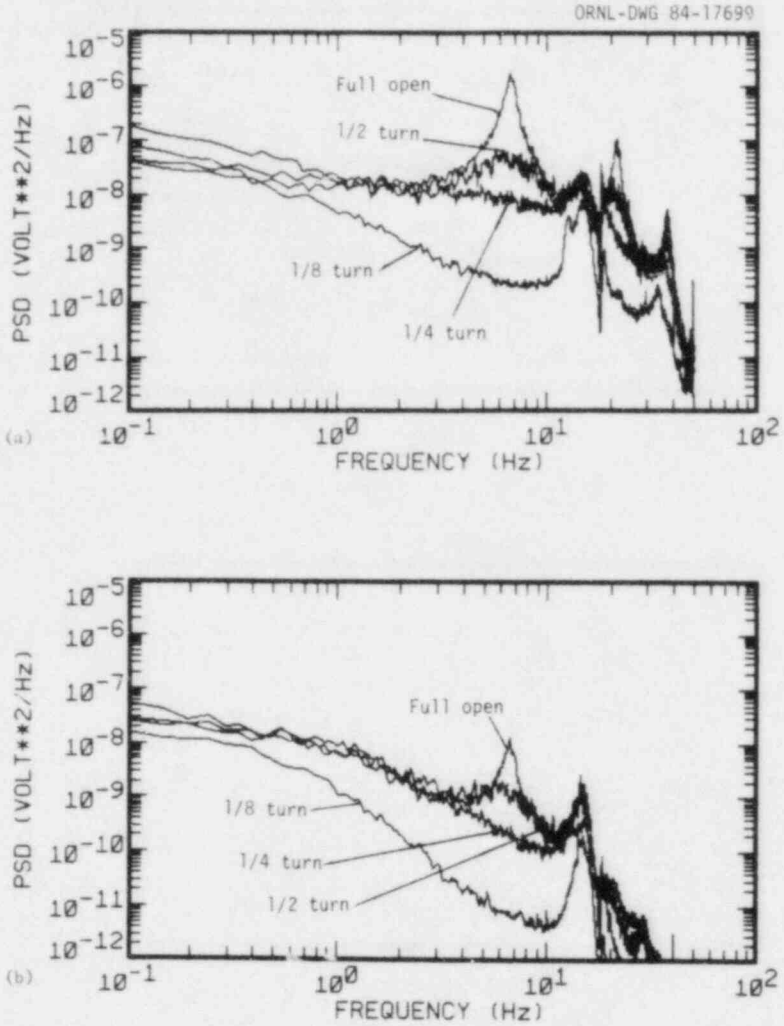

Fig. 2.9. Power spectral density as a function of sensing line resistance located at the inlet of the sensing line: (a) Validyne and (b) Foxboro.

(>100 Hz) than the Foxboro, also detects the changes in the standing-wave resonances. It is clear from this figure that the output noise contains the necessary information to detect severe sensing line degradations.

Several methods can be used to quantify the time delay from the output pressure noise. One method could consist of obtaining a baseline PSD when the pressure measurement system is in a known good condition; then, subsequent measurements can be compared to the baseline. In particular, the presence or absence of the Helmholtz resonance has to be determined. If the resonance is not apparent, low-frequency poles, which contribute large time delays, should be identified. The time delay can be quantified by several methods:

1. Making fits to the PSD in terms of poles and zeros. The delay is obtained from the damping in the Helmholtz resonance relative to the reference case or from the break frequency when the real pole is present.

2. Measuring the signal root mean square (rms). If a baseline PSD is available, a conversion table of rms versus time delay can be approximately constructed by calculating the rms of the product of the baseline PSD times a first-order time delay of the form $1/[1 + (\tau\omega)^2]$ for several values of τ.

3. Comparing the measured PSD with the baseline. Of particular interest for this comparison should be the identification of the Helmholtz resonance and its approximate width. If the resonance is not present, the time delay can be estimated from the frequency of the low-frequency real pole.

These methods were successfully applied to pressure noise data from the high-pressure loop at the FCTF at ORNL (see Sect. 3).

We have demonstrated in the laboratory that pressure noise data may contain the necessary information to detect degradations of the line or pressure sensor, even when only the process sensor is available. Several methods have been proposed and evaluated to identify and quantify changes in the time delay based on pressure noise. However, there may be situations in plants where the natural pressure noise is not suitable to obtain this information.

2.3 TRANSIENT PRESSURE REDUCTION (TPR) METHOD

2.3.1 Introduction

Nuclear Regulatory Commission Regulatory Guide 1.118 sets forth recommendations for response in the testing of instrumentation for nuclear power plants. In particular, the delay between the time that the process obtains a specific state and the time that the instrumentation output obtains its corresponding value should be determined. Thus, the technical specifications of some plants require that pressure transmitters be tested periodically with a pressure-ramp generator. This method directly determines the delay time associated with the pressure transmitter, but it does not incorporate the sensing line dynamics. The tests proposed herein should allow the determination of the response characteristics of the sensing line and the response time of force-balance pressure transmitters.

The test documented in this report has been performed at The University of Tennessee Department of Nuclear Engineering (UTNE) at low pressures and at intermediate pressures (up to 1000 psig). The test has also been performed at 2000 psig on an experimental facility (FCTF) at the Oak Ridge National Laboratory (ORNL).

2.3.2 Description

The TPR test is a proposed method for dynamic testing of liquid-filled pressure-sensing lines. It involves connecting a small air-filled chamber at atmospheric pressure (the TPR chamber) to a test port near the pressure sensor, as shown in Fig. 2.10. Flow from the pressurized sensing line into the TPR chamber is inhibited by a fast-acting solenoid valve, which is initially shut. A test is initiated by opening the solenoid valve. As pressure equilibrium is established between the process and the TPR chamber via flow through the sensing line, a reference pressure transducer records the TPR chamber pressure. Because the sensing line is used to establish pressure equilibrium, the recorded pressure transient may be used to infer the dynamic characteristics of the sensing line.

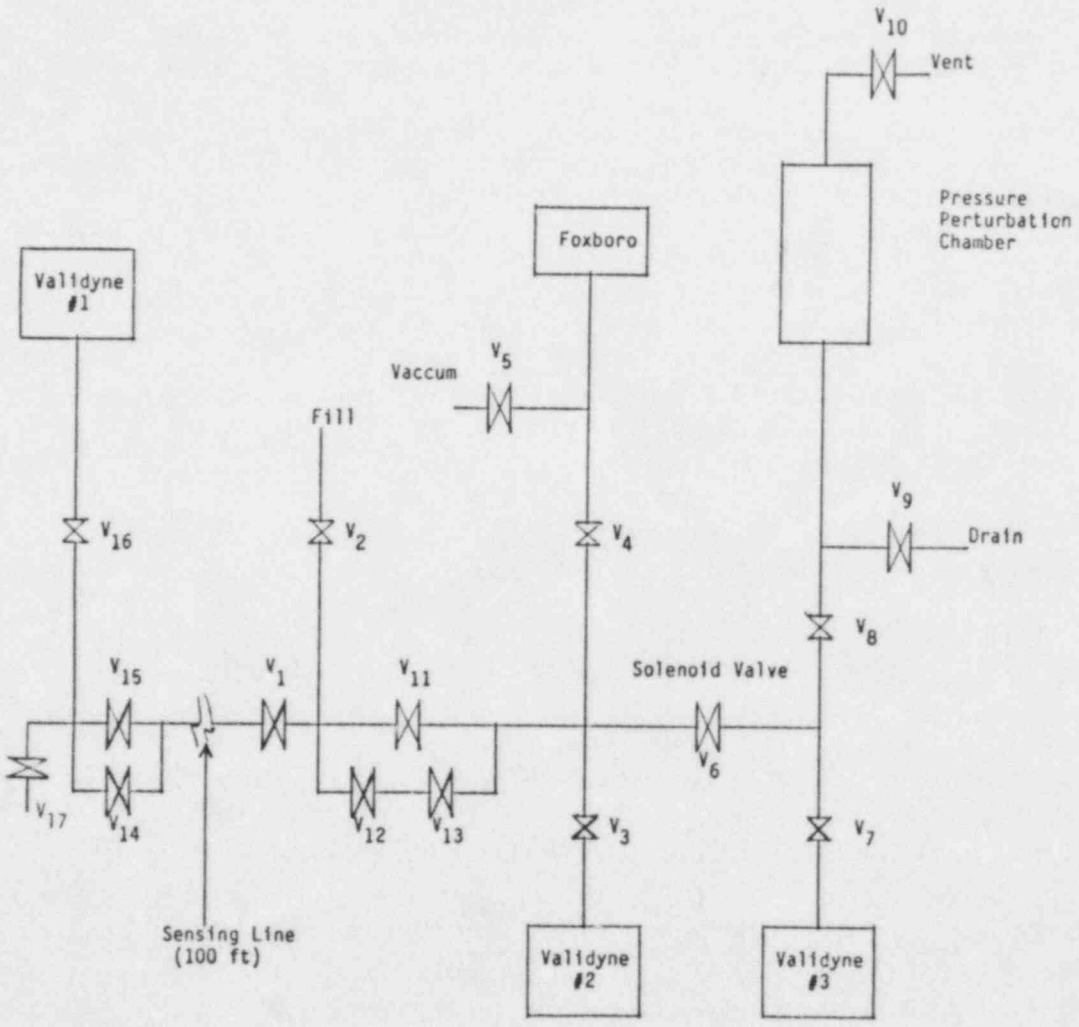

Fig. 2.10. Schematic diagram of ORNL high-pressure perturbation test equipment.

The purpose of the test is to measure the asymptotic ramp delay time, τ, of the sensing line. When there is a low confidence in the estimate of τ, assurance must be provided that the estimate is conservative (high). Even when the sensing line blockage is not great enough to cause a change in the estimate of τ, a qualitative examination of the transient can detect degradation.

2.3.3 Theoretical Basis of TPR Test

Two models were developed for analysis of TPR test data. One model assumed a quarter-wave resonance, and the other was based on a second-order model of the sensing line. For the second-order model, the time constant is determined from the model assuming a ramp input (see Appendixes A and B). The following development is for the model that assumes that the line resonates at the quarter-wave frequency.

It can be shown[2] that the asymptotic ramp delay time, τ, of a sensing line depends on the magnitude and distribution of resistance and capacitance throughout the sensing line in accordance with

$$\tau = \int_0^{\ell} [r(x) \int_x^{\ell} c(x)dx] dx \qquad (2.5)$$

where

x = position, measured from sensing line origin,
$r(x)$ = resistance per unit length as a function of x (see Appendix B, Sect. B.2),
$c(x)$ = capacitance per unit length as a function of x (see Appendix B, Sect B.2), and
ℓ = sensing line length.

Since in a TPR test the pressure is recorded at only one location in the sensing line, it is not possible to measure the distributed parameters in Eq. (2.5). A simplified model is required. Thus, the fluid-transmission-line equation for a uniform line is chosen.[2] In the uniform-line case, Eq. (2.5) can be integrated to give

$$\tau = rc \frac{\ell^2}{2} . \qquad (2.6)$$

It can be shown[2] that a transmission line in oscillation near its quarter-wave frequency can be treated approximately as a single-lump network having series inertance and resistance and shunt capacitance given by

$$\hat{L} = m\ell,$$

$$\hat{R} = r\ell, \qquad (2.7)$$

$$\hat{C} = \frac{4}{\pi^2} c\ell,$$

respectively, where m = inertance per unit length of line (see Appendix B, Sect. B.2). This network is shown in Fig. 2.11.

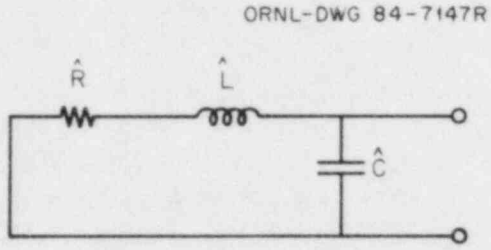

Fig. 2.11. Single-lump model of a sensing line.

The most prominent resonant frequency in a TPR test can be controlled to some extent by the size of the TPR chamber. Larger TPR chambers result in lower resonant frequencies. However, an upper limit is imposed by the sensing line itself. This is the quarter-wave resonance of the line. Experimental measurements have shown (see Fig. 2.12) that if the TPR chamber and the process sensor capacitances are small in comparison with the total capacitance of the sensing line, the system will resonate at a frequency slightly lower than the quarter-wave frequency of the sensing line.

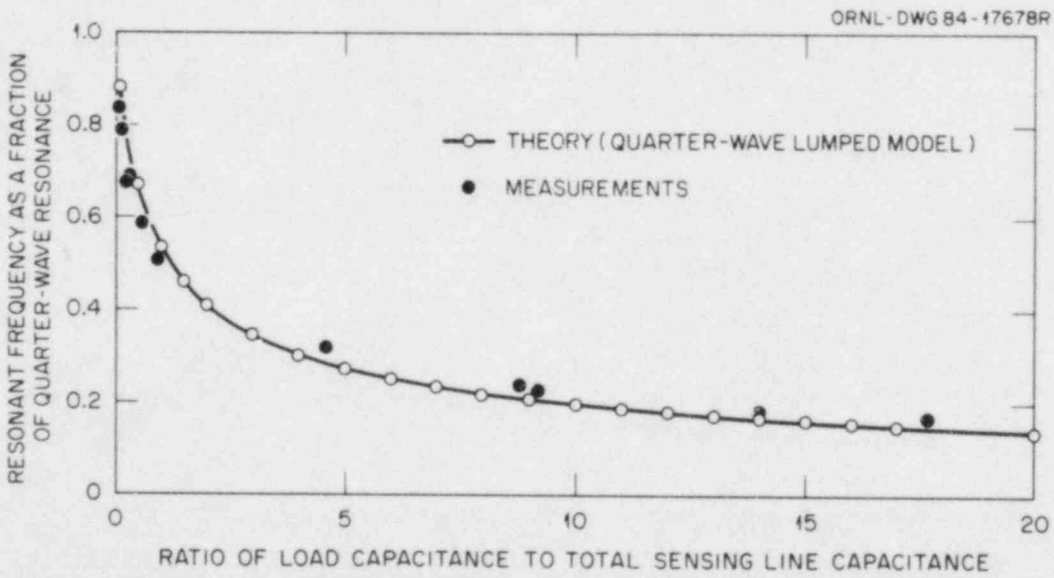

Fig. 2.12. Effect of load capacitance on resonant frequency of a sensing line.

If the single-lump model just described is taken to represent the sensing line in a TPR test, the product, $\hat{R}\hat{C}$, can be estimated from the recorded trace of pressure vs time (as described in the next paragraph), provided sufficient oscillation takes place. Then τ can be estimated from Eq. (2.6) as

$$\tau = rc\,\frac{\ell^2}{2} \tag{2.8}$$

$$= \hat{R}\hat{C}\,\frac{\pi^2}{8}$$

After the solenoid valve is opened, the TPR chamber takes some time to fill. During this time, the pressure recorded by the reference transducer is approximately constant. Then, the chamber fills up producing decaying pressure oscillations. Time zero can be chosen so that the pressure during the decaying oscillation is approximately described by

$$p(t) = p(0)e^{-\alpha t}\cos \omega t \tag{2.9}$$

where $p(t)$ = pressure at time t, and the symbols α and ω denote, respectively, the real and imaginary components of the complex root of the characteristic equation which corresponds to the single-loop model. (Reference 2 gives a clear exposition.)

The imaginary component, ω, is simply the angular frequency of oscillation. The real component, α, can be estimated by plotting the amplitude of the pressure oscillations versus time on semilog paper and drawing a straight line through the points. The slope of the line determines α. Finally, the product $\hat{R}\hat{C}$ is given by (see Appendix B)

$$\hat{R}\hat{C} = \frac{2\alpha}{\alpha^2 + \omega^2} \tag{2.10}$$

and Eq. (2.8) is used to estimate τ, the asymptotic ramp delay time of the sensing line.

2.3.4 Sources of Error

Energy is dissipated as the fluid flows into and out of the TPR chamber through the solenoid valve. This additional energy loss increases the damping above that for the sensing line alone, which tends to increase the estimate of τ.

The presence of the TPR chamber also changes the distribution of capacitance in the system. The effect of this is apparent by examination of Eq. (2.5). The integral

$$W(x) = \int_x^{\ell} c'(x')\,dx' \tag{2.11}$$

can be viewed as a weighting factor. Then Eq. (2.5) can be written as

$$\tau = \int_0^{\ell} W(x)\,r(x)\,dx \tag{2.12}$$

The weighting factor is equal to the total downstream capacitance. If an additional capacitance (the TPR chamber or the process sensor) is added at the downstream end, the dynamic effect of the sensing line resistances throughout the line is increased. This effect also tends to increase the estimate of τ.

We have seen that, ideally, the TPR chamber and process sensor capacitances should be small in comparison to that of the sensing line. However, the presence of the TPR chamber always tends to increase damping and to decrease the resonant frequency. Both of these effects tend to increase the estimate of τ derived from a TPR test. This ensures that the TPR test gives a conservative estimate of τ.

2.3.5 Predicted Effect of Blockage on Response Time

Consider a sensing line with constant capacitance per unit length, c', but with resistance per unit length, $r'(x)$, varying as depicted in Fig. 2.13.

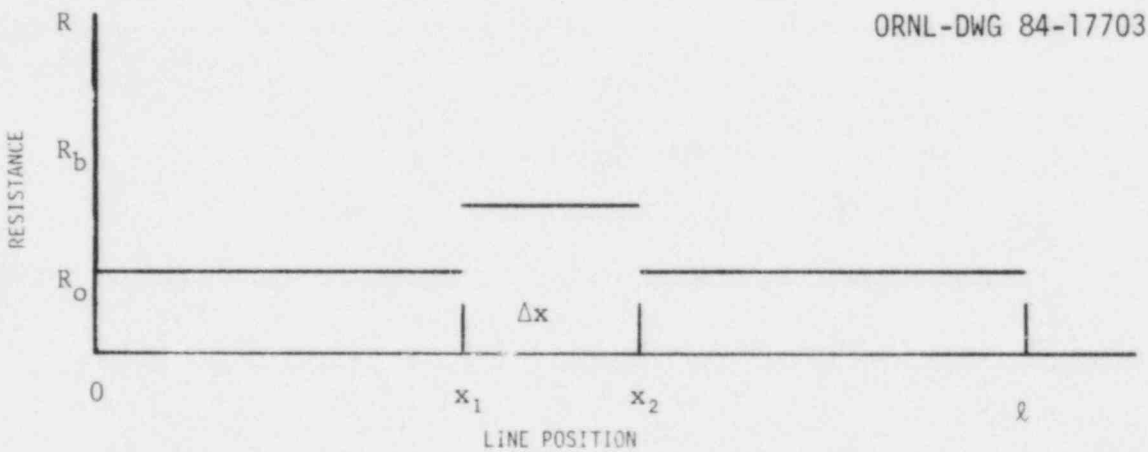

Fig. 2.13. Variation of resistance versus length for an idealized sensing line with localized blockage.

Assume that the blockage is a uniform constriction in a cylindrical sensing line. Using Eq. (2.5), an expression can be developed[2] which relates the ramp delay time of the blocked line, τ_b, to that of the line in its normal, unblocked condition, τ_n. The expression is, in terms of the nominal cross-sectional flow area A_n of the sensing line and the flow area of the blocked section, A_b,

$$\frac{\tau_b}{\tau_n} = 1 + \frac{\Delta x}{\ell}\left[2\left(1 - \frac{x_1}{\ell}\right) - \frac{\Delta x}{\ell}\right]\left[\left(\frac{A_n}{A_b}\right)^2 - 1\right] . \qquad (2.13)$$

This equation is plotted in Fig. 2.14 for values of the dimensionless ratios $\left(\frac{\Delta x}{\ell}\right)$ and $\left(\frac{A_n}{A_b}\right)$ which correspond to an inch-long constriction in a

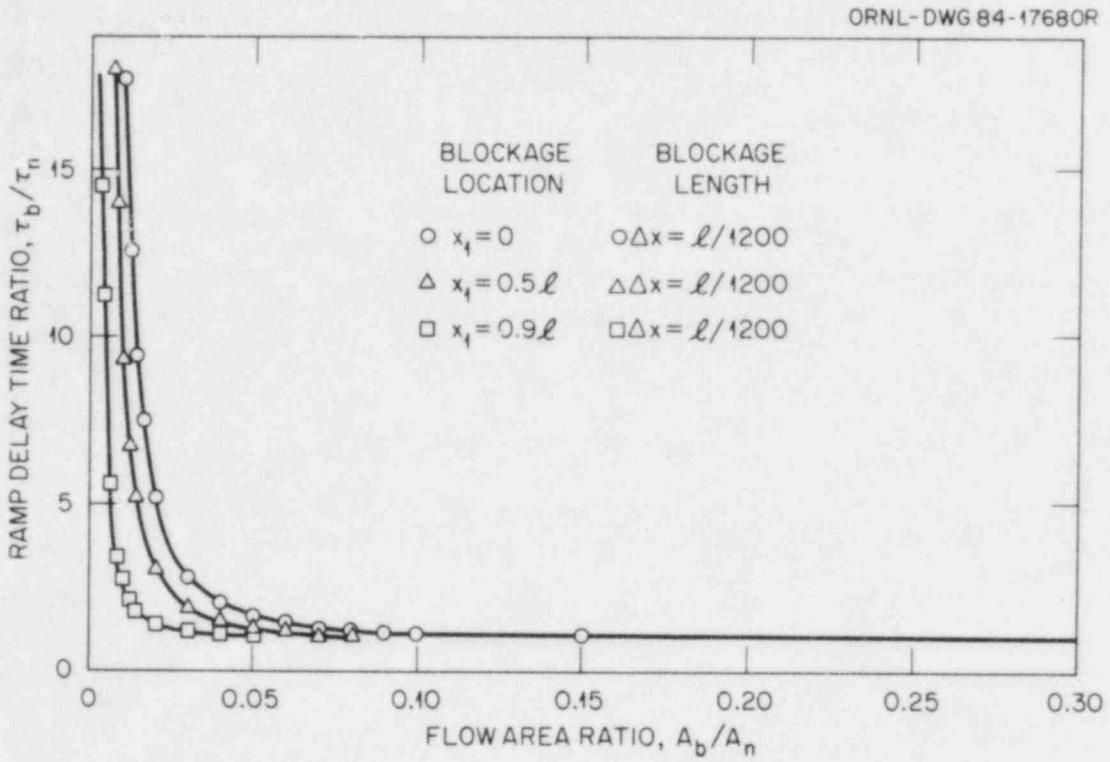

Fig. 2.14. Predicted effect of localized flow constriction on ramp delay time. Consistent units must be used for sensing line length ℓ, blockage length Δx, and blockage location x_1.

100-ft-long sensing line. The equation is plotted for various blockage locations as described in the figure.

Equation (2.13) is based on fully developed laminar flow and therefore ignores entry effects into the blocked region. Thus, Fig. 2.14 demonstrates that a sensing line blockage must be nearly complete before any dynamic effect is observed. It also reveals the importance of the location of the blockage. It is seen that blockages near the process end have a greater effect than similar blockages near the sensor end.

2.3.6 Critical Condition for Success of the Method

The success of the TPR-test method requires the existence of damped pressure oscillations. This requirement is made more precise in this section.

Consider the second-order system described by

$$\hat{L}\hat{C}\,\frac{d^2p}{dt^2} + \hat{R}\hat{C}\,\frac{dp}{dt} + p = 0 \qquad (2.14)$$

which serves as a representation of a sensing line equivalent to Fig. 2.11. The natural frequency of this system is

$$\omega_n = \frac{1}{\sqrt{\hat{L}\hat{C}}} \tag{2.15}$$

The relationship between ω_n and the parameters α and ω as previously defined is depicted in Fig. 2.15.

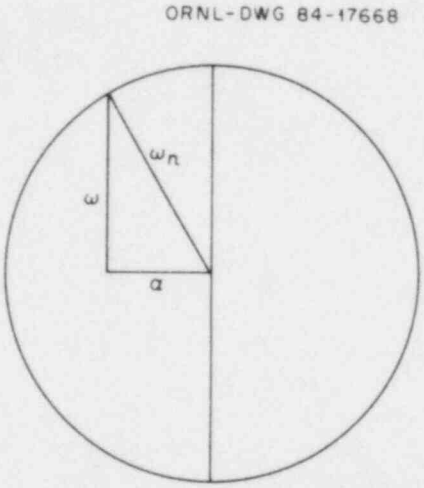

Fig. 2.15. Depiction of the relationship between the natural frequency ω_n and the parameters ω and α of a second-order system.

The circle in Fig. 2.15 with ω_n as its radius is intended to stress the constancy of ω_n with respect to changes in $\hat{R}$. The other parameters, α and ω, depend on $\hat{R}$ in accordance with

$$\alpha = \frac{\hat{R}}{2\hat{L}} \tag{2.16}$$

and

$$\omega^2 = \omega_n^2 - \alpha^2 \ . \tag{2.17}$$

Thus, increases in $\hat{R}$ cause increases in α and decreases in ω until the limiting condition $\alpha = \omega_n$ is reached. At this point, the system is no longer oscillatory. This condition may be translated into a statement about the maximum ramp delay time which can be obtained from a TPR test:

$$\tau_{max} = \left[\left(\frac{\pi^2}{8}\right) \frac{2\alpha}{\alpha^2 + \omega^2}\right] \quad \alpha = \omega_n, \ \omega = 0 ,$$

$$= \left(\frac{\pi^2}{8}\right) \frac{2}{\omega_n} , \tag{2.18}$$

$$= \frac{\pi^2}{4\omega_n} .$$

Thus, given a TPR-test record for which α is known to be small ($\alpha \ll \omega$), one can immediately estimate what maximum τ could be measured for that particular sensing line using the TPR test method, since $\omega \cong \omega_n$ if $\alpha << \omega$.

2.3.7 When the Method Fails

Suppose that the critical condition for oscillation is violated. It is immediately known that

$$\tau \geq \tau_{max} \tag{2.19}$$

where τ_{max} was defined in the previous section. It is not possible to pinpoint the value of τ, but the TPR-test record still contains some information about the severity of the blockage. However, it is not advisable to use a second-order model to estimate the ramp delay time of an overdamped system because any fitting procedure which could be devised would be mathematically ill-conditioned unless the two roots were widely separated. In any case, the failure of the sensing line to oscillate during a TPR test would indicate the presence of a severe blockage (unless a snubber were present).

2.4 STEP PRESSURE PERTURBATIONS

If the response of a stationary linear system is known for a particular input with zero initial conditions, it is frequently possible to determine the predicted response of this system for other inputs. (Practical difficulties are encountered when output data do not adequately represent system dynamics or when they are contaminated with extraneous signals.) A mathematical development that relates systems outputs to various inputs is given by ref. 3. The system output that results from a ramp input is of interest since technical specifications are frequently defined by the ramp delay time between input and output signals. In particular, the ramp delay time is the difference between the time when the input and output signals obtain a specified value based on an input that varies linearly with time. For the case of a relaxed system

(zero initial conditions), the response for a ramp input is the integral of the output from a step input to a relaxed system. The output based on a step input is, in principle, as useful as one based on a ramp input and is usually much easier to obtain. Thus, step changes of the input pressure are used for determining the ramp delay time associated with (1) a restricted sensing line and (2) a Foxboro pressure transmitter for positive and negative signals.

Note from Fig. 2.10 that fast-responding Validyne pressure transmitters are located near each end of the sensing line. Note also that isolation valves for the sensing line provide a convenient means for obtaining step changes in pressure. Detailed procedures for measuring the sensing line delay time for various conditions of line resistance are presented in Appendix A.

Step changes in pressure input to a Foxboro pressure transmitter must be less than approximately 15% of the calibrated range in order to ensure that the response is describable by linear system theory.[4,5] This is because large perturbations drive the transmitter lever system to a physical constraint. Consequently, particular attention must be paid to the magnitude of the step pressure changes. This is accomplished by somewhat different methods for positive and negative pressure inputs to the Foxboro transmitter. In particular, valve sequencing differs for setup and execution of experiments for inducing positive and negative pressure transients. Procedures utilized for the experiments cited for this effort are described in Appendix A and results are discussed in Sect. 3.2.2.

2.5 REMOTE TEST USING A POWER INTERRUPT (PI) METHOD

2.5.1 Principles of Operation of Pressure Transmitters

Motion-balance transmitters allow elastic elements (diaphragms, bellows, or Bourdon tubes) to flex under the influence of a pressure differential. The displacement is measured with a strain gauge or capacitative detector and converted into an electrical signal that is proportional to pressure.

Force-balance transmitters use a position-detection device to detect displacement of the elastic element and a force motor to balance the pressure force and null the displacement. A feedback control system uses the displacement signal to control the force-motor operation. The force-motor current provides an electrical signal that is be related to pressure. Force-balance transmitter operation is determined by the performance of a complex electromechanical device. Because of the design features of a transmitter based on the force-balance principle, remote in situ response time testing is possible. In particular, Foxboro models series E10, E11, and E13 are suitable for application of the remote test described in this section.

2.5.2 Foxboro Transducer Operation

It is necessary to understand how the Foxboro transducer works in order to understand the in situ test. Figure 2.16 is a simplified diagram for a Foxboro transducer model E13DM transmitter. The sensing element for model E13DM is the diaphragm (D) as shown in Fig. 2.16. The sensing element is subject to a high pressure (H) on one side and a low pressure (L) on the other side. The product of the difference in pressure and the effective area of the diaphragm results in a force that propagates

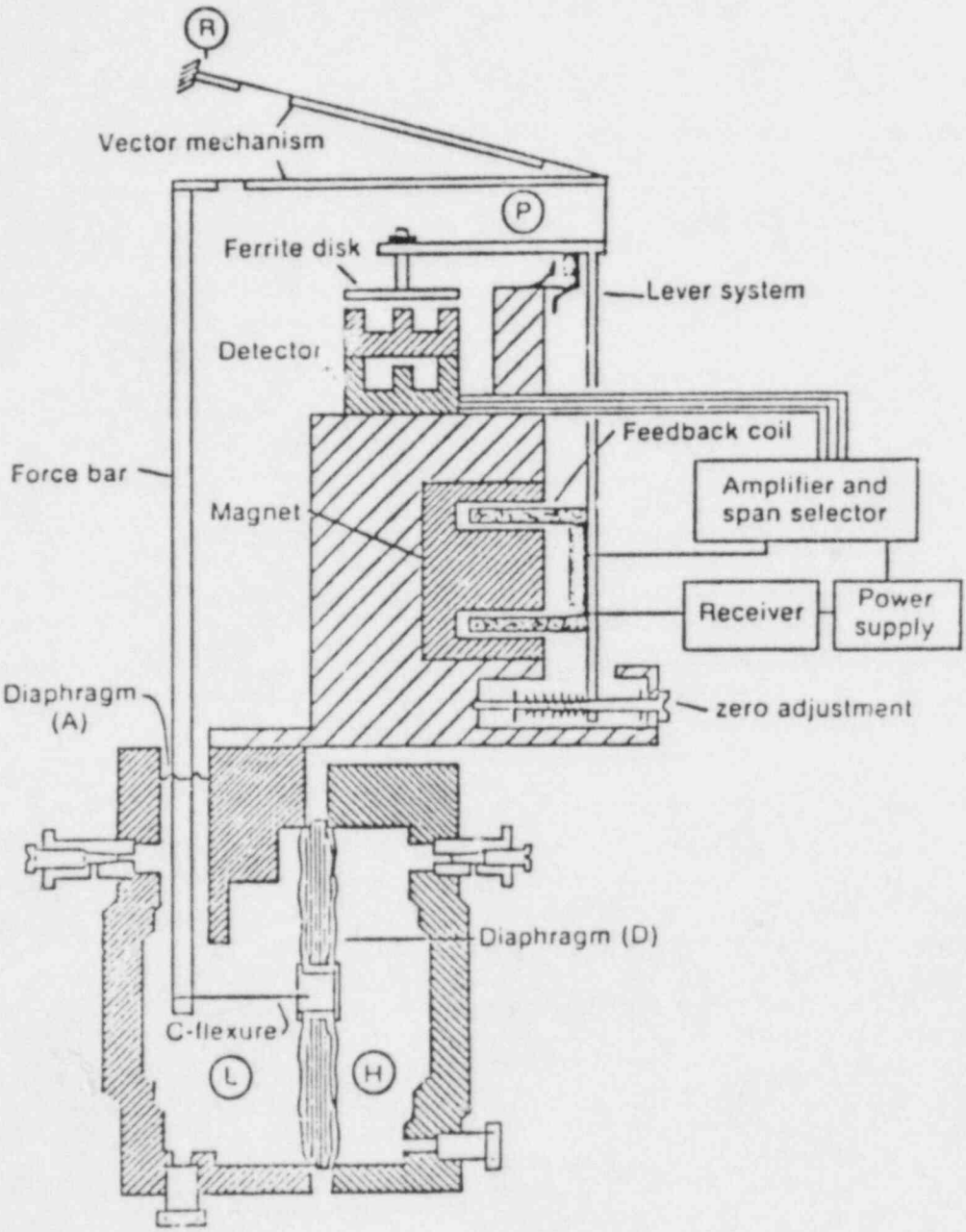

Fig. 2.16. Foxboro pressure transducer Model E13DM.

through the mechanical system to move the lever system and the ferrite disk. The displacement of the ferrite disk from its equilibrium position is an error signal that causes the direct current in the electronic system to change. The current is proportional to the time integral of the displacement. The direct current, which is the output of the transducer, flows through a feedback coil placed perpendicular to a magnetic field and generates a magnetic force. This magnetic force is the feedback action of the transducer and causes the ferrite disk, along with all parts of the mechanical system, to return to the original position. The output of the sensor is a current signal (4 to 20 mA or 10 to 50 mA for full span) proportional pressure. The pressure may be determined by measuring the voltage drop across a resistor in the current loop.

The motion of the lever system is restricted in both directions. It is restricted in the counter-clockwise direction by a stop located beneath the force motor, and in the clockwise direction, by the structure of the transducer. Thus, the displacement of the ferrite disk is limited. Since the displacement of the ferrite disk is an error signal, a limitation in the motion of the disk implies a limitation of the magnitude of the error signal, which makes the transducer a nonlinear system.

Experimental work has shown that a step change in pressure of about 15% of the adjusted span causes the lever system to engage a stopping point until the feedback force is strong enough to return the system to the original position. While the lever system stays at the stopping point, the magnitude of the error signal (the displacement of the ferrite disk) is maximum. The portion of the step response that occurs while the lever system is limited by a stopping point gives the largest gradient that can be present in the output of the transducer. We define this gradient as the critical ramp rate. The corresponding ramp is defined as the critical ramp.

For ramp inputs with ramp rates lower than the critical, the stopping point is not reached, and the transducer behaves as a linear system. For linear systems, the ramp response is as shown in Fig. 2.17. An important feature of linear systems is that the ramp time delay is constant and independent of ramp rate. For ramp inputs with a ramp rate higher than the critical, the stopping point is reached, and the transducer becomes a nonlinear system. For these inputs, the output of the transducer includes the critical ramp, and the time delay increases as the applied pressure ramp rate increases (see Fig. 2.18). The maximum time delay is expected when the transducer is submitted to a large (greater than 15% of span) step perturbation (a ramp with ramp rate equal to infinity).

2.5.3 Power Interrupt (PI) Test

The transmitter can be activated by turning the electric power off then back on. When the power is turned off, the lever system relaxes against a stopping point. When the power is turned back on, three phases of

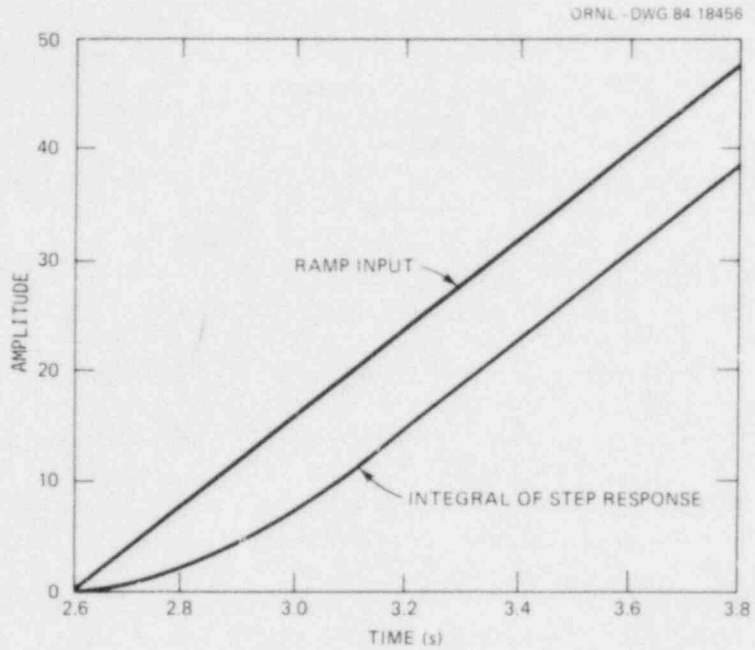

Fig. 2.17. Illustration of time delay based on ramp input pressure and integration of step response.

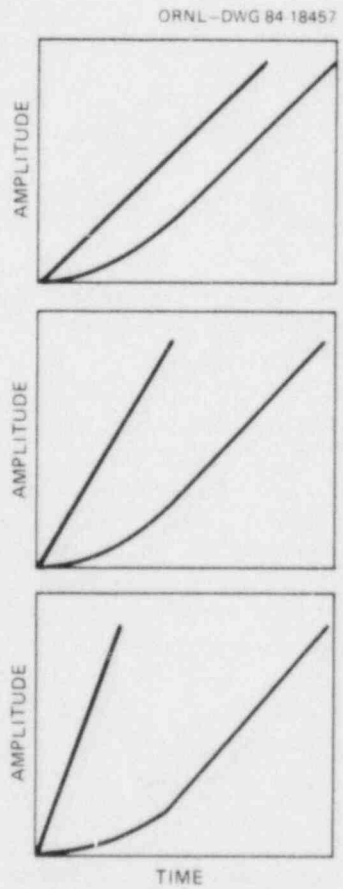

Fig. 2.18. Response of transducer to ramp inputs for different ramp rates.

operation occur (see Fig. 2.19 for a measured response after reinitiation of power):

1. An electronic transient occurs as the electronic detection and feedback system begins operation.
2. The period of operation takes place during which the lever system is still in contact with the stopping point. During this time, the error signal to the feedback system stays constant, and the transmitter output signal changes linearly.
3. A period of operation begins when the lever system first disengages from the stopping point. During this time, the error signal to the feedback control system decreases as the lever system is driven back to the null position.

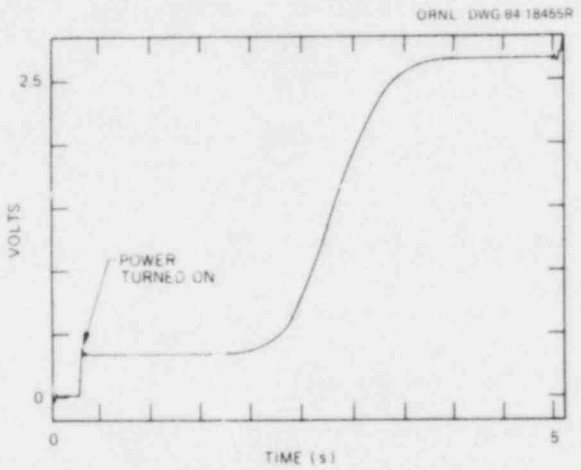

Fig. 2.19. Remote test of Foxboro Model E11GM (10 to 50 mA) pressure transmitter.

These three phases of operation are shown in Fig. 2.20.

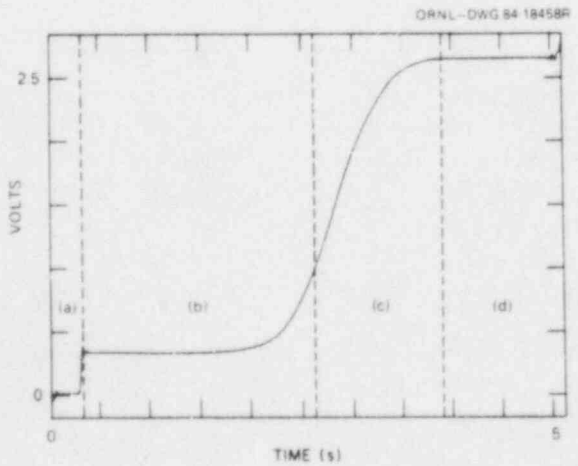

Fig. 2.20. Illustration of a remote test. Region (a) powerup phase, (b) activation of electronics, (c) critical ramp response, and (d) movement of ferrite disk back to equilibrium position. Note that the pressure response is proportional to the voltage.

The value of the data from the PI test may be understood by considering the response to a pressure perturbation. For example, a pressure step causes the lever system to displace suddenly. The feedback system then actuates to drive the lever system back to the null position. For small perturbations, the lever does not reach the stopping point, but for large perturbations, the stopping point is encountered. Consequently, the feedback system faces the same condition at the start of a pressure perturbation as it does during phase b or phase c of the response to turning on sensor power.

To show the equivalence of the pressure step response and the remote test response, an experiment was performed in which a transducer was subjected to a sudden pressure perturbation. After reaching steady state, the remote test was performed by turning power off then back on. Figure 2.21 shows the results for both tests. Clearly, the remote test yields the same response as the pressure perturbation step.

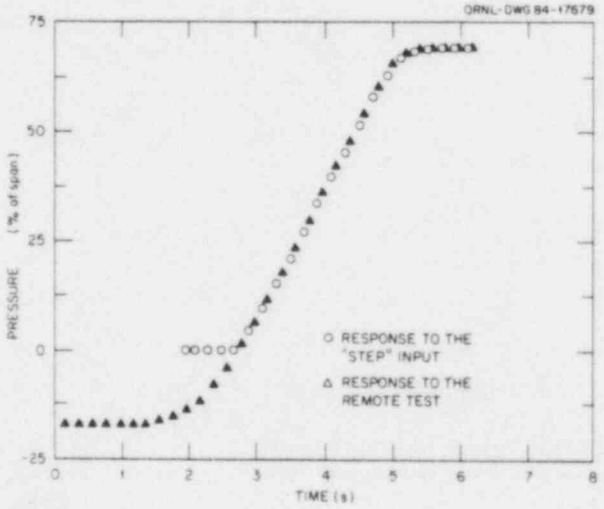

Fig. 2.21. Comparison of response from remote test and step pressure perturbation test.

The remote test may also be used to determine the response to small pressure perturbations in which the stopping point is not encountered. In this case, only phase c of the remote test transient is pertinent. During this phase, the system behaves as a linear dynamic system. This means that the time required to cover any fraction of the total response is the same regardless of the size of the input.

2.5.4 Sensor Dynamic Analysis

For small pressure perturbations, the Foxboro force-balance transmitter can be approximated as in Fig. 2.22. This model applies force perturbations that do not result in driving the lever system to the mechanical stop. The mechanical transfer function, G_m, converts a force imbalance into a displacement and the electrical transfer function, G_e, converts a

ORNL-DWG 84-17667

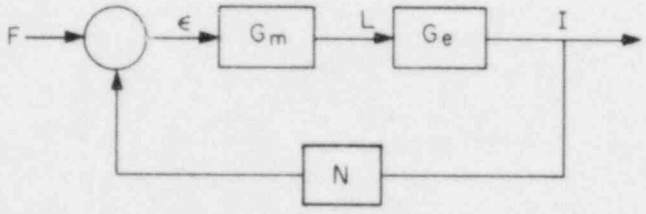

Fig. 2.22. Simplified transmitter block diagram where
N = feedback loop gain.
F = pressure force,
ε = imbalance,
L = diaphragm displacement,
I = current to transmitter feedback motor (assumed proportional to motor force),
G_m = mechanical transfer function for the transmitter,
G_e = electrical transfer function for the transmitter.

displacement into a force-motor current (and equivalently, an output current signal from the transmitter). To a first approximation, G_m and G_e may be represented as first order lags.[5] That is

$$G_m = L/\varepsilon = \frac{A}{s + B} , \qquad (2.20)$$

$$G_e = \frac{I}{L} = \frac{\alpha}{s + \beta} .$$

These may be converted into differential equations as follows:

$$\frac{dL}{dt} + BL = A\varepsilon , \qquad (2.21)$$

$$\frac{dI}{dt} + \beta I = \alpha L .$$

Since the output of interest is the current, I, it is useful to eliminate L from this set of equations. The result is

$$\frac{d^2I}{dt^2} + (B + \beta)\frac{dI}{dt} + (-\alpha AN + B\beta)I = \alpha AF \qquad (2.22)$$

or

$$\frac{d^2I}{dt^2} + K_1 \frac{dI}{dt} + K_0 I = C \qquad (2.23)$$

where

$K_1 = B + \beta$,
$K_O = -\alpha AN + B\beta$, and
$C = \alpha AF$.

Note that steady-state conditions require that $C = K_O I_\infty$.

Equation (2.23) may be used to analyze sensor dynamics for a pressure perturbation or for an PI test. Figure 2.21 shows a typical PI transient and a typical pressure step transient. The condition for the mechanical components of the system is the same at the start of a pressure step transient as the time when the level system first disengages from the stop in the PI test. However, the electrical system is in a different condition at these two time points. In a pressure perturbation, the electrical system is initially at rest $dI/dt = 0$. At the time of disengagement in the PI test, the electrical system is operating at its maximum rate and $dI/dt \neq 0$. This implies that the transient for a pressure step perturbation is not identical with the after-disengagement transient in the PI test unless the effect of the nonzero initial derivative is negligible in the PI test.

Laplace transforming Eq. (2.23) gives

$$(s^2 + K_1 s + K_O)I - \left.\frac{dI}{dt}\right|_o = \frac{cK_O I_\infty}{s} \qquad (2.24)$$

where I is measured relative to its value at the breakaway point. Solving for I/I_∞ gives

$$I/I_\infty = \frac{s\left(\frac{1}{I_0}\left.\frac{dI}{dt}\right|_o\right) + K_O}{s\,(s^2 + K_1 s + K_O)} \; . \qquad (2.25)$$

This shows that the transform of the transient after the breakaway point has one zero, a pole at zero, and two nonzero poles (real or complex). That is, the form is

$$y(s) = \frac{M(s + z)}{s(s + p_1)\,(s + p_2)} \; . \qquad (2.26)$$

The time-domain response may be obtained by inverse Laplace transformation. The result is

$$y\,(t) = M\frac{z}{p_1 p_2} + \frac{(z - p_1)}{(-p_1)(p_2 - p_1)}\,e^{-p_1 t} \qquad (2.27)$$

$$+ \frac{(z - p_2)}{(-p_2)(p_1 - p_2)}\,e^{-p_2 t} \; .$$

The final value, $y(\infty)$, is $\frac{Mz}{p_1 p_2}$. Subtracting the response from its final value gives

$$y'(t) = y(\infty) - y(t) = \frac{M(z - p_1)}{p_1(p_2 - p_1)} e^{-p_1 t} + \frac{M(z - p_2)}{p_2(p_1 - p_2 t)} e^{-p_2 t} . \tag{2.28}$$

The Fourier transform of $y'(t)$ is given by

$$F = \frac{M}{2\pi} \int_0^\infty y'(t) e^{j\omega t} dt . \tag{2.29}$$

Performing the integration gives

$$F = \frac{M}{2\pi} \frac{(z - p_1)}{p_1(p_2 - p_1)(p_1 + j\omega)} + \frac{M}{2\pi} \frac{(z - p_2)}{p_2(p_1 - p_2)(p_2 + j\omega)} . \tag{2.30}$$

Algebraic manipulation yields

$$F = \frac{\frac{Mz}{2\pi p_1 p_2} \left(j\omega + p_1 + p_2 - \frac{p_1 p_2}{z} \right)}{-\omega^2 + j\omega (p_1 + p_2) + p_1 p_2} . \tag{2.31}$$

The form of the Fourier transform is

$$F = \frac{A (j\omega + B)}{(D - \omega^2) + jC\omega} . \tag{2.32}$$

That is, the Fourier transform of $y'(t)$ has the form of a frequency response of a function with one zero and two poles.

2.5.5 Frequency-Domain Data Analysis of Remote PI Test Data

The theoretical results presented above provide a basis for analysis of actual data from an PI test. The steps are

1. Record the transient output from the transmitter after it is turned on.
2. Identify the breakaway point.
3. Form a new data set consisting of the portion after the breakaway point.
4. Subtract each point in the new data set from the final value.

This provided data for performing a numerical Fourier transform.

The next step is to identify the poles and the zero by analysis of the Fourier transformed data.

Fitting a transfer function to data is often done by a nonlinear search method, which minimizes the error between the data and the fit. For the present problem, a closed-form linear analytical method was developed. The Fourier transform yields complex numbers at each frequency, ω. That is

$$F = R + jI \ . \tag{2.33}$$

The problem is to find the values of A, B, C, and D in Eq. (2.32) which cause a fit at all measurement frequencies. This requires the following equality at each frequency:

$$R + jI = \frac{A(j\omega + B)}{(D - \omega^2) + jC\omega} \ . \tag{2.34}$$

Algebraic manipulation and equating real parts and imaginary parts yields:

$$\begin{aligned} RD - I\omega C - AB &= \omega^2 R \ , \\ ID + R\omega C - \omega A &= I\omega^2 \ . \end{aligned} \tag{2.35}$$

The second equation is a linear algebraic equation with R, I, and ω known. Therefore, a solution for the unknowns (D, C, and A) may be evaluated if Fourier transform data are available for at least three frequencies. After D, C, and A are found, B may be found from Eq. (2.35) as follows

$$B = \frac{\omega^2 R - RD + I\omega C}{A} \ . \tag{2.36}$$

The poles may be evaluated as follows

$$p_i = - \frac{C \pm \sqrt{C^2 + 4D}}{2} \ . \tag{2.37}$$

Note that real or complex poles are possible.

The fit gives the zero and the poles, but only the poles are needed to construct the responses that would have followed a pressure step, as may be seen by using Eq. (2.25). For a pressure step, $\left.\frac{dI}{dt}\right|_o$ is zero, and the Laplace transform of the response is

$$I/I_\infty = \frac{K_o}{s(s^2 + K_1 s + K_o)} \ . \tag{2.38}$$

This function has the same poles as the poles for the PI transient, but there is no zero. The transfer function may be written

$$I/I_\infty = \frac{p_1 p_2}{(s + p_1)(s + p_2)} \quad . \tag{2.39}$$

The response is

$$I(t)/I_\infty = 1 + \frac{p_1 p_2}{(-p_1)(p_2 - p_1)} e^{-p_1 t} + \frac{p_1 p_2}{(-p_2)(p_1 - p_2)} e^{-p_2 t} \quad . \tag{2.40}$$

Note that the poles (available from the fit of the Fourier analysis results from the PI test) provide all the information needed to evaluate the response to a pressure step.

2.5.6 Time-Domain Data Analysis of Remote (PI) Test Data

The transient response of a Foxboro pressure transmitter that results from a remote PI test is, in part, assumed to be that of a linear time-invariant system. In particular, the portion of the response that corresponds to the time when the lever system moves from the stop to the equilibrium position is assumed to be a step response of a linear time-invariant system with nonzero initial conditions. Thus, parameters of a linear time-invariant model must be identified from the data subject to nonzero initial conditions in order to determine the delay time associated with a ramp input to a relaxed system.

First consider a general model of a linear time-invariant system of order n,

$$dx(t) = Ax(t) + Bu(t) \tag{2.41}$$

where x(t) is vector of n functions, A is an n × n constant matrix, B is an n × m constant matrix, and u(t) is a vector of m functions. The solution to this equation is given by

$$x(t) = \Phi(t)\, x(o) + \int_o^t \Phi(t,\tau) B u(\tau) d\tau \tag{2.42}$$

where $\Phi(t,\tau)$ is called the state transition matrix. For a linear time-invariant system, the state transition matrix is the matrix exponential $\exp [A(t - \tau)]$. For a single-input, second-order system, Eq. (2.31) can be written as

$$\begin{bmatrix} x_1(t) \\ x_2(t) \end{bmatrix} = \begin{bmatrix} \phi_{11}(t) & \phi_{12}(t) \\ \phi_{21}(t) & \phi_{22}(t) \end{bmatrix} \begin{bmatrix} x_1(0) \\ x_2(0) \end{bmatrix} \tag{2.43}$$

$$+ \int_0^t \begin{bmatrix} \phi_{11}(t-\tau) & \phi_{12}(t-\tau) \\ \phi_{21}(t-\tau) & \phi_{22}(t-\tau) \end{bmatrix} \begin{bmatrix} b_1 \\ b_2 \end{bmatrix} u(\tau)d\tau$$

Because a linear system is invariant under any linear transformation one may define the following without modifying dynamic characteristics of the system,

$$x_1(t) = [V(t) - V_o]/(V_\infty - V_o) \tag{2.44}$$

where

$V(t)$ = recorded voltage output data,
V_o = voltage at the start of the analyzed transient,
V_∞ = voltage at the end of the analyzed transient.

Thus, $x_1(o)$ is zero, and $x_1(\infty)$ is unity under this transformation. Another consequence of this invariance is that any linear time invariant system of order n may be placed in the canonical form corresponding to state variables being defined by $x_2(t) = \dot{x}_1(t)$, $x_3(t) = \dot{x}_2(t)$ and likewise for higher-order state variables where only the last entry in the b vector is not zero. For a second-order system, this representation is,

$$\begin{pmatrix} x_1(t) \\ x_2(t) \end{pmatrix} = \begin{matrix} 0 & 1 \\ -\alpha_1 & -\alpha_2 \end{matrix} \begin{matrix} x_1(t) \\ x_2(t) \end{matrix} + \begin{matrix} 0 \\ 1 \end{matrix} U(t) \Bigg), \tag{2.45}$$

where α_1 and α_2 are coefficients of the characteristic equation. Thus, applying these transformations and transforming the integral so that $\tau = t - \tau$, for a step input, Eq. (2.43) becomes (letting $\tau = \tau$)

$$\begin{bmatrix} x_1(t) \\ x_2(t) \end{bmatrix} = \begin{bmatrix} \phi_{11}(t) & \phi_{12}(t) \\ \phi_{21}(t) & \phi_{22}(t) \end{bmatrix} \begin{bmatrix} 0 \\ x_2(0) \end{bmatrix} \tag{2.46}$$

$$+ C \int_0^t \begin{bmatrix} \phi_{11}(\tau) & \phi_{12}(\tau) \\ \phi_{21}(\tau) & \phi_{22}(\tau) \end{bmatrix} \begin{bmatrix} 0 \\ 1 \end{bmatrix} d\tau$$

Note that now a single integral equation can be written for $x_1(t)$. In particular,

$$x_1(t) = \phi_{12}(t)\, x_2(0) + \frac{c}{x_2(0)} \int_0^t x_2(0)\, \phi_{12}(\tau)d\tau \qquad (2.47)$$

Because the initial condition on the first derivative of $x_2(t)$ is not known explicitly and because C must satisfy the final condition, one may rewrite Eq. (2.47) by redefining ϕ_{12} and C so that,

$$x_1(t) = \psi_{12}(t) + \gamma \int_0^t \psi_{12}(\tau)d\tau \qquad (2.48)$$

where $\psi_{12}(t) = x_2(0)\phi_{12}(t)$ and $\gamma = c/x_2(0)$. Since $x_1(0)$ is zero, it is apparent that $\psi_{12}(0) = 0$. For the response to be bounded, $\psi_{12}(t)$ must go to zero as time increases to infinity. Thus, since $x_1(t)$ goes to unity,

$$\gamma = 1/\int_0^\infty \psi_{12}(\tau)d\tau \qquad (2.49)$$

Note that the measured data provide $x_1(t)$ [defined as $x_m(t)$] and that $\psi_{12}(t)$ must be identified from the data. If one differentiates Eq. (2.48), a differential equation for $\psi_{12}(t)$ is obtained. In particular,

$$\dot{\psi}_{12}(t) + \gamma\, \psi_{12}(t) = \dot{x}_m(t) \qquad (2.50)$$

or

$$\psi_{12}(t) = e^{-\gamma t}\, \psi_{12}(0) + e^{-\gamma t} \int_0^t e^{\gamma\tau} \left[\frac{dx_m}{d\tau}\right] d\tau \qquad (2.51)$$

Since $\psi_{12}(0)$ is zero, Eq. (2.51) becomes

$$\psi_{12}(t) = e^{-\gamma t} \int_0^t e^{\gamma\tau} \left[\frac{dx_m}{d\tau}\right] d\tau \qquad (2.52)$$

and γ is an unspecified parameter. Thus, the problem of identifying $\psi_{12}(t)$ becomes one of finding γ so that $x_1(t)$ calculated from Eq. (2.48), defined as $x_c(t)$, approximates $x_m(t)$ as well as possible. In particular, γ is chosen so that

$$f(\gamma, x_m, T) = \int_0^T \left\{[x_c(\tau) - x_m(\tau)]\right\}^2 d\tau \qquad (2.53)$$

is minimized where T represents the time corresponding to the end of the data to be analyzed.

A. The minimization is accomplished as follows:

1. choose a value for γ,
2. solve for $\psi_{12}(t)$ and $x_c(t)$ by numerical integration of Eqs. (2.52) and (2.48),
3. evaluate the functional defined by Eq. (2.53),
4. test the functional (f) to determine if the minimum is found,
5. determine a new value for γ if f is not minimized,
6. repeat steps 2 through 5 until convergence is obtained.

There are a variety of methods for choosing new values for γ. The method used for results reported here uses a Fibonacci line search in combination with halving the interval.[6]

The delay time associated with a unit ramp input [D(t)] is given by

$$D(t) = t - \int_0^t [x_m(\tau) - \psi_{12}(\tau)]\, d\tau \qquad (2.54)$$

This follows because the unit ramp response is the integral of a relaxed system response to a unit step input. Note that ψ_{12} in the integral of Eq. (2.54) eliminates the effect of the nonzero initial conditions in the remote test data.

3. RESULTS

3.1 NOISE EXPERIMENTS

This section presents the results of the analysis of pressure noise data obtained at the FCTF high-pressure loop. The experimental setup is described in Appendix A.

3.1.1 Pressure Sensor Time Delay

An important characteristic of the Foxboro pressure sensor used for our tests is the inherent nonlinearity which causes steps of negative magnitude to be faster than steps of positive magnitude regardless of the actual magnitude of the step (see Sect. 3.2.2). It was determined that the time delay introduced by this sensor is 0.11 s for negative steps and 0.32 s for positive steps. The pressure noise contains perturbations of positive and negative magnitudes; therefore, we hypothesize the effective delay lies between the two previous ones.

Figure 2.8 in Sect. 2 shows the sensor transfer function calculated by simultaneously measuring the pressure noise with the Foxboro sensor and a high-frequency-response Validyne sensor located near it. The dominant factor in this transfer function contributing to the time delay is the low-frequency real pole at about 1 Hz. This pole introduces a delay of 0.159 s ($1/\omega$), which lies between the delays measured with perturbative techniques using positive and negative perturbations step pressure changes.

3.1.2 Sensing Line Time Delay

The effect of increased friction on the sensing line transfer function was presented in Fig. 2.6. This figure shows the line transfer function for several positions of a needle valve located near the line inlet. These positions are (a) fully opened, (b) opened 1/2 turn, (c) opened 1/4 turn, and (d) opened 1/8 turn. These four cases have been analyzed using the techniques described in Sect. 2.1. The results are presented in Table 3.1.

The first line in Table 3.1 gives the results of the nonlinear fit to the sensing line open-loop transfer function. These results proved to be accurate when compared to the pressure step tests (see Sect. 3.2.2) and can be used for benchmarking the other calculations. As expected, the best agreement is obtained from the nonlinear fitting of either the Validyne or Foxboro sensor. The other three methods are only approximations which should be used to predict only trends, not absolute values.

The PSD fitting methods yield systematically larger values of the time delay. This effect can be explained by the fact that the transfer function method measures the open-loop transfer function between the inlet and outlet pressure sensors; whereas the PSD methods measure the closed-loop transfer function, which includes the interactions with the test loop. We hypothesize that the closed-loop feedback produces an increased

Table 3.1. Sensing line time delays (ms) estimated from noise analysis

Method	Time delay (ms) for valve position			
	Open	1/2 turn	1/4 turn	1/8 turn
Transfer function nonlinear fit*	1.8	10.5	13.0	215.1
Transfer function -45° frequency*	23.2	28.9	45.5	227.4
Validyne PSD: nonlinear fit†	2.6	14.7	28.8	212.5
Validyne PSD: rms value†	N/A	42.0	96.0	425.0
Foxboro PSD: nonlinear fit†	3.1	12.7	24.3	240.8
Foxboro PSD: rms value†	N/A	6.0	225.0	>500

*Open-loop result.
†Closed-loop results.

damping that increases the time delay. The closed-loop time delay is the one that can be observed by perturbative methods such as the TPR test.

The rms method has given relatively good results when applied to the Validyne sensor but not when applied to the Foxboro sensor. In general, it predicts a longer time delay than the actual delay. This effect is due to the damping of the resonances in the real case thus reducing the rms value more than the superposition of the first-order time delay used to create the conversion table from rms to time delay. Because of the reduced dynamic range of the Foxboro sensor, this method does not have sensitivity for small time delay changes when this sensor is used, and, therefore, the degradation must be severe to be observable. Consequently, this method should be used only to monitor for severe changes in the line damping, not to obtain an absolute value of the delay.

3.1.3 Discussion of the Noise Results

The general terminology "noise techniques" includes several methods to estimate time delays introduced by the sensing line or pressure sensors. These methods have been divided in two broad categories: (a) transfer-function measurements and (b) output-noise measurements. The main difference between the two categories of methods is the number of sensors that are used. Output-noise measurements can utilize the plant's existing instrumentation, but transfer-function measurements require the installation of a second sensor in the line.

The results of this research show that transfer-function measurements based on the existing process noise in our test facility (without external perturbations) are possible, and they compare well with pressure step measurements. Using these methods, both the sensing line and the pressure sensor time delays can be estimated. However, measuring the sensing line transfer function requires the installation of a second sensor at the inlet of the line; this is easily accomplished in laboratory conditions, but it is currently impractical in nuclear plants. The measurement of the sensor transfer function, however, requires the installation of a second sensor close to the original process sensor. This is a more accessible location. The current procedure for testing pressure sensors requires that an operator disconnect the sensor from service and test it with a portable pressure-ramp generator. The ramp test is sometimes difficult to perform because of extreme environmental conditions inside the containment. A simpler method that would replace the ramp test and still yield equivalent results could be based on a sensor transfer-function measurement. It would require the installation of a second sensor at the sensing end of the line. This sensor could be installed permanently for continuous measurements or temporarily if the measurement is performed periodically.

Two different methods have been proposed to estimate sensing line time delays from output-noise measurements using only the process sensor: (a) rms measurement and (b) fitting to the pressure PSD. Both methods have been shown to work for all the blockage simulations studied in Sect. 3.1.2; however, their application in a real plant environment still needs to be assessed. The results in a plant will probably depend on the quality of the instrumentation (including the electronics), interferences from the primary system noise, and proper interpretation analysis of the results. The rms measurement is a very robust method in that it will detect severe line blockages with a high degree of confidence, but its accuracy for response time measurement is very low. Therefore, the rms method should be used primarily to indicate blockages or for trend analysis, not to quantify the time delays. Fits to the PSD may yield a quantitative value of response time for short time delays but the interpretation of the results require a detailed physical description of the system, which is not always readily available.

It has been shown that all the noise methods proposed work under laboratory conditions simulating those in a power plant. The transfer-function methods yield good estimates of response time when compared to pressure step tests, but they require the installation of additional

instrumentation. The rms method can be implemented with great simplicity and can be used to detect trends or to set a threshold limit to indicate severe degradation. The PSD fits are capable of yielding the correct response time under the right conditions, but they require detailed analyses by a noise analyst.

3.2 TRANSIENT PRESSURE REDUCTION (TPR) TESTS

3.2.1 Low-, Medium-, and High-Pressure TPR Tests

Three facilities were used for the evaluation of the TPR test method. Main features and results are presented here, and details are given in Appendix A.

The purpose of the low-pressure facility was to determine whether further investigation of the TPR test concept was merited. The TPR test was shown, in low-pressure tests, to be sensitive to changes in sensing line blockage. On the basis of that encouraging qualitative result, further experiments were planned at pressures up to 2000 psi.

The development of the theory behind the TPR test was greatly aided by results from the medium- and high-pressure facilities. The theory requires that the capacitance of the TPR chamber be small in comparison to that of the sensing line itself. The small-TPR-chamber-capacitance assumption is satisfied in the medium- and high-pressure facilities but not in the low-pressure facility. The presence of the TPR chamber may be accounted for by augmenting the capacitance in the single-lump model as shown in Fig. 3.1. The relationship between TPR chamber capacitance (as a fraction of total sensing line capacitance) and resonant frequency is plotted in Fig. 2.12. The theoretical relationship was determined according to the model in Fig. 3.1. The measurements shown in Fig. 2.12 are from the medium- and high-pressure facilities. The wide range of frequencies was attained by using different TPR chamber sizes and static pressures in the medium-pressure facility. The reason for the vast differences in TPR chamber capacitance in Fig. 2.12 is that, for a given TPR chamber, the capacitance is inversely proportional to the square of the absolute pressure.

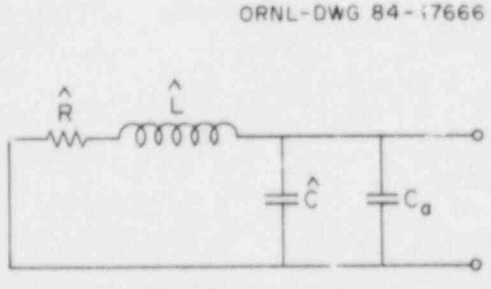

Fig. 3.1. Single-lump model of a sensing line with load capacitance, C_a.

Since the capacitance of the TPR chamber is a function of pressure (being larger at lower pressure), a departure from linear behavior occurs for large-amplitude pressure oscillations. Figure 3.2 shows semi-logarithmic plots of amplitude versus time for TPR tests with different blockage conditions in the medium-pressure facility. In some cases the data can be fitted rather well with two straight lines. (In other cases, the magnitude of the oscillations is so small that only a few data points can be accurately read.) Figure 3.3 shows a typical

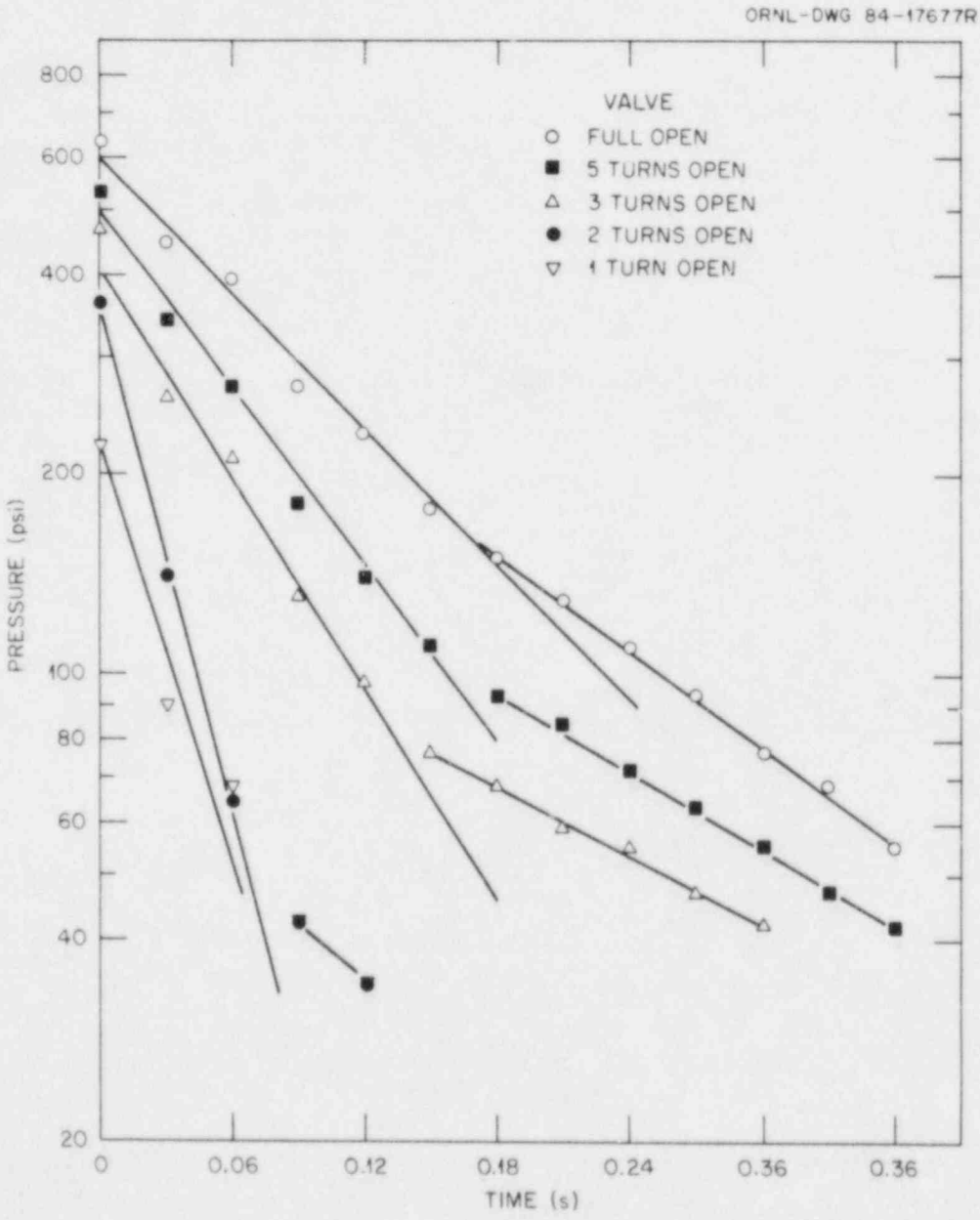

Fig. 3.2. Pressure amplitude plots for different blockage from a TPR test of the medium-pressure facility.

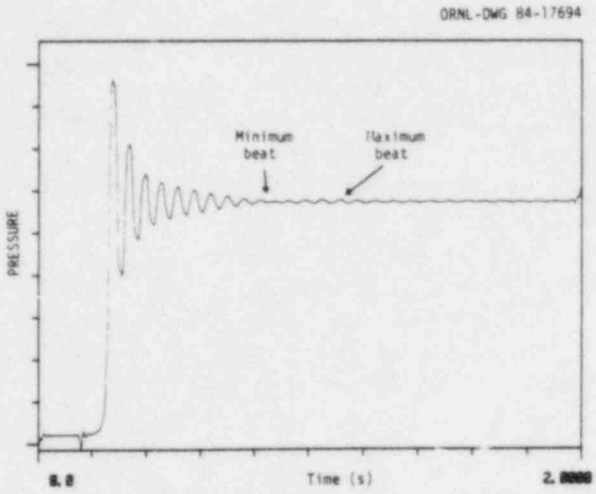

Fig. 3.3. Typical TPR test record from the medium-pressure facility (medium blockage, valve 4 turns open).

trace (from the medium-pressure facility) in which the blockage simulation valve near the process was four turns open. (The same valve was one turn out of nine open for the test in Fig. 3.4.)

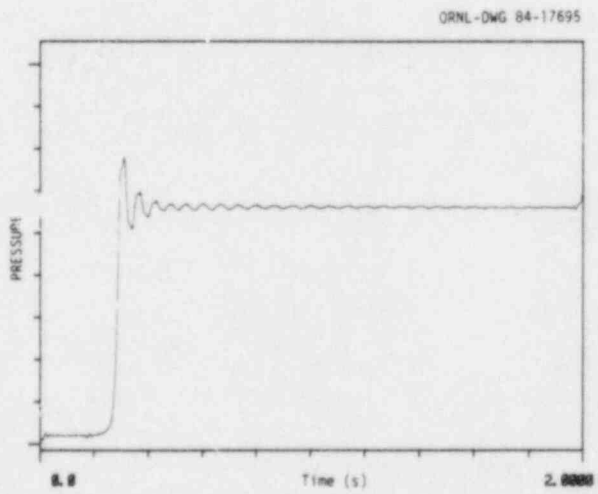

Fig. 3.4. Typical TPR test record from the medium-pressure facility (large blockage).

Since no single line fits the data well (Fig. 3.2), determining τ is ambiguous. The steeper of the dashed versus solid lines (Fig. 3.2) yields the larger value. For the sake of conservatism, the steeper line

should be used. However, since the capacitance of the TPR chamber is insignificant for small oscillations about a large pressure, a better indication of the ramp delay time may result from using the slopes of the dashed lines. But the slopes of these lines are independent of the valve positions (Fig. 3.2). This may be a reflection of the fact that a severe blockage is required before there is a significant change in ramp delay time (see Fig. 2.14).

To illustrate the method of determining τ from a TPR test, the following procedure is presented; this is followed by a concrete example. Each point in Fig. 3.2 represents the pressure (as recorded by the fast-acting pressure sensor) at either a local maximum (peak) or local minimum (trough) alternately. Therefore, the time between points represents half a cycle. Thus the angular frequency is given by

$$\omega = \frac{n\pi}{t_2 - t_1} \tag{3.1}$$

where

n = number of half cycles separating t_1 and t_2,
t_1 = first time point,
t_2 = second time point.

A pressure corresponds to each time point. Thus (t_1,p_2) and (t_2,p_2) represent data points in Fig. 3.2 or just arbitrarily chosen points on the line of best fit drawn through the data points. The rate of decay of the pressure oscillations is characterized by the slope of the line of best fit. Thus, we calculate

$$\alpha = \frac{\ln p_1 - \ln p_2}{t_2 - t_1} = \frac{\ln \dfrac{p_1}{p_2}}{t_2 - t_1} \quad . \tag{3.2}$$

Having calculated α and ω, we proceed to calculate

$$\tau = \frac{\pi^2}{8} \quad \frac{2\alpha}{\alpha^2 + \omega^2} \tag{3.3}$$

$$= \frac{\pi^2\alpha}{4(\alpha^2 + \omega^2)} \quad . \tag{3.4}$$

The relationship between τ and α and ω was discussed in Sect. 2.3. In particular see Eqs. (2.8) and (2.10).

For example, referring again to Fig. 3.2, to estimate the τ associated with the five-turns-open case, we choose the following points arbitrarily

$$(t_1, p_1) = (0.03,\ 280)\ ,$$

$$(t_2, p_2) = (0.18,\ 46)\ .$$

In accordance with the procedure just described,

$$\omega = \frac{5\pi}{0.18 - 0.03}\ ,$$

$$\cong 104.7\ \frac{\text{rad}}{\text{s}}\ ,$$

and

$$\alpha = \frac{\ln\left(\frac{280}{46}\right)}{0.18 - 0.03}\ ,$$

$$\cong 12.04,$$

and, finally,

$$\tau \cong \frac{\pi^2}{8}\ \frac{2\,(12.04)}{(12.04)^2 + (104.7)^2} \qquad (3.5)$$

$$\cong 2.7\ \text{ms}\ .$$

Figure 3.5 shows a characterization of the valves used for blockage simulation in the medium-pressure facility. The flow coefficient is defined to be the flow in gal/min which would result from a steady-state pressure difference of 1 psi across the valve.

The beat phenomenon was not observed in the high-pressure facility. Typical traces (Figs. 3.6 and 3.7) show the effect of 9 and 1 turns open, respectively, of the blockage valve near the process. Note that the blockage is so severe in the one-turn case that there is no oscillation. In this case, τ cannot be determined by the method described here. However, the absence of oscillation indicates a severe line blockage.

Typical plots (from a high-pressure facility) for determining α are shown in Fig. 3.8). Some of the curves in Fig. 3.8 exhibit the same sort of nonlinearity observed in the low-pressure facility. In some highly blocked cases the amplitude of a "trough" exceeds that of the preceding "peak." This could be due to the longer time that the TPR chamber takes to fill under high-blockage conditions. In these cases

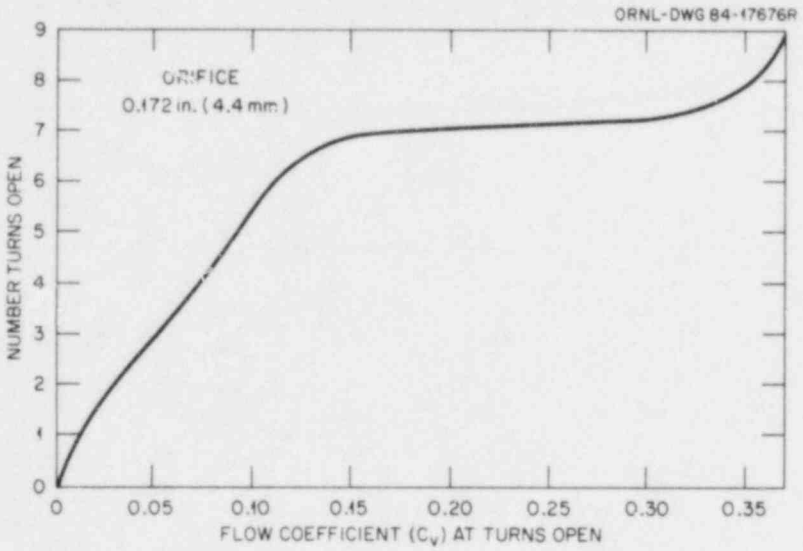

Fig. 3.5. Valve characterization for regulating stem (medium-pressure facility).

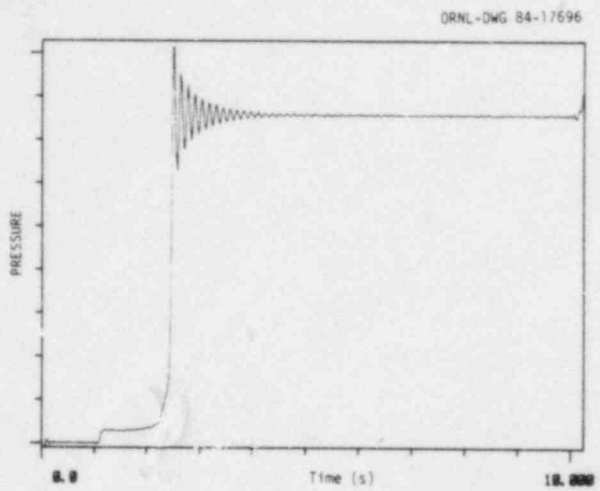

Fig. 3.6. Typical TPR test record from the high-pressure facility (low blockage, valve 9 turns open).

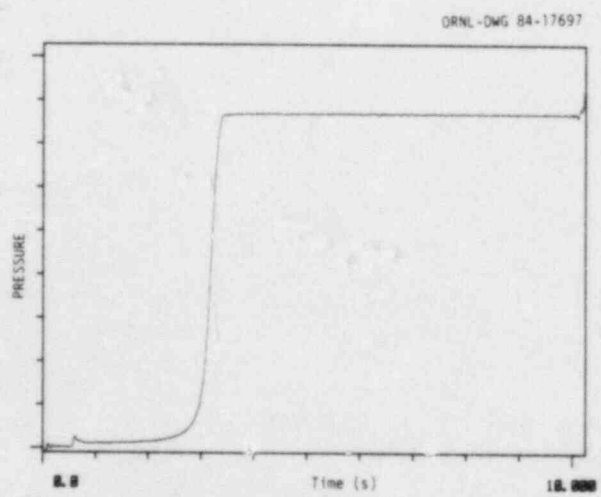

Fig. 3.7. Typical TPR test record from the high-pressure facility (large blockage, valve 1 turn open).

(notably the two-turns-open case in Fig. 3.8), it is still possible to draw a line which crudely fits the data, and thereby estimate τ.

Typical plots (from the high-pressure facility) for determining α are shown in Fig. 3.8.

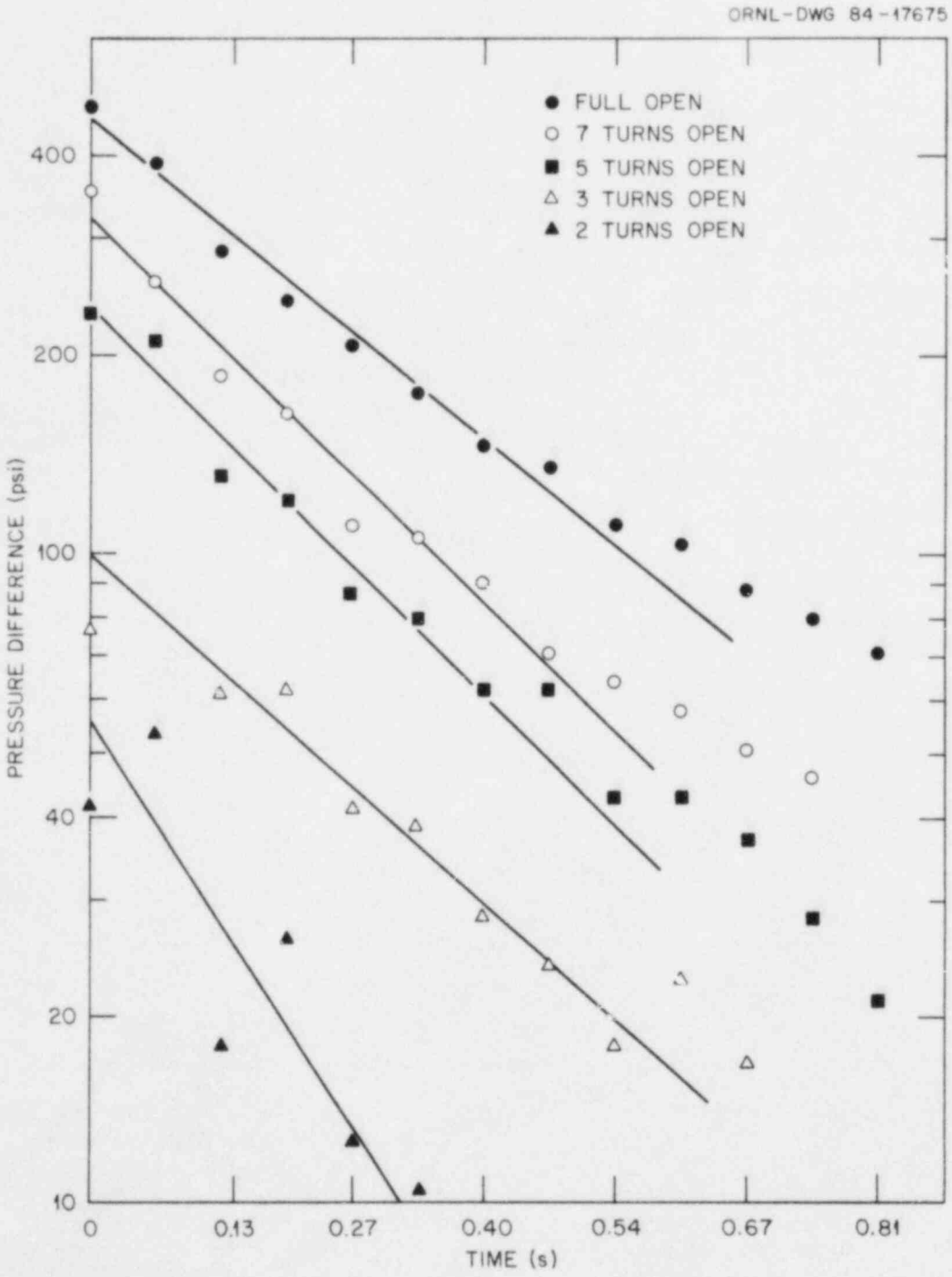

Fig. 3.8. Pressure amplitude plots for different blockages from TPR tests of the high-pressure facility.

The blockage simulation valve near the process end of the sensing line had a much greater dynamic effect than the one near the sensor in both the high-pressure and the medium-pressure facilities. This is readily explained by noting that the dynamic effect of resistance is dependent on the total downstream capacitance [see Eq. (2.12)]. No results are presented for blockage near the sensor.

Figure 3.9 is a plot of an asymptotic ramp delay time, τ (as estimated from TPR tests) versus valve flow coefficient for the medium-pressure facility.

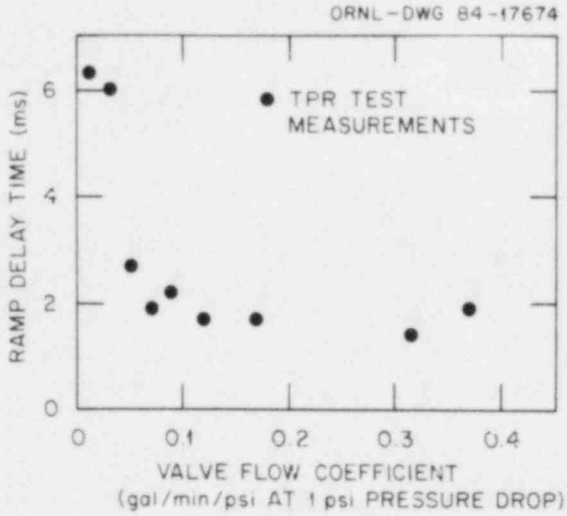

Fig. 3.9. Ramp delay time measurements from the medium-pressure facility.

Using Eq. (2.6) and formulas[2] for r and c, theoretical predictions of τ can be made for an unblocked sensing line. The formulas take no account of bends, valves, or other irregularities. Comparisons of the theoretical predictions of τ with those obtained from TPR tests are provided in Table 3.2.

Table 3.2 Comparison of Theoretical and Measured values of τ

Case	Theoretical* (ms)	TPR (ms)	Noise (ms)
High-pressure	0.25	2.7	2.6
Medium-pressure			
6.2-cc TPR chamber	0.11	1.9	
12-cc TPR chamber	0.11	2.1	
19-cc TPR chamber	0.11	2.2	

*Theoretical values of τ are independent of TPR chamber size since the theoretical treatment ignores the TPR chamber.

It is not surprising that the theoretical predictions of τ are much smaller than the TPR-test results. The theoretical prediction would be expected to underestimate τ. The TPR test is expected to overestimate τ. This leads to the conclusion that the true value in the high-pressure facility lies within these limits.

3.2.2 TPR Test Evaluation for use in Blocked Lines

The objective of the TPR test is to measure indirectly the ramp delay time of a sensing line. The measured value may then be added to the ramp delay times of the other components of the instrument channel to obtain the response time of the entire channel. The latter value must be below a certain maximum. Typical pressure sensors used in nuclear power plants have response times in the range of 100 ms to 500 ms. It has been demonstrated here that an idealized (but otherwise typical) sensing line has an asymptotic response time on the order of 5 ms or less. The maximum allowable response time of the entire channel is typically 2 s. Thus, we see that the contribution from the sensing line to the total response time of the channel is negligible under normal circumstances. It also has been shown here that the response time of a sensing line remains negligible unless the line is severely blocked.

Depending on the severity of the blockage, a determination of τ by the TPR test may or may not be possible, since such a determination requires damped pressure oscillations.

The TPR test allows one to distinguish among three possible sensing line conditions: unblocked, partially blocked, and severely blocked.

An unblocked line would exhibit decaying pressure oscillations and would have a negligible response time. A partially blocked line also would exhibit the decaying oscillations and would also have a negligible response time. However, its response time would be greater than that of the unblocked line. A severely blocked line would not exhibit the damped oscillations; therefore, the response time determination would be possible with methods described herein.

Evaluating the usefulness of the TPR test requires examining its advantages and disadvantages in light of other possible methods. First, whether or not it represents significant advantages over simpler methods should be considered. A crude method of sensing line testing would be to open a valve on a test port near the sensor end of the sensing line and observe the resulting flow. By this method, an unblocked line could easily be distinguished from a severely blocked one. Also, a partially blocked line could be diagnosed by measuring the flow rate, provided that a benchmark flow-rate measurement had been made. Since the response time of a properly functioning sensing line is negligible, the TPR test provides no more information than the crude flow-rate test and at considerably more expense. Second, in addition to the amount of information gained in a test, possible harm to the system should be considered. Damage from water hammer could be a problem in some cases. Also, since the coolant water in a PWR contains dissolved boric acid,

each test would introduce a fresh supply of concentrated solution that could precipitate solid boric acid when cooling. Third, the real need for the information should be assessed. A sensing line can tolerate much blockage before ceasing to work well (see Figs. 3.3 through 3.7), and severe blockages have obvious symptoms (e.g., dead sensor response and very limited frequency response) that could be detected in other ways. For example, a more fruitful approach would be to monitor the frequency spectrum of pressure sensor output for high-frequency signal degradation.

3.3 STEP PRESSURE PERTURBATION TESTS

Step pressure perturbation results are obtained for determining the delay time associated with the sensing line and with the Foxboro transmitter for positive and negative perturbations. Results discussed in this section are obtained from the high-pressure experiments performed at the FCTF and based on procedures presented in Appendix A. Table 3.3 lists results of delay time for values of simulated sensing line resistance obtained from various positions of the needle value V_{14} shown in Fig. 3.10. Note that for an unrestricted line, the delay time for the pressure signal to move down the sensing line is determined to be approximately the line length divided by the speed of sound in water (~30 ms for the FCTF). This is expected from theoretical considerations. Likewise, based on an analysis of the wave equations with damping, it is apparent that the delay time will increase to infinity as the resistance is increased to infinity. On the other hand, the solution to the wave

Table 3.3. Sensing line response times for simulated line restrictions at the FCTF high-pressure test facility on May 22, 1984*

Value configuration	Response time (ms)
V_{14} 1/16 turn open	1300
V_{14} 1/4 turn open	230
V_{14} 1/2 turn open	100
V_{14} 1 turn open	45
V_{15} full open	30

*Refer to Fig. 3.10 for determining the test setup. All inputs are positive step pressure perturbations.

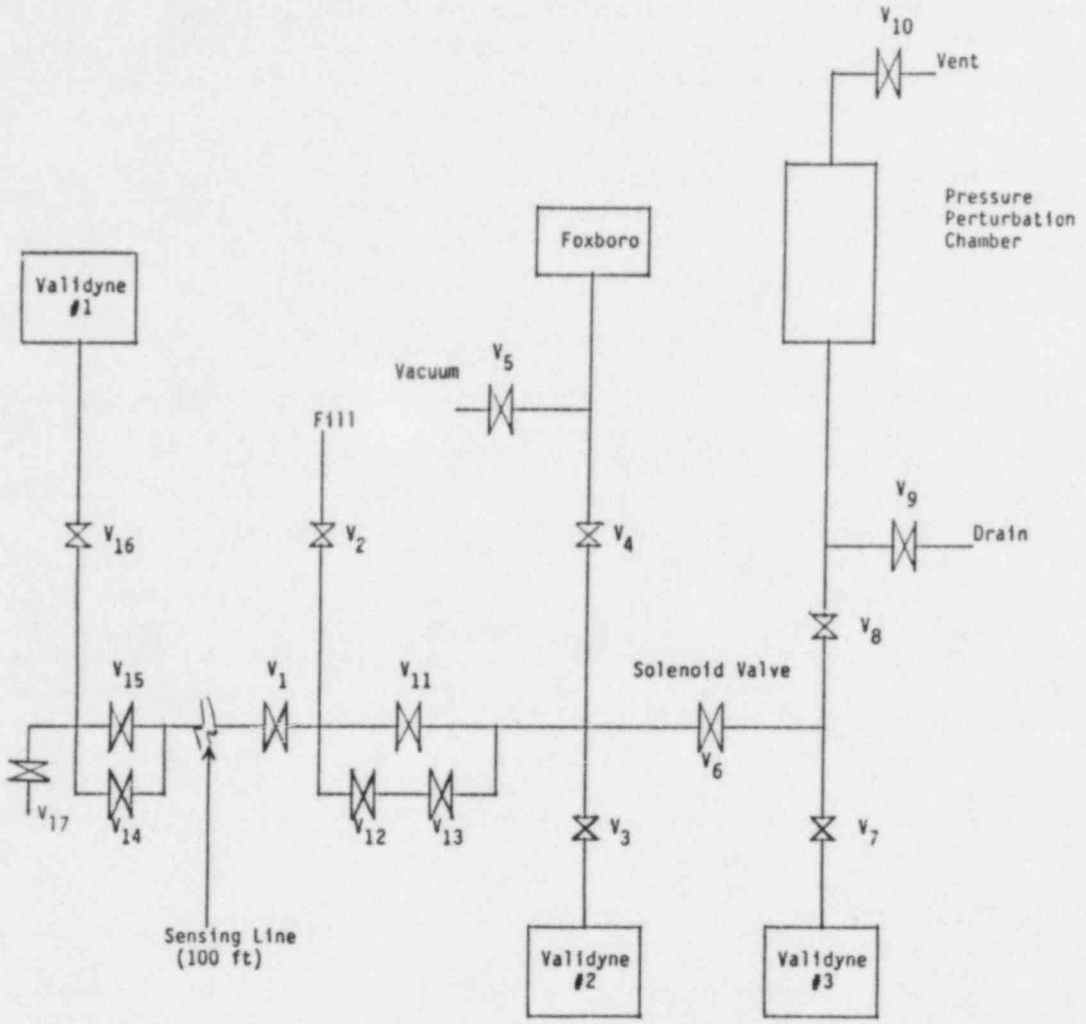

Fig. 3.10. Schematic diagram of ORNL high-pressure perturbation test equipment. (See also Fig. A.6.)

equation for no line resistance (with a ramp input and a reflected output) illustrates that the output will periodically lead and lag the input by the length divided by the speed of sound in water. Thus, the asymptotic time delay for a ramp input is, on the average, zero. Results (shown in Table 3.3) for the unrestricted line and for the case of V_{14} greater than 1/2 turn open represent the transient delay for the first pressure wave to move the length of the sensing line. Results (Table 3.1) for V_{14} at 1/4, 1/8, and 1/16 turns open are based on the time required for the output to obtain 63% of its final value; hence, these results are characteristic of the asymptotic delay and compare reasonably well with the noise analysis results shown in Table 3.3 since valve positioning is visually estimated.

Measurements of the response times of the Foxboro pressure transmitter for positive and negative transients are shown in Table 3.4. Note that the delay time for the negative transient is approximately one third of

Table 3.4. Response time measurements of the Foxboro pressure transmitter at the FCTF high-pressure test facility for positive and negative step input

Test date (1984)	Type of input	Response time (s)
4/6	Positive	0.39
4/6	Positive	0.40
5/22	Positive	0.32
5/22	Positive	0.32
5/22	Negative	0.11
5/22	Negative	0.15
5/22	Negative	0.12

that for the positive transient. For a positive-going transient, the response is expected to be dominated by the electronic characteristics of the force motor (and associated electronics); whereas, for the negative-going transient, the restoring force of the calibration spring may (or may not) dominate the response (depending on the setup of a particular transmitter). Details relative to the operation of a Foxboro transmitter are discussed in Sect. 2.4.

3.4 REMOTE POWER INTERRUPT (PI) TESTS

Laboratory tests were performed on 11 different transmitter combinations. Ten of these were tested when they were reverse calibrated (high pressure is applied to the low side of differential transmitter and the zero is adjusted with the zeroing spring). Different testing methods were used at low pressure (<15 psi) and at higher pressure.

Low-pressure testing was accomplished with an electronically controlled pressure signal generator. Sawtooth pressure signals were generated. The pressure was monitored with a Validyne Model PP-15 high-speed transmitter in parallel with the signal from the Foxboro transmitters. The signals from the Validyne and the Foxboro transmitters were recorded simultaneously on a Hewlett-Packard Model 7402A strip chart recorder. To obtain adequate resolution, the recorder was run at its maximum speed (125 mm/s). This gives a time resolution of 8 ms/mm. Since the Foxboro transmitters have ramp time delays of approximately 100 to 500 ms, the ability to resolve a few millimeters is important. Furthermore, some of the signals had low-level electrical noise contamination. These factors contribute to a measurement uncertainty that is estimated to be approximately 100 ms.

A summary of remote test analyses and experimental data are given in Table 3.5. Data for the experimental determination of delay times are

Table 3.5. Comparison of measured and calculated (PI) remote test delay times for Foxboro Pressure Transmitters

Sensor ID	Measured time delays (ms)				Remote PI test results (ms)	
	(+) Ramp*	(-) Ramp*	(+) Step*	(-) Step*	Time domain	Frequency domain
1B	131	137	226		230	160
1E			205	125	240	
2B	150	127			200	143
2E				112		
3B	174	122			250	182
3E			220	135		
NE11GM Absolute			360	130	525	411
E133DM (3094892) Differential	324		321		330	287
E133DM (3010955) Differential			492		436	382
(reverse cal.)			438		370	346
E133DM (3032882) Differential			412		340	331
(reverse cal.)			392		378	450
E11GM (4504106) Absolute			179		150	146
(reverse cal.)			155		200	203

*Measured ramp delay times are asymptotic values. Measured step delay times are the time required for the output to obtain 63% of its final value (note that 1B, 1E, 2B, 2E, 3B, and 3E are Foxboro sensors).

obtained for positive and negative ramp inputs and for positive and negative step inputs. The delay times reported for the ramp inputs are determined as illustrated by Fig. 2.4, and those for the step input are determined by the time required for the output to obtain 63% of its final value. Variations in measured delay times of approximately 100 ms are expected based on the resolution of data-recording equipment and on the overall consistency of repeated measurements.

Results from analyses of remote (PI) tests are reported for two methods: (1) a frequency-domain method and (2) a time-domain method. Asymptotic time delays reported for the analyses represent averages of calculated

values for several PI (remote) tests. Variations in results from the analyses of several tests for a particular transmitter are as large as 30% for the time-domain method and are approximately 20% for the frequency-domain method. Thus, the differences between delay times calculated with either analysis method or between measurements and analyses of PI test data are within expected variations. The results listed in Table 3.5 provide an adequate database for the observation that the PI test (in conjunction with the analysis methods described in Sect. 2) should be considered as an alternative method to the current ramp test method for determining the response time of Foxboro pressure transmitters.

4. CONCLUSIONS

Three methods for assessing the response time of pressure sensor/sensing line systems were evaluated: (1) interruption of ac power to force-balance pressure sensors (PI method); (2) pressure perturbation (TPR) method; and (3) noise analysis of the noise on the pressure signal. We conclude that the PI method yields satisfactory values of the response time of force-balance pressure sensors and therefore may provide an alternative to the pressure ramp method now used on these sensors in some plants. The major advantages of this method are that it can be performed without entering containment and requires only a momentary interruption of the system service. A typical nuclear-grade sensor was tested by this method in our laboratory and found to have a response time of approximately 0.4 s.

The TPR method can be used to determine whether a sensing line is unblocked, partially blocked, or severely blocked, but other methods maybe more suitable from an operations viewpoint. We conclude that this method does not offer significant advantages over the commonly employed and much simpler techniques of sensing line blockage evaluation.

We conclude that analysis of the noise on the pressure signal can yield useful information regarding the condition of the pressure-sensing system. Our tests in the laboratory indicate that noise analysis can detect degradation in response time resulting from simulated sensing line blockages or voids. Also, if an additional fast-response reference sensor is installed at the sensor end the line, a quantitative value of process sensor response time can be inferred. It also appears that quantitative values of sensing line response time may be obtained by fitting the pressure power spectrum to obtain parameters related to the line dynamics. However, more research is needed to verify this method. We were able to verify that the response time of an unblocked line is negligible (2 to 3 ms) by computing the transfer function between fast-response sensors located at both ends of the line. This, of course, is a very good way to measure the line response under all conditions but is not practical in most plant situations.

We conclude that the noise analysis method may be useful for remotely assessing the general condition of pressure sensing systems during plant operation; however, the success of this method depends very much on the particular installation and the bandwidth and amplitude of the pressure fluctuations in the process that stimulates the sensing system. Therefore, we recommend that if the noise method is used, that baseline measurements be made under known system conditions (i.e., after the system response is verified by other means).

In summary, our theoretical and experimental studies have shown that the combined response time of typical process pressure sensors and sensing lines is considerably less than the response time required by plant specifications for all but severely blocked lines. Although, based on our industry survey, degradation of response time of pressure-sensing systems does not seem to be a significant problem in the industry, it may be desirable to monitor key plant pressure-measuring systems for the

types of degradation that have been experienced such as frozen sensing lines, lines blocked by valves that are inadvertently left closed during maintenance, and electronic failures of pressure sensors.

Since those types of failures can occur during operation, the noise analysis method appears to be the only practical way to provide remote and continuous monitoring of pressure sensor/sensing line systems to detect severe degradation of response time. However, if noise analysis is contemplated, we strongly suggest that baseline measurements of noise on typical in-plant systems be performed to further evaluate the reliability of this approach.

REFERENCES

1. J. A. Mullens and J. A. Thie, "Pressure Noise in Pressurized Water Reactors," ORNL/TM-9773, NUREG/CR-4389, in preparation.

2. G. E. Ragan, "The TPR Test: A Method for In-Situ Response Time Testing of Pressure-Sensing Lines in Nuclear Power Plants," M.S. Thesis, The University of Tennessee, Knoxville, June 1985.

3. J. J. DiStefano, A. R. Stubberud, and I. J. Williams, Theory and Problems of Feedback Control Systems, Schaum's Outline Series, McGraw-Hill, New York, 1967.

4. G. T. Chen, Introduction to Linear System Theory, Holt, Rinehart and Winston, Inc., New York, 1970.

5. A. J. Soares, "Study and Dynamic Modeling of a Pressure Transducer that is based on the Principle of Force Balance," Ph.D. Dissertation, The University of Tennessee, Knoxville, December 1982.

6. P. J. Wilde and C. S. Beightler, Foundations of Optimization, Prentice-Hall, Inc., Englewood Cliffs, N.J., 1967.

7. J. A. Thie, personal communication, August 1984.

APPENDIX A. TEST FACILITIES AND PROCEDURES

A.1 NOISE ANALYSIS FACILITIES

The purpose of this procedure is to provide instructions for recording and reducing pressure noise data to be used to detect degradations of the sensing line and/or the pressure sensor.

A.1.1 Equipment

This procedure can be divided in two main tasks: (a) signal conditioning and (b) signal reduction. The equipment needed for the first task is a set of matched antialiasing filters and amplifiers. For the second task, a dedicated multichannel Fourier analyzer can be used. Alternatively, an FM tape recorder, which produces a tape that later can be analyzed with a multipurpose computer, can be used.

A.1.2 Method for Signal Conditioning

Prior to recording or reduction, the pressure-noise signals must be ac-coupled to remove the dc component. The oscillating part of the signal is then filtered to avoid biasing. The filter's cutoff frequency must be set at 80% of the Nyquist frequency (40% of sampling frequency). The filtered-noise signal must then be amplified to an appropriate rms level in order to increase the signal-to-noise ratio while taking care not to overload the tape recorder or A/D converter.

A.1.3 Method for Signal Reduction

The sampled time data is reduced to the required power spectral densities (PSDs) and/or transfer functions using the fast Fourier transform (FFT) technique. In order to calculate the sensor transfer function, a frequency resolution of 0.02 Hz or less is needed (i.e., minimum 50 s per analysis block). To monitor the sensing line dynamics, a larger frequency resolution can be used. In this case, the Nyquist frequency should be determined so that it properly defines the expected frequency range of the Helmholtz resonance.

A.1.4 Data Analysis

After the PSDs and/or transfer functions have been obtained, any of the analysis methods described in Sect. 2.2 can be applied. The choice of method will depend on the available instrumentation.

A.2 PRESSURE PERTURBATION AND TPR TEST FACILITIES

A transient pressure reduction (TPR) test is performed by introducing a pressure pulse into the sensing line with a fast-action solenoid valve and recording the output of a fast-responding reference pressure transmitter. The recorded data are analyzed by identifying a parameter directly related to the delay time of the sensing line based on a second-order model of the system. Because the delay time associated with the sensing line is a function of line length, line resistance, and

capacitance of the process transmitter diaphragm, some fluid in the line needs to be moved. It has been observed that a pressure perturbation chamber of several hundred cubic centimeters provides excellent sensitivity for determining sensing line resistance and capacitance.

A.2.1 Equipment

The equipment and materials needed for conducting a pressure perturbation test of the sensing line are illustrated by Fig. A.1. Note that valve V_1 is connected to the plant test-port isolation valve and that

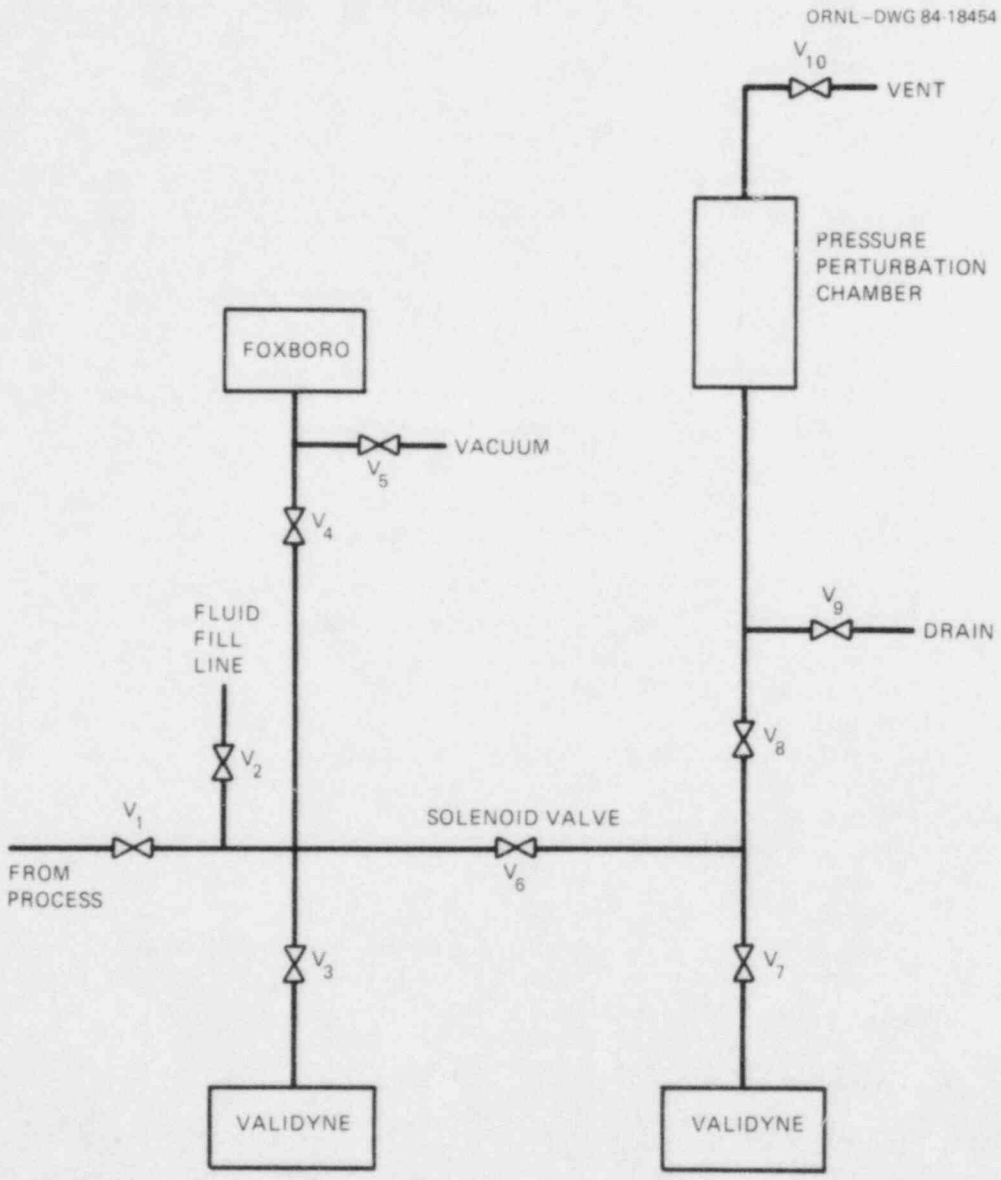

Fig. A.1. Schematic diagram of the test configuration for determination of the sensing line response time. A Foxboro process pressure transmitter is included for evaluation of its response time by a method that uses electrical preturbation.

valve V_6 is a remotely operated solenoid valve used to initiate the pressure perturbation. Valves V_3 and V_7, V_4 and V_8 isolate the two Validyne reference pressure transmitters, the Foxboro force-balance pressure transmitter and the pressure perturbation chamber, respectively. Valve V_2 is provided so that the system can be filled with reactor-grade nonradioactive water. Valves V_9 and V_{10} allow for draining the pressure perturbation chamber. Note that the Foxboro pressure transmitter is included in order to evaluate its response time by an electrical perturbation method and that it need not be present for routine response time tests of sensing lines.

A.2.2 Data-Recording Equipment

The data-recording equipment must preserve a permanent record of the test data and also provide sufficient on-line diagnostic capability. In addition, a hardcopy readout of test results should be available during data acquisition to ensure that the time-dependent responses have the expected form and that test parameters, such as initial and final valve positions, have prescribed values. Experience obtained from laboratory experiments and from other field tests for similar experiments is sufficient to conclude that these objectives will be satisfied by using the following components:

1. a voltmeter with a digital readout,
2. an oscilloscope that can temporarily store transient data,
3. a dual-channel strip chart recorder,
4. a frequency-modulated analog tape recorder with a voice channel, and
5. a time-code generator.

The voltage meter provides an accurate readout of initial and final values of transient responses and allows for cross checking data shown on the oscilloscope. The oscilloscope gives an immediate readout of the data and can be used to cross check the traces obtained with the strip recorder. The strip chart data can be used for inspecting preliminary results of the test and is a backup for analog data. The analog data contain a wide range of frequency-dependent information and can be digitized for later off-line analysis. The voice channel and time code generator provide a convenient mechanism for identifying the beginning of particular data.

A.2.3 Data Analysis for the TPR Test

The primary objective of this test is to identify a delay time associated with a sensing line and associated plant instrumentation. In particular, this is the time difference (τ_1) between a linear pressure ramp input at the process and the output pressure at the sensor end of the sensing line when observed at a fixed pressure. A secondary objective is to identify the time lag (τ_2) between a fast-responding reference pressure transmitter (a Validyne) and a typical process pressure transmitter.

The pressure transient, p(t), induced into the sensing line system by opening the solenoid valve normally consists of damped oscillations of a frequency (f_o). The damping constant, α, and f_o are identified from p(t). The damping (or decay) constant is given by[7]

$$\alpha = f_o \ln[A(t)/A(t + f_o^{-1})] \qquad (A.1)$$

where t corresponds to the time of the first peak of the oscillations. Given α and f_o, the desired delay is given by[7]

$$\tau_1 = 2\alpha/[\alpha^2 + (2\pi f_o)^2] \; . \qquad (A.2)$$

However, if damped oscillations are not obtained from the test, a more detailed analysis must be performed in which p(t) is compared to system model calculations. One cause of this type of off-normal behavior is due to a significant sensing line blockage that prevents oscillatory response.

It may also be possible to obtain the time lag, τ_2, between the Validyne and a process pressure transmitter. In particular, if both transmitters respond with damped resonant oscillations, τ_2 can be obtained from the phase lag between the two recorded pressure transients. If the two pressure transients are not similar, a detailed analysis that compares data with system models is required. Examples of causes for a nonoscillatory response of the process transmitters are nonlinearities and low-pass filtering by the system or by the process transmitter.

The time delay associated with the sensing line and pressure transmitter system is computed directly from the sum of τ_1 and τ_2.

A.2.4 Pressure Perturbation Test Procedures at the Forced Convection Test Facility (FCTF) for Sensing Line Dynamics

The sensing line dynamics are obtained by introducing a pressure perturbation (TPR test) into the sensing line and then monitoring the transient response. The test is performed as follows:

1. Eliminate air from the test facility.
2. Initialize the fluid level in the test facility with atmospheric pressure downstream of the process isolation valve.
3. Pressurize the test facility upstream of the solenoid valve.
4. Drain pressure perturbation chamber.
5. Open the solenoid valve and monitor the transient response of the pressure.
6. Shut the solenoid valve and reinitialize fluid level and pressure in the pressure perturbation chamber.
7. Repeat steps 4 and 5 for additional tests.

A detailed procedure is listed below:

1. Shut valves V_1, V_2, V_9, and V_{10}.
2. Open valves V_3, V_4, V_5, V_6, V_7, and V_8.
3. Establish a vacuum at the vent valve V_5.
4. Close valve V_5.
5. Open valve V_2.
6. Bleed both Validyne pressure transmitters.
7. Shut V_4.
8. Open V_5.
9. Establish a vacuum at V_5.
10. Close V_5.
11. Open V_4.
12. Shut valves V_2 and V_6.
13. Open valve V_1.
14. Shut valve V_8.
15. Open drain valve V_9.
16. Open vent valve V_{10}.
17. Wait approximately three minutes to ensure that the pressure perturbation chamber is drained.
18. Shut valves V_9 and V_{10}.
19. Verify that the recording equipment is ready and initiate data recording.
20. Open valve V_8.
21. Open solenoid valve V_6.
22. Shut valve V_6 when the transient is complete.
23. Repeat steps 14 through 22 for additional tests.

A.2.5 Procedures for Step Pressure Perturbation Tests at the FCTF

The step pressure perturbation experiments documented in this report include response-time tests for:

1. a restricted sensing line with a variety of line resistances and
2. a Foxboro pressure transmitter for positive and negative transients.

Refer to Fig. 3.10 for references to valves and pressure transmitters cited in the following sections that describe procedures used at the Forced Convection Test Facility.

A.2.5.1 Experimental Procedure for Determining the Sensing Line Delay Time at the FCTF

The sensing line delay-time test is performed as follows:

1. Verify that V_1, V_3, V_4, V_7, V_8, V_{11}, V_{15}, V_{16}, and V_{17} are open.
2. Verify that V_2, V_5, V_6, V_9, V_{10}, V_{12}, V_{13}, and V_{14} are shut.
3. Shut V_{17}.
4. Open V_6 and V_{10}.

5. Shut V_6, V_{10}, and V_{15}.
6. Position the needle valve, V_{14}, at the desired position.
7. Open V_{17} and record the transient signal from all of the pressure transmitters.
8. Shut V_{15}.
9. Repeat steps 1-8 for subsequent tests.

A.2.5.2 Experimental Procedure for Determining the Foxboro Pressure Transmitter Response Time From a Positive Pressure Step

One important factor in performing these tests is that the magnitude of the step pressure change must be less than 15% of the calibrated range so that the transmitter will respond with linear dynamic characteristics. Following are valving operations to achieve this objective and to obtain a suitable positive step pressure signal.

1. Verify that V_1, V_3, V_4, V_7, V_8, V_{11}, V_{15}, V_{16}, and V_{17} are open.
2. Verify that V_2, V_5, V_6, V_9, V_{10}, V_{12}, V_{13}, and V_{14} are shut.
3. Shut V_{17}.
4. Open V_6 and V_{10}.
5. Shut V_6, V_{10}, and V_{15}.
6. Open V_{17} and V_6.
7. Gradually open the needle valve, V_{14}, so that the pressure indicated by Validynes 2 and 3 and the Foxboro increase slowly to a value about 15% below the system pressure.
8. Shut V_{14} and V_{17}.
9. Open V_{15}.
10. Verify that the pressure indicated by the Validynes and the Foxboro are within 15% of the system pressure.
11. Open V_{17} and record the transient signal from all of the pressure transmitters.
12. Shut V_{16} and V_{17}.
13. Repeat steps 1-12 for subsequent tests.

In order to perform this test with the pressure perturbation chamber excluded from the response, open only V_{17} in Step 6.

A.2.5.3 Experimental Procedure for Determining the Foxboro Pressure Transmitter Response Time From a Negative Pressure Step

Following are valving operations to obtain a negative step pressure change of less than 15% of the calibrated range.

1. Verify that V_1, V_3, V_4, V_7, V_8, V_{11}, V_{15}, V_{16}, and V_{17} are open.
2. Verify that V_2, V_5, V_6, V_9, V_{10}, V_{12}, V_{13}, and V_{14} are shut.
3. Shut V_4 and V_{17}.
4. Open V_6 and V_{10}.
5. Shut V_{10} and V_{15}.
6. Open V_{17}.
7. Gradually open needle valve V_{14} so that the pressure indicated

by Validynes 2 and 3 increase slowly to a value about 15% below the indicated pressure of the Foxboro.
8. Shut V_{14} and V_{17}.
9. Verify that the pressure indicated by the Foxboro is less than 15% greater than the pressure indicated by Validynes 2 and 3.
10. Open V_4 and record the transient signal from the Foxboro pressure transmitter.
11. Open V_{17} and record the transient signals from all of the pressure transmitters to obtain a transient response for a positive step pressure perturbation.
12. Repeat Steps 1-11 for subsequent test.

A.2.6 Facilities for TPR Test

Three experimental facilities were used in the investigation of the TPR-test method. The facilities can be described according to pressure regime as

1. low-pressure (<30 psig),
2. medium-pressure (<1000 psig), and
3. high-pressure (<2300 psig).

A.2.6.1 Low Pressure (<30 psig)

The low-pressure facility was built first to determine whether further investigation of the TPR-test concept was merited. The facility consisted of a 42-gal tank (to act as a pressure reservoir), a 50-ft-length of 3/8-in.-OD copper tubing (as a sensing line), a regulating valve (to introduce line blockage), a solenoid valve (to initiate the tests), and interchangeable TPR chambers of 50, 100, and 1000 cc. A schematic diagram of the low-pressure facility is provided in Fig. A.2.

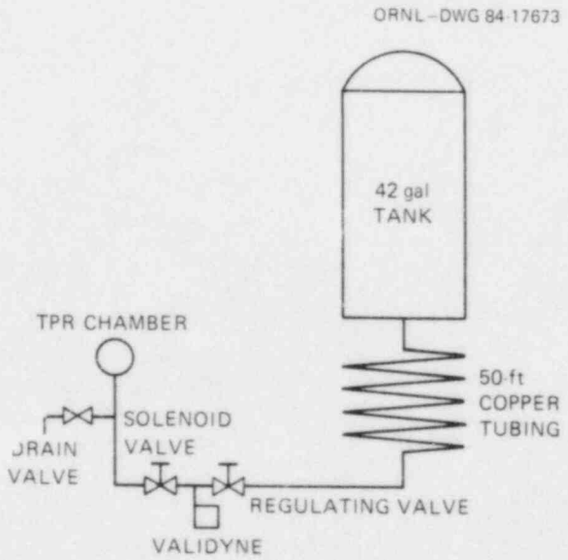

Fig. A.2. Schematic diagram of low-pressure facility.

A.2.6.2 Medium Pressure (<1000 psig)

The medium-pressure facility increased pressure by a factor of 20. This is only a factor of 2 less than typical reactor pressures. The major difference resulting from the increase in pressure was that the capacitance of the TPR chamber was greatly reduced in the higher-pressure case. Thus, the distributed nature of the sensing line itself became significant. Therefore, the facility was designed so that the location of the blockage could be varied. The facility was also designed so that entrained air could be introduced in the sensing line.

A schematic diagram of the facility is provided in Fig. A.3. Table A.1 describes the facility in detail.

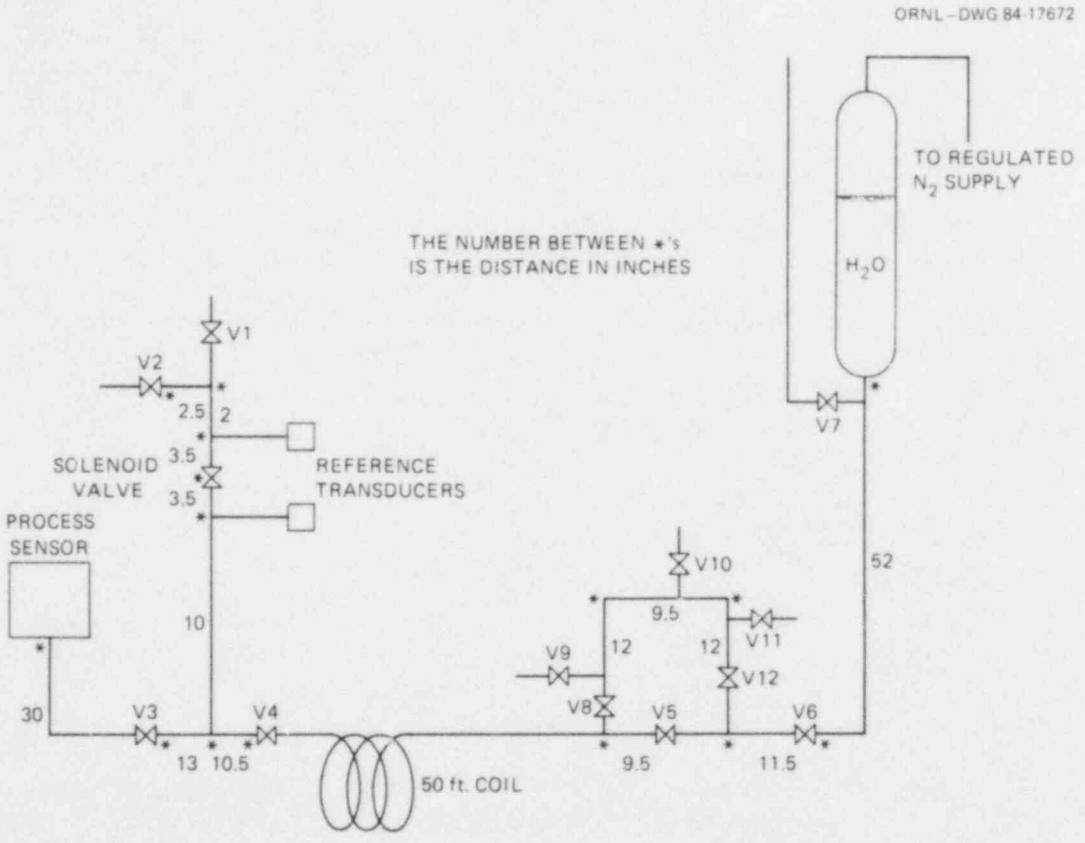

Fig. A.3. Schematic diagram of medium-pressure facility.

Table A.1. Detailed description of medium-pressure facility

Item	Designation in Fig. A.4	Function	Description
Tubing	--	Sensing line	1/4-in.-OD, 0.03-in. wall copper tubing
Solenoid valve	Solenoid valve	Test initiation	
TPR chamber	TPR chamber	See text	Section of 3/8-in.-OD copper tubing
Reference transducers	Reference transducers	Data acquisition	Validyne
Pressure reservoir	Pressure reservoir	Pressure reservoir	1 gal tank, pressure rating 1800 psi
Process sensor	Process sensor	Not used	
Valve	V4	Blockage introduction "near sensor"	Whitey
Valve	V5	Blockage introduction "near process"	Whitey
Misc. valves	Vmn	Miscellaneous	Whitey
Level indicator	Level indicator	Indication of tank water level (when depressurized)	Plexiglass tube
Pressure supply	To regulated He supply	Provides pressure source for reservoir	2000-psi He tank with regulator

A.2.6.3 High pressure (<2300 psig)

The high-pressure tests were conducted at the ORNL FCTF, which is capable of simulating a large PWR reactor during a small break event. The facility is a high-pressure, high-temperature, forced-circulation water loop configured as shown in Fig. A.4. The loop can be operated at temperatures and pressures up to 650°F and 2250 psig with a water flow through the test section of up to 50 gal/min at variable test-section power inputs of up to 30 kW. The pressure perturbation fixture was connected to the spool piece on the discharge side of the 100-A pump, feeding the test section in the FCTF. The test configuration, as shown in Fig. A.5, consisted of connection tubing to the process spool piece with an isolation valve, input pressure sensor, Validyne pressure sensor model DP-15, valves to simulate blockage at input, and a 100-ft, 3/8-in.-OD, .065-in.-wall coiled stainless steel sensing line. The sensing line is connected to a typical PWR pressure panel configuration as shown in Figs. A.6 and A.7. The TPR chamber and associated pressure

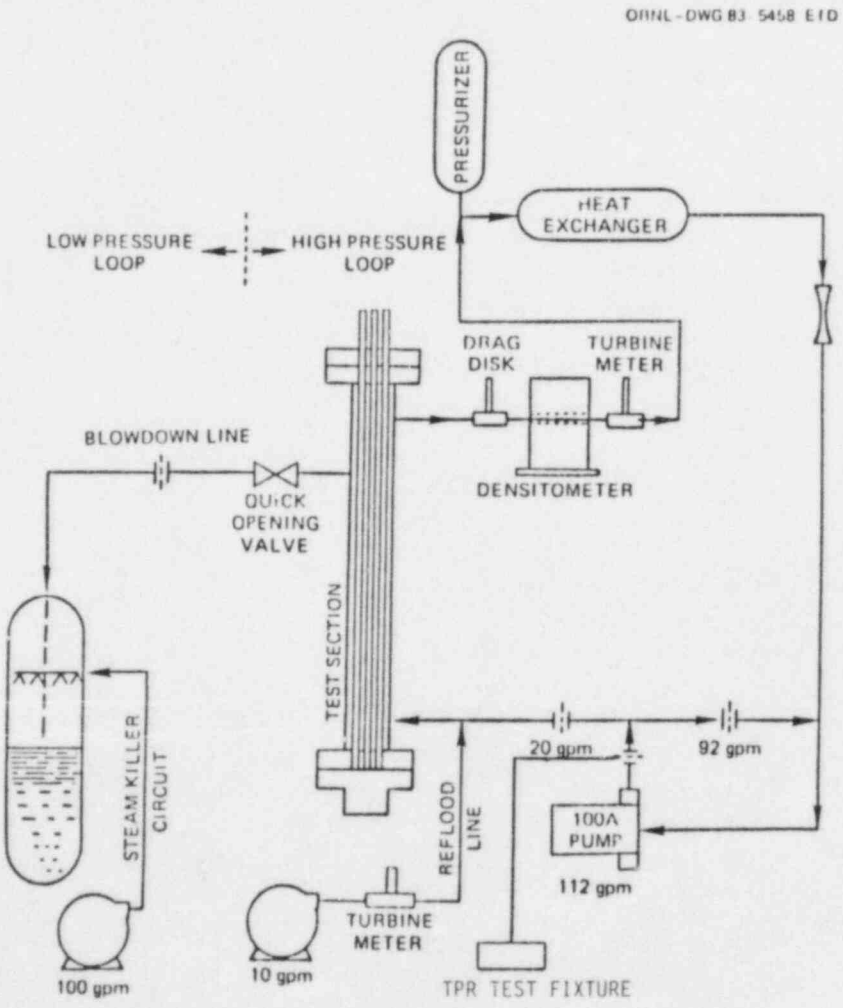

Fig. A.4. Schematic diagram of ORNL Forced Convection Test Facility (FCTF).

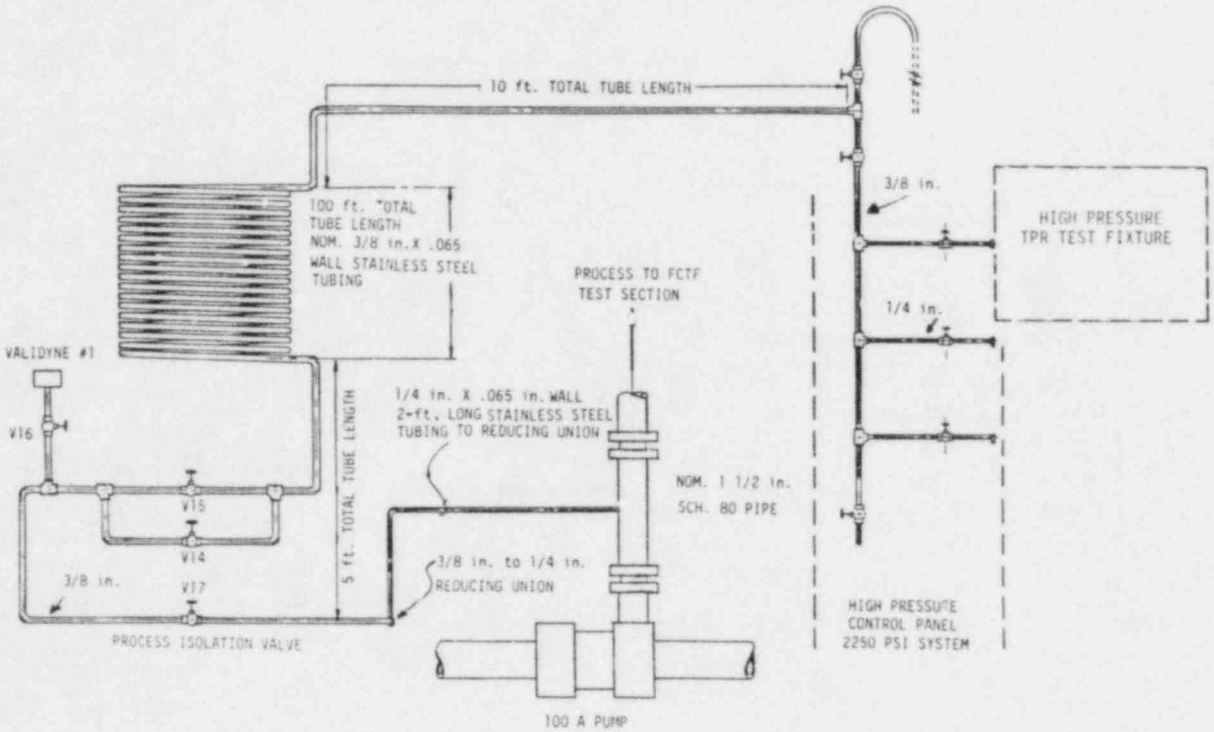

Fig. A.5. ORNL FCTF high-pressure perturbation test configuration.

sensors and valves are connected to the calibration port of the pressure panel. The pressure perturbation test fixture as shown in Figs. A.8 and A.9, is constructed of 1/4-in.-OD, .065-in.-wall stainless steel. Two Validyne Model DP-15 pressure sensors and a Foxboro Model NE11GM pressure transmitter are connected to the fixture. The TPR chamber is welded construction of stainless steel with a volume of 150 cc. The solenoid valve is remotely controlled. The fixture was mounted in the FCTF so each of the valve handles could be accessed without opening the safety barrier when the FCTF is in operation.

A.3 REMOTE TESTING

The purpose of this procedure is to provide instructions for response-time testing of pressure transmitters using a remote testing method. This method permits testing a pressure transmitter from outside the reactor containment while the plant is operating and is applicable only to Foxboro force-balance pressure transmitters.

The Foxboro force-balance pressure transmitters measure pressure and transmit it as a proportional current signal. This transmitter uses a dc power supply in its circuitry that is usually located outside the containment and, thus, is easily accessible. A momentary interruption of the power supply output to the transmitter constitutes the basis for the remote response time testing.

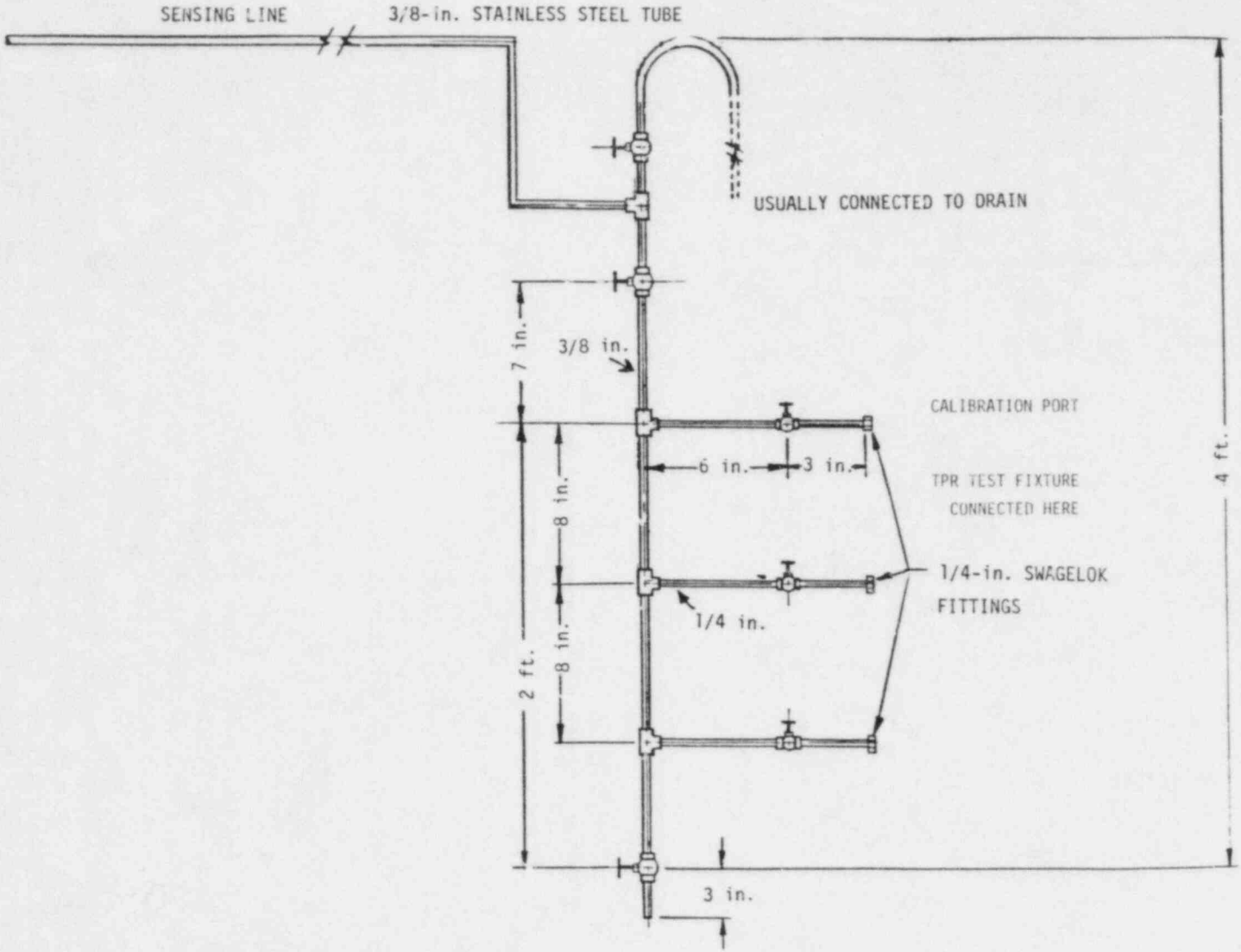

Fig. A.6. Schematic diagram of typical connection to a pressurized water reactor pressure panel used at FCTF.

ORNL PHOTO-7915-83

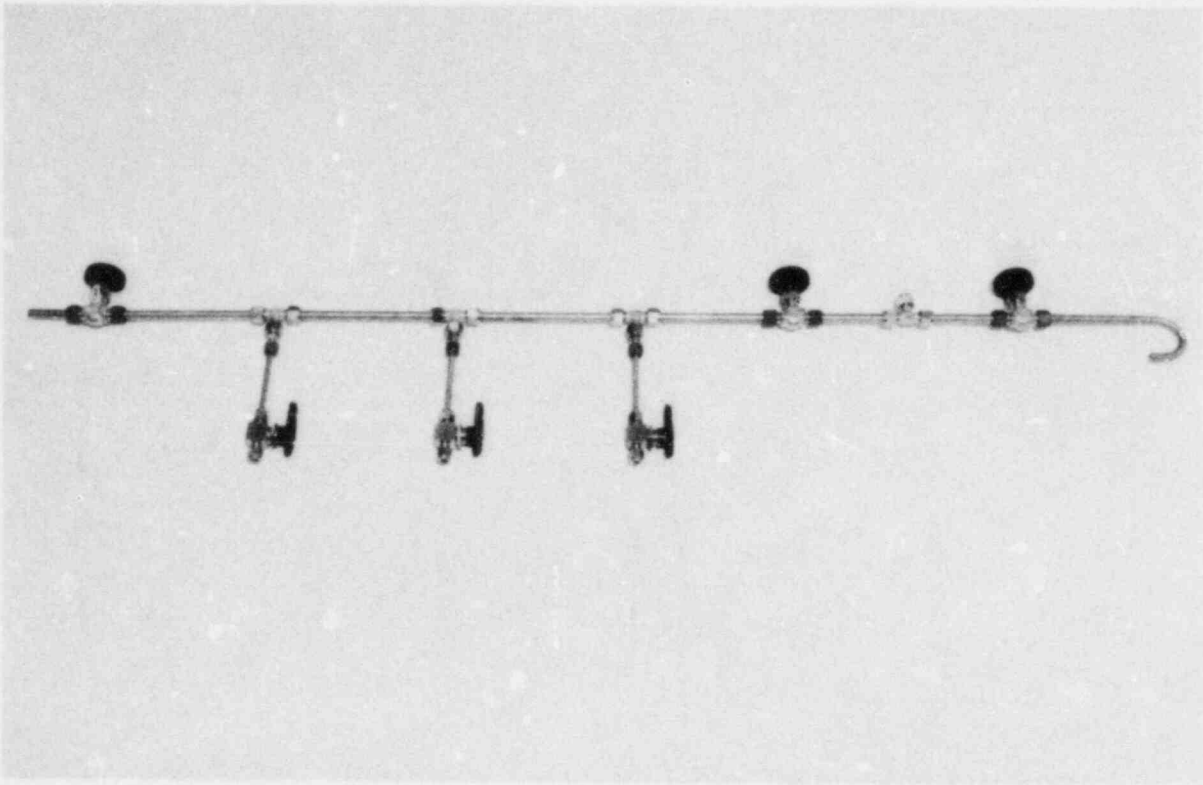

Fig. A.7. Photograph of typical connection to pressurized water reactor pressure panel used at FCTF.

It has been shown[5] that the step response of a Foxboro pressure transmitter may be obtained from the output after the dc voltage is turned off and then on. That is, a momentary interruption of the dc voltage to a Foxboro pressure transmitter results in an output that may be used to determine the response of the sensor to a step change in process pressure.

A.3.1 Equipment

The following equipment is needed for remote testing of the response of Foxboro pressure transmitters (see Fig. A.10):

1. a strip chart recorder (or equivalent),
2. a test-box that consists of a switch and a fixed resistor, (the switch is used to interrupt the current in the transmitter circuitry, and the resistor is used to convert the current in the circuit to a voltage to be monitored and stored.)
3. a data storage device (analog or digital), and
4. a multimeter.

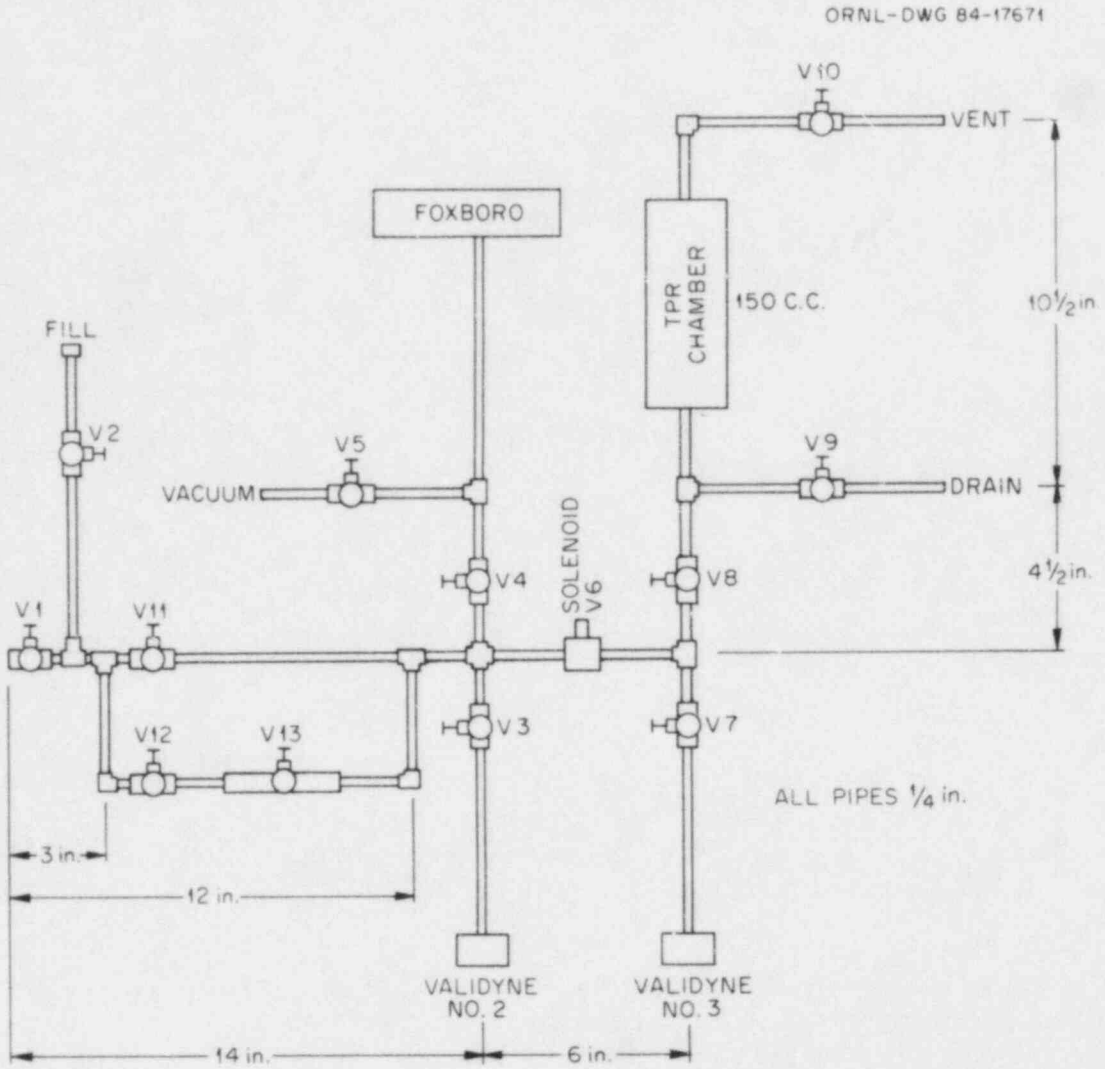

Fig. A.8. Schematic diagram of pressure perturbation test fixture.

A.3.2 Data Analysis

Two methods for analyzing data from remote tests of Foxboro force-balance pressure transmitters were evaluated. One method uses a frequency-domain approach, and the other a time-domain method.

The frequency-domain analysis is accomplished in essentially three steps:

1. Perform a Fourier transform of the applicable data.
2. Identify the gain poles and zeros of a transfer function model with a linear least-squares method.
3. Determine the delay time associated with a ramp response by integrating the differential equation that corresponds to the identified model with relaxed initial conditions.

ORNL PHOTO-7916-83

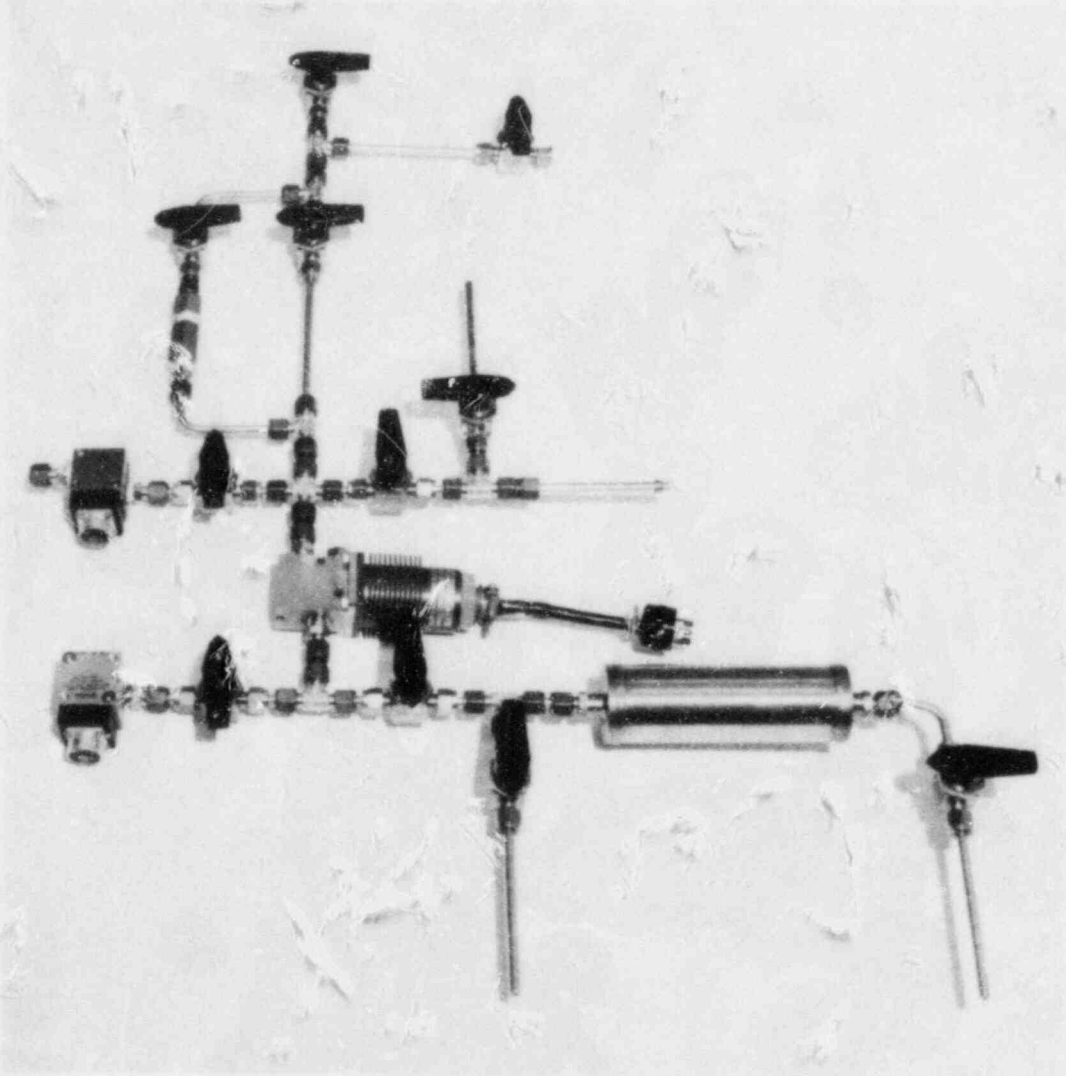

Fig. A.9. Photograph of pressure perturbation test fixture.

The analysis of the data in the time domain proceeds as follows:

1. Perform a nonlinear least-squares minimization for a single parameter of an integral equation that describes the transient response of a second-order system with nonzero initial conditions.
2. Determine the delay time associated with a ramp response by integrating the differential equation that corresponds to the identified model with relaxed initial conditions.

Both of these methods have been used to analyze data from laboratory experiments, and both yield delay times that are in good agreement with direct experimental results. However, they need to be tested on field

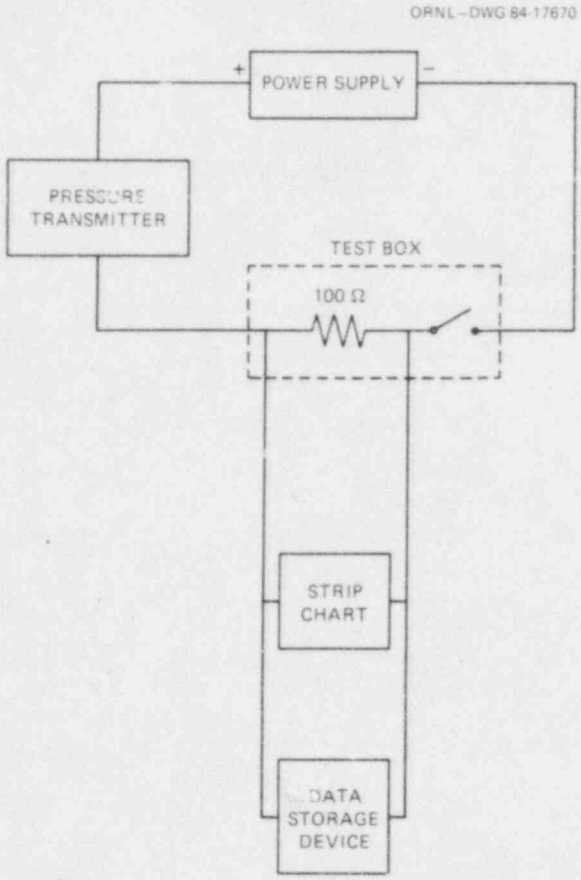

Fig. A.10. Schematic diagram of electrical configuration for a remote test of a Foxboro pressure transmitter.

data and other Foxboro pressure transmitters before definitive conclusions should be drawn about the expected consistency between standard ramp tests and results from the analysis of remote (PI) tests.

A.3.3 Test Procedure

The remote testing of a Foxboro pressure transmitter involves monitoring the transmitter response to a momentary interruption of the dc voltage normally used to activate the transmitter's circuitry. The following procedure may be used:

1. Set up the test equipment near the cabinet where the power supplies for the pressure transmitters are located.
2. Select a plant transmitter to be tested and record its tag number and serial number.
3. Bypass the channel in which the transmitter is connected. (This must be done by qualified plant personnel using an approved plant procedure.)
4. Place the switch on the test box to OPEN.

5. Connect the test box to the transmitter circuit (in series) as shown in Fig. A.10.
6. Connect the data monitoring and data storage equipment across the fixed resistor in the test box.
7. Initiate data recording.
8. Place the switch on the test box to CLOSE to close the current loop.
9. Record the voltage drop across the fixed resistor in the test box.
10. Wait until the output settles and terminate data recording.
11. Place the switch on OPEN.
12. Repeat from step 7 to obtain more of the same data if needed.
13. Remove the test box from the transmitter's circuitry.
14. Restore the transmitter circuitry to its as-found configuration.
15. Place the transmitter in service.
16. Start with step 2 to test another transmitter.

APPENDIX B. DYNAMICS OF PRESSURE-SENSING SYSTEMS

This section applies the well-established technology of the theoretical methods of acoustical engineering to pressure sensing systems. The sequence is first to formulate the general applicable equations and then to formulate special simpler cases. In the latter part of this section, the model is checked against experiment to achieve confidence in using its parameters as system characterizations.

B.1 DISTRIBUTED PARAMETER MODEL

The sensing line and its attachments (i.e., primary piping and terminating transducers) constitute a hydraulic system. Figure B.1 is a general drawing of such a system, and special cases of this drawing will be considered throughout this section. Because of the close analogy with electrical circuits, electrical symbols represent components of the system. The general equations which follow pertain to any hydraulic subsystem of this figure, particularly to those having the sensing line traversing a distance ℓ and having boundary conditions at its endpoints $x = 0$ and ℓ.

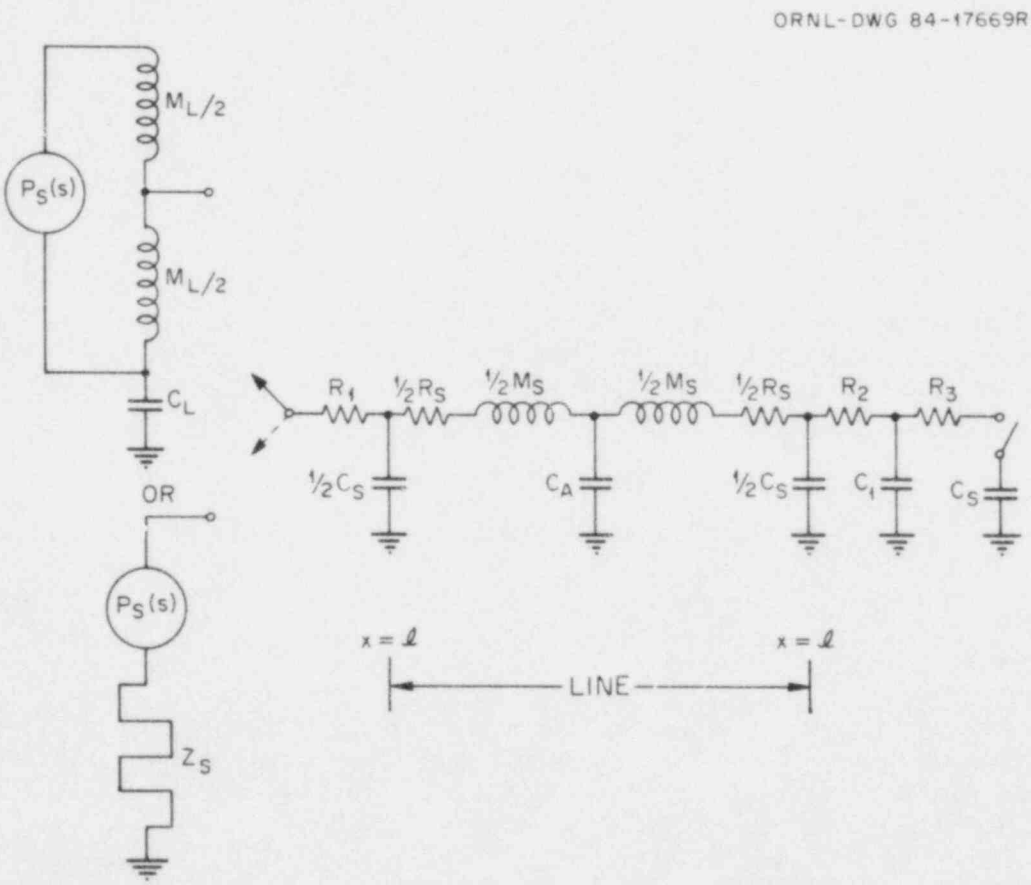

Fig. B.1. Impedance diagram describing two possible source networks (left) and a sensing system connected to one of these (see Table B.1 for specific configurations).

The momentum equation for this line is one dimensional when transverse velocities are not important, and when

$$v \frac{\partial v}{\partial x} << \frac{\partial v}{\partial t}$$

$$\rho \frac{\partial v}{\partial t} + Fv + \frac{\partial p}{\partial x} = 0 \qquad (B.1)$$

Here ρ, v, and p are the local density, velocity, and pressure. A linear friction factor F is assumed (but in turbulent flow it is, in fact, dependent on velocity). The continuity equation when velocity gradients are more important than density gradients is

$$\frac{\partial \rho}{\partial t} + \frac{\partial}{\partial x}(\rho v) \cong \frac{\partial \rho}{\partial t} + \rho \frac{\partial v}{\partial x} = 0 \ . \qquad (B.2)$$

The fluid also obeys its equation of state

$$\frac{\partial \rho}{\partial p} = \frac{\rho}{B} \ , \qquad (B.3)$$

where B is the bulk modulus. While a conservation of energy equation can also be written for the fluid and its surroundings, it would not be useful for the applications here. (However its effects on fluid temperature are discussed below.)

The above equations may be combined to give a wave equation in the volumetric flow $u = v$ times pipe cross-sectional area A, and to give a simple pressure/flow relation:

$$\underset{M/\ell}{\frac{\rho}{A}} s^2 u + \underset{R/\ell}{\frac{\rho F}{A}} su - \underset{\ell/C}{\frac{B}{A}} \frac{\partial^2 u}{\partial x^2} = 0 \qquad (B.4)$$

$$\frac{1}{A} \frac{\partial u}{\partial x} = - \frac{s}{B} p \qquad (B.5)$$

The coefficients in Eq. (B.4) may be identified with impedance gradients as indicated for this Laplace transform formulation in which s is the Laplace variable. The M/ℓ, R/ℓ, and ℓ/C are respectively the inertance, resistance, and reciprocal capacitance gradients.

This wave equation may be solved with boundary conditions of terminating impedances Z_S and Z_R at its two endpoints as depicted in Fig. B.1 and Table B.1. The result is

$$\frac{p(o,s)}{p_S(s)} = \frac{Z_o Z_R}{(Z_S Z_R + Z_o^2) \sinh \gamma\ell + Z_o (Z_S + Z_R) \cosh \gamma\ell} \qquad (B.6)$$

Table B.1. Specific configurations for two possible source networks illustrated in Fig. B.1.

Source configuration	Impedances	Switch
Lower	$R_1 = 0$; Z_R = network of R_2 C_T, R_3 and C_C; Z_O = distributed parameter line approximated by C_S, M_S, R_S and C_A	Closed
Lower	$R_1 = R_2 = 0$; $Z_S = 0$; $C_A = 0$	Closed
Lower and $p_S = 0$	$Z_S = 0$; $C_A = C_S = 0$; $R_3 = 0$	Closed
Upper	$C_A = 0$	
Lower and $p_S = 0$	$R_1 = R_2 = R_3 = R_S = 0$; $Z_S = 0$; C_A = both 0 and nonzero	Closed

where the propagation constant γ and the characteristic line impedance Z_O are respectively

$$\gamma = \sqrt{(R + sM)sC}/\ell \tag{B.7}$$

$$Z_O = \sqrt{(R + sM)/sC} \tag{B.8}$$

The ability of a sensing line to exhibit standing wave behavior is a direct consequence of the solution Eq. (B.6). Half-wave resonances occur when Z_S and Z_R approach zero and R is small, and then $\gamma\ell \cong j\omega\ell/c$ = an integral multiple of $j\pi$. Quarter-wave resonances occur when Z_S and Z_R approach zero and infinity respectively (corresponding to open and closed ends respectively), and then $j\omega\ell/c$ = odd integral multiple of $j\pi/2$. Where c is the sound velocity from

$$c = \sqrt{B/\rho} \tag{B.9}$$

With boundary conditions evidently strongly influencing a line's behavior, it is convenient to express terminating impedances in terms of a so-called reflection coefficient r:

$$r_p = \frac{\frac{Z}{Z_o} - 1}{\frac{Z}{Z_o} + 1} \quad , \tag{B.10}$$

where Z is the terminating Z_S or Z_R. For example, if this coefficient is zero at the chamber end (when impedances are matched, $Z_R = Z_o$), and -1 at the source end, then there is no reflection and the transfer function Eq. (B.6) becomes simply $\exp(-\gamma\ell) \cong \exp(-j\omega\ell/c)$. In these idealized conditions the primary system pressure would be delayed without reflection with a delay time equal to the sonic transit time ℓ/c.

In the case of typical power plant sensing systems and test configurations used in this research, the reflection coefficient is close to unity at the chamber end at the low frequencies of interest. Here the transfer function Eq. (B.6), for small Z_S had in these systems, simplifies to

$$\frac{p(0,s)}{p_S(s)} \cong \frac{1}{1 + sR(C_B + C_T + \frac{C_S}{2}) + \text{terms of order } s^2} \tag{B.11}$$

Thus the low-frequency behavior is that of a time constant determined by line resistance and effective capacitance.

A simple consequence of Eq. (B.11) having practical application is for $p_S(t)$ being a very slow period of ramp (i.e., change fractionally little in a time equal to R times the total capacitance). Then $p(0,t)$ will have this same asymptotic time behavior except for being delayed by this time constant of R times total C. This same asymptotic result also has been obtained by solving this distributed parameter model's equations entirely in the time domain.

B.2 ACOUSTICAL IMPEDANCE METHODOLOGY

It is noted above in discussing Eq. (B.4) that impedances can be associated with terms in the basic description of the pressure-flow relationship. This conveniently allows the use of well-established methodologies for solving impedance networks. In the previous section, the impedances were continuously distributed. In this and the following sections, the lumped approximation will be used. This approximation is permissible when the dimensions of a chamber or pipe are somewhat smaller than a wavelengths $\lambda = c/f$ for frequencies of interest.

That the lumped impedance approximation indeed works may be seen by applying it to Fig. B.1 for the conditions applicable to Eq. (B.4). The small $\gamma\ell$ assumption for the latter corresponds to a small ℓ/λ for which the lumped impedance approximation may be used. A π approximation is used for the line--half of its capacitance at each end. The transfer

function of Eq. (B.11) may be computed by a straightforward solution of the impedance network. (As in electrical networks, one uses equalities of pressure drops, which are volumetric flows times impedances, between points via different paths; and one uses continuity of volumetric flows at junctions.) The result is the same as in Eq. (B.11) for this same low-frequency application.

Obtaining specific impedance parameters from system characteristics may be done from the following equations, stemming from identifications made in Eq. (B.4):

$$M = \rho \ell / A \quad , \tag{B.12}$$

$$R = \rho F \ell / A \quad , \tag{B.13}$$

and

$$C = V/B \quad , \tag{B.14}$$

where V has been used as a more general chamber volume than a pipe's $A\ell$ product.

Transducers attached to fluid-containing components of the sensing system also may be represented by the pressure to volumetric flow ratio (i.e., impedance) that they present. For example, Fig. B.1 shows a test transducer. Its capacitance is

$$C_T = \frac{\text{volume displaced}}{\text{pressure causing displacement}} \quad . \tag{B.15}$$

This simplicity is permissible where a diaphragm's spring constant dominates a transducer's response.

After impedance parameters are computed and a network drawn, the solution for the pressure at any point may be obtained knowing the exciting source pressure. Examples of the latter are

a. a random-noise source in the process piping,
b. a step imposed at the process end of the sensing line,
c. a step imposed by closing the switch, (i.e., opening a valve in Fig. B.1), and
d. an external pressure source inserted at the switch in Fig. B.1.

In the frequency domain, the computing of transfer functions between the pressure excitation source and the pressure at the test transducer C_T can be done for each of these cases. The results for cases (a) and (b) are the same:

$$\frac{p(s) \text{ at } C_T}{p_S(s)} =$$

(B.16)

$$\frac{Z(C_T, \frac{1}{2} C_S)\, Z(R_3, C_c)}{Z(C_T, \frac{1}{2} C_S)Z(R_3, C_c) + Z(M_S, R_s)[Z(C_T, \frac{1}{2} C_S) + Z(R_3, C_c)}$$

The results for case (c) and (d) are the same

$$\frac{p(s) \text{ at } C_T}{p(s) \text{ across switch}} =$$

(B.17)

$$\frac{Z(C_T, \frac{1}{2} C_S)\, Z(M_S, R_S)}{Z(C_T, \frac{1}{2} C_S)Z(M_S, R_S) + Z(R_3, C_C)[Z(C_T, \frac{1}{2} C_S) + Z(M_S, R_S)]}$$

Here the impedances Z(i and j) are used to designate the combinations of the individual impedances i and j in specific branches of the network. All of these expressions have a resonance when the inertance and capacitance contributions in the denominator cancel each other at a resonant frequency.

Corresponding to cases (b) and (c) the time-domain solutions are of interest as they represent the transients obtained from the two types of pressure perturbation tests investigated. (Note that within the type of test for case (c) either an empty chamber or a transducer may be valved in to obtain a terminating capacitance change.) These time-domain solutions are calculated by inverse Laplace transforming Eqs. (B.16) and (B.17). In both test types the solution has the form

$$p = p_o \exp(-\alpha t) \cosh(\omega_o' t - \phi') \qquad (B.18)$$

for an overdamped system where the resistance is large, and has the form

$$p = p_o \exp(-\alpha t) \cos(\omega_o t - \phi) \qquad (B.19)$$

for an underdamped system with a small resistance. Virtually all of the tests conducted here are of this latter type where the coefficients of t are related to effective network parameters

$$\alpha = R_S/2M \qquad (B.20)$$

$$\omega_o = \sqrt{\frac{1}{MC} - \alpha^2} \qquad (B.21)$$

In these equations ϕ' and ϕ are phase angles, p_o the excited amplitude, and ω may be regarded as an imaginary angular velocity in the overdamped case. (The steady-state system pressure, existing after the transient, has been subtracted and therefore these expressions decay to zero.)

A priori expressions for the excited amplitude p_o may be obtained for various test configurations. They are directly proportional to the pressure differential in the system before the transient, and the proportionality constant depends on system impedances, particularly the capacitance being valved in. For the simple case of no resistances R_2 and R_3 in Fig. B.1, the valving in of the chamber capacitance C_C will result in instantaneous redistribution of stored volumes of fluid, q, according to the relation, stemming from the definition of capacitance:

$$p\,(0_+) = \frac{q_T(0_-) + q_C(0_-)}{C_T + C_C} = \frac{p_T(0_-)C_T + p_C(0_-)C_C}{C_T + C_C} \qquad (B.22)$$

where $p(0_+)$ and $p(0_-)$ are the gauge pressures immediately before and after the valving in respectively.

It should be noticed that the theory of this section uses linear equations. This assumption of linearity may still be implemented in oscillations even if R is flow dependent, if an appropriate average value over a cycle is used. If a highly nonlinear process is involved in exciting the transient, linear theory would not be used until after the oscillations start. The next section will treat these nonlinear processes by formulating a more exact equation of fluid motion than Eq. (B.4).

B.3 NONLINEAR SOLUTION OF STEP TESTS

In a pressure perturbation test, a sequence of events involves somewhat distinct phases. The final phase was discussed in the preceding section, namely linearly damped oscillations. The phases prior to this occur as follows:

1. The solenoid valve separates the system from the chamber opens.
2. Before flow starts, pressure equalizes among the elements at the end of the sensing line according to their capacitances; this occurs at the speed of sound.
3. Flow progresses from laminar to turbulent to possibly choked conditions (i.e., fluid velocity at the solenoid's orifice is limited to the speed of sound) while the gas in the chamber compresses.
4. Gas compresses beyond the system's equilibrium point and eventually decelerates the flow to zero at the time of peak chamber pressure.

5. Gas decompresses and flow reverses as a damped oscillation ensues.

This section treats the predictive calculation of these phases using knowledge of system parameters.

The following assumptions are made in the nonlinear model used in this section:

1. The lumped impedance approximation may be used at the low frequencies of interest here.
2. One resistance in series with the sensing line is considered, and its velocity dependence is taken into account.
3. The test configuration identified in Fig. B.1 is used.
4. Nonlinear gas volume changes are taken into account by the use of a power law in the pressure-volume relationship, with conservation of energy not being explicitly used in the model.

The last assumption amounts to using either the adiabatic or isothermal gas law and is discussed further in Sect. B.5.

With these assumptions, the system may be described by the momentum equation and a pressure balance equation:

$$\rho \ell \frac{dv}{dt} + AR(v)v + p_S + p_{at} - \frac{p(0) + p_{at}}{\left(1 + \frac{\Delta V}{V_o}\right)^{\gamma}} = 0 \qquad (B.23)$$

where p_S and $p_{(o)}$ are the time-dependent pressures at the measured system and transducer ends of the sensing line, respectively.

$$p(0) + p_{at} + \frac{V_o}{C_T}\left(\frac{\Delta V}{V_o} - \frac{A\int_o^t v\,dt}{V_o}\right) = \frac{p(0) + p_{at}}{\left(1 + \frac{\Delta V}{V_o}\right)^{\gamma}} = 0 \qquad (B.24)$$

The first two terms of the momentum equation are readily identifiable with those in Eq. (B.1) multiplied by ℓ; the remaining terms give the net pressure that moves the sensing line fluid. In Eq. (B.24), the initial absolute pressure, $p_o + p_{at}$, adjusted by the pressure on C_T, is equal to the balancing pressure from the gas law. Here γ would be 1.0 for isothermal behavior and 1.4 for adiabatic behavior of air. The fractional change in the chamber's air volume is $\Delta V/V_o$. (If the latter is $<<1$ and R is constant, Eq. (B.1) reduces to the linear equation used in solving the networks of the previous section.)

The numerical solution of these two equations is quite straightforward using a computer and a time-stepping, Runga-Kutta technique as an efficient algorithm. This algorithm has been used to compare the model with

a University of Tennessee test at 20 psig on a 50-ft sensing line terminated with a 50-cc chamber, with the measuring sensor's C_T being negligible. The nonlinear resistance was approximated by the function expected in turbulent flow,

$$R(v) = \frac{K|v|}{2A} \tag{B.25}$$

where K is the only parameter in the model to be adjusted. With a properly adjusted K, the computer output plots fit data reasonably well, the transient plots like Fig. 3.3 being used to make comparisons. The results in Table B.2 indicate a good a priori-calculated damped resonant frequency and that a K of approximately 4,570 lb/ft^3 fits best. For more precise fitting, a better representation than Eq. (B.25) is required.

The overshoot ratio in Table B.2 is defined for a pressure perturbation transient as

$$\frac{\text{first peak pressure - equilibrium pressure}}{\text{system initial gauge pressure}} \tag{B.26}$$

Table B.2. Predictions of the nonlinear model compared with features of a test transient

	Calculated values for assumed K (lb/ft^3)			Measured value
	0	4,570	22,850	
Resonant frequency (Hz)	0.89	0.93	0.91	1.03
Overshoot ratio	4.1	0.82	0.17	0.37
α (s)	0	0.81	0.72	1.2
Time to first peak from start (s)	0.55	0.72	1.20	0.72

The damping constant α in this table is that obtained from the first cycle of the computed or experimental transients according to its definition in Eq. (B.19):

$$\alpha = \frac{\ln[p(t_2)/p(t_1)]}{t_1 - t_2} \qquad (B.27)$$

where t_1 and t_2 are times of successive maxima.

Note that α determined from experimental data varies significantly from cycle to cycle, unlike expectations from linear theory in Eq. (B.19). This is due to the nonlinearity in the resistance. The nonlinear model here has the average R in a cycle as being amplitude dependent, and thus exhibits α variations akin to those in the data.

B.4 HELMHOLTZ RESONANCE

It has been noted above that the behavior of the denominator of Eq. (B.16) or (B.17) is responsible for a resonance in lightly damped systems. Physically, this corresponds to a cancellation of the inertance and capacitance effects in Eqs. (B.23) and (B.24), whose linearized form is

$$Msu + Ru + \frac{1}{sC}u = \text{forcing pressure} \quad . \qquad (B.28)$$

This resonant frequency

$$f_1 = \frac{1}{2\pi}\sqrt{\frac{1}{MC} - \frac{R^2}{4M^2}} \approx \frac{1}{2\pi}\sqrt{\frac{1}{MC} - \alpha^2} \qquad (B.29)$$

where M is the sensing line inertance and C is the total effective series capacitance and has historically been called the Helmholtz resonant frequency when C is dominated by a chamber of gas. Long sensing lines and large chamber capacitances (due to large volumes) lead to low frequencies, and the system is oscillatory as long as $\alpha < 1/\sqrt{MC}$.

Perturbation tests can be designed to use a chamber volume that gives a resonant frequency suitable for the sensors used. For example, calculations using Eqs. (B.12), (B.14), and (B.29) will show whether the resonant frequency is low enough for sensing by existing system transducers, or whether wide bandwidths must be added. Also in test design, any resistance added--such as by the orifice of a solenoid value--becomes a part of the network of Fig. B.1, combining with others to contribute to the damping.

With Helmholtz resonant behavior appearing in phases 4 and 5 of the transient discussed in Sect. B.3, the appropriate gas volume to use in Eq. (B.14) is the equilibrium volume and not the initial volume. With chamber pressure changing from p_{at} to $p_{at} + p_S$ (where p_S is the system-end of the sensing lines pressure), the gas volume changes from V_o to the equilibrium V needed for capacitance calculation. The gas law

$$\frac{p_{at} + p_S}{p_{at}} = \left(\frac{V_o}{V}\right)^{\gamma} \qquad (B.30)$$

to be applied (i.e, the value of its γ) is discussed in the next section.

Figure B.1 shows how capacitances combine at the end of a sensing line where a π approximation is used for the line: half the line's capacitance, a sensor's capacitance, and the chamber capacitance is a parallel combination (with possible resistances between). Also this combination is in series with the C_L of the main loop. (In practice, the latter is normally so large that it does not significantly lower the terminating parallel combination.) Hence in lightly damped systems, the C to use in Eq. (B.28) is the sum, $0.5C_S + C_T + C_L$.

Impedances for the main loop part of Fig. B.1 are depicted because their values and configuration can sometimes influence test behavior. One such phenomenon is a Helmholtz antiresonance or sink frequency that results in the pressure noise spectrum at $x = \ell$. It is due to a wave-trap effect. In a wave-trap, its impedance at its resonant frequency is low. This has the effect of "shorting out" pressure fluctuations at this point. The transfer functions computed (under simplifying assumptions of negligible C_S and R_s) for the pressure amplitudes at $x = \ell$ and 0 are respectively

$$p_x = \ell(s) = \frac{\frac{1}{2} p_S(s) \left[sM_s + R + \frac{1}{sC},\right]}{s(M\frac{1}{S} + \frac{1}{4} M_L) + R + \frac{1}{sC}} \qquad (B.31)$$

and

$$p_x = 0(s) = \frac{\frac{1}{2} p_s(s) \frac{1}{sC}}{s(M_S + \frac{1}{4} M_L) + R + \frac{1}{sC}} \qquad (B.32)$$

The capacitance combinations used here are $C = C_T + C_c$ and $C = C_L C / (C_L + C)$. The resistance combination is $R = R_s + R_1 + R_2$. The pressure at the primary loop end of the line exhibits both a sink and a resonance, while the other end of the line exhibits only resonance. Also, the different total inertances and capacitances for the sink and resonant frequencies will displace these from each other. This prediction of the theory is borne out in spectra taken at the ORNL FCTF (discussed in Sect. 3.1 where these spectra are used). These two closely spaced frequencies are found to be 8.4 and 7.4 Hz respectively. The separation is primarily due to M_L.

While linear theory has been used in this discussion of Helmholtz resonances, its applicability to interpreting the damping behavior in the relatively large amplitude pressure perturbation tests needs to be treated. An energy balance model in which damping losses are averaged

over a cycle is useful in applying this linear theory--the effective resistance being allowed to vary from cycle to cycle as amplitudes change.

From the terms of Eq. (B.4) the theory of second-order systems gives for the peak potential and kinetic energies, occurring a quarter of a cycle apart,

$$\text{Potential energy stored via capacitance} = Cp_{max}^2/2 \qquad (B.33)$$

$$\text{Kinetic energy of sensing line fluid} = Mu_{max}^2/2 \; . \qquad (B.34)$$

where u_{max} is the line area times the largest velocity in the cycle. The losses from a dynamically averaged resistance R are expressed

$$\text{Resistance energy loss in a cycle} = Ru_{max}^2/2f \; . \qquad (B.35)$$

The theory also defines a damping ratio which is

$$\delta = \frac{\text{loss of energy per cycle}}{4\pi \text{ (maximum energy stored)}} = \frac{R}{4\pi M} = \frac{\alpha}{\omega_o} \; . \qquad (B.36)$$

In the practical application of these expressions to a transient, α and δ may be determined for a particular cycle. Then the effective resistance can be calculated using this last equation and an a priori value for M (which can be confirmed via resonant frequency investigation). This empirically determined resistance parameter would characterize the system. Its value in similar transient amplitudes in tests from time to time would be a quantitative method of characterizing any blockage growth.

B.5 THERMAL EFFECTS

Conservation of energy has not been incorporated explicitly into model equations above, so it is treated next. The local temperature is allowed to vary in space and time as a consequence of energy conservation between the sensing system and its environment. The numerical method of Sect. B.3 is appropriate to use for calculation of transients involving this additional complexity: the varying temperature becomes reflected into the model as a varying density as long as no fluid phase changes are involved. For example, this approach would be used in an accurate modeling of a transient in the ORNL high-temperature loop in which a significant fraction of the sensing line fills with hot water during phase 3 of the transient when the chamber fills.

Another thermal consideration is whether gas in a pipe or chamber behaves adiabatically or isothermally. This decision is made by computing the thermal time constant of the element, which for a cylinder of radius r, heat capacity C_H, and conductivity K_H is

$$\text{time constant} = \frac{6K_H}{C_H \rho r^2} . \qquad (B.37)$$

If it is long or short compared to the reciprocal of the ω_o of interest, the element behaves adiabatically or isothermally respectively. For example a 0.2-in.-ID sensing line having air within behaves isothermally below 5 Hz, whereas a 2-in.-ID air chamber behaves isothermally only below 0.05 Hz.

Equation (B.37) is intended for use in a single phase. Considerable turbulence and mist in a chamber during its initial filling process makes calculation of the instantaneous gas volume more complex. However, it may be bracketed by making adiabatic and isothermal assumptions.

The only effect of main-loop temperature seen experimentally in ORNL loop transients at 2250 psig was to raise the Helmholtz frequency 14% when the main loop was at 490°F compared to when it was at room temperature. Since one sixth of the sensing line's ambient temperature water is replaced by loop water, calculations show that this should raise the Helmholtz frequency by 2% due to the density effect in M. It is believed that the remainder of the increase is due to the substantial decrease in M_L from room temperature to 490°F in Eq. B.32. (This would not be noticed in power plants where M_L is negligible compared to M_S.)

In all tests reported, the subcooling was always sufficient to prevent local flashing. Whether flashing occurs can be determined by comparing local pressures and temperatures to saturation conditions. For example, flashing would take place if an atmospheric pressure chamber were suddenly filled with water above 212°F.

B.6 MODEL VERIFICATION

Discussions in other sections compare aspects of the model to test findings for purposes of verification:

1. Table B.2 indicates how one friction parameter can be used to approximately describe nonlinearity,
2. Section B.4 explains the presence of both a Helmholtz resonance and antiresonance, and
3. Section B.7 gives model calculations which enable an understanding of the effect of a sensing line air bubble on the Helmholtz frequency.

The purpose of this section is to compile a number of other comparisons of the model and data. The versatility in test conditions and configurations at the University of Tennessee and at ORNL afforded the unique opportunity of a rather stringent overall model checkout: Data and theory can be compared for the effects of many parameters being individually varied.

The individual parameter or test condition variations whose effects calculated are summarized in Table B.3. In all these model calculations, a priori information was used (i.e., geometric configuration). The individual parameter or test condition variations whose effects and fluid properties used as input information for impedance parameter calculations. An exception is that friction parameters are deduced from the data, since it is beyond the scope of the research here to go into these nonlinearities a priori. Comments on comparing these calculations with measurements are as follows:

- The standing-wave frequency in Table B.3 is that which is excited in the initial phases of pressure perturbation tests as well as by process-loop pressure noise. The quarter-wave resonance discussed in Sect. B.1 is calculated here.

- In making comparisons of the Helmholtz frequency of tests, the slight increase caused by removing the small (in comparison to the test chamber) capacitance of a Rosemont sensor is verified. The calculation method of the ORNL loop frequency as measured from transients required bracketing the result by assuming adiabatic and isothermal gas laws in the chamber's compression.

- The sensing line length and test chamber volume make up the inertance and capacitance respectively in Eq. (B.21) and change the Helmholtz frequency inversely as the square root of these parameters in lightly damped systems. On the other hand, Table B.3 shows that the very large capacitance of a pressure accumulator tank in series with the sensing line essentially does not influence resonant frequency because of the manner in which series capacitive impedances combine.

- Table B.3 attempts only a comparison of ratios of friction changes induced in a transient test by various numbers of turns open on a throttling blockage valve in the line. In applying the model, the frictional approximation of Eq. (B.25) was assumed, and its parameter, K, fits empirically to individual test damping behavior. These changes in K are compared in this table with those deduced from the valve manufacturer's pressure drop, flow, and turns-open characteristics. The good agreement should be qualified because it deduced Ks from transients; these Ks depend somewhat on amplitude of the cycle used since Eq. (B.25) is not a precise description. Nevertheless, it is quite encouraging that a meaningful parameter may be quantitatively determined from test data and used to characterize closely the extent of a blockage.

- The effect of test pressure on a transient shown in the last table entry is bulk modulus and volume influence. The volume used in capacitance calculations during Helmholtz oscillations is the compressed (not original) chamber volume. The bulk modulus in Eq. (B.14) is proportional to pressure. As a result, in isothermal initial compression cases the resonant frequency varies essentially inversely as $\sqrt{C}$ $\underline{C}$ and, hence, inversely as absolute pressure.

B.7 SENSING SYSTEM CHARACTERIZATION WITH MODEL FEATURES

Having a model which satisfactorily describes a sensing system test, it is appropriate to use test data to obtain specific features of the system. Thus, a methodology for understanding a test could be as follows:

1. Obtain selected descriptors (e.g., resonant frequencies, damping constants, etc.) directly from the data;
2. Use theoretical relationships between these descriptors and system parameters (e.g., inertances, capacitances, and resistances) to obtain the latter; use confident a priori values (e.g. sensing line inertance), and deduce only hard-to-determine parameters (e.g., resistance) so the data are fit.
3. Use the resulting best-fit model to answer questions (e.g., What anomaly might be indicated by off-normal values? How will the system behave if a change is made or if some transient is postulated?).

This section discusses this methodology of model usage.

Table B.3. Comparison of model calculations with transient test results

Quantity compared	Test used	Measured value	Calculated value
Standing wave-frequency (Hz)	ORNL, cold	10	10.1
Helmholtz frequency (Hz)			
• with Rosemont present	UT, low pres.	1.04	1.08
• without Rosemont	UT, low pres.	1.08	1.16
Helmholtz frequency (Hz)	ORNL, cold	6.4	5.6 to 7.3
Line length effect on resonance, f_o(32 ft)/ f_o(101 ft)	UT, low pres.	1.60	1.63
Chamber volume effect on resonance, f_o (50 cc)/ f_o(100 cc)	UT, low pres.	1.43	1.41
Accumulator air volume effect on resonance, $f_o(.87\ ft^3)/f_o(1.86\ ft^3)$	UT, low pres.	1.00	1.0005*
Blockage valve turns effect on K, $\Delta K(9T \rightarrow 3T)/\Delta K(3T \rightarrow 1T)$	UT, interm. pres.	0.18	0.16
Pressure effect on resonance, f_o(25 psia)/f_o(45 psia)	UT, low pres.	0.54	0.54

*Model calculations in general are not this precise, but this particular ratio can be quite precisely calculated when only a volume value changes.

A distinction is first made between transient and noise tests that describe data. For the former, distinctly different usable features are found in phases 2 and 3 (see Sect. 2.3) compared to later phases. For phases 2 and 3 of transient tests one finds the following useful descriptions:

1. immediate pressure amplitude changes occurring within the transit times of sound,
2. standing-wave resonant frequency (if excited by this amplitude),
3. damping constant of the decaying standing wave (if found), and

4. time interval until the chamber's absolute pressure first reaches its ultimate equilibrium value or time interval until the first pressure peak is reached.

For example, this last is mentioned in Table B.2. The standing wave's damping constant, like that of the Helmholtz frequency, is due to line resistance.

The next source of data descriptors in pressure perturbation tests is in phases 4 and 5 of the transient and include:

1. the overshoot ratio Eq. (B.26) characterizing the amplitude of the excited Helmholtz frequency,
2. the Helmholtz frequency, and
3. the oscillations' damping constant.

More detail on system nonlinearity may be obtained if the latter is measured for various amplitudes.

Convenient descriptors in noise tests exist which correspond to the amplitude, frequency, and damping measures in transients. These are

1. the peak value of the spectrum (in absolute units or dimensionless if divided by the spectral value of the loop's pressure noise if this is measured),
2. the resonant frequency, and
3. the frequency width Δf of the resonance 3 dB below the peak.

These three quantities may be determined for both standing wave and Helmholtz resonances. The last of these may be related to the damping constant and system parameters by the following relationships from the theory of resonant systems.

$$\frac{\Delta f}{f_o} = 2\zeta = 2\,\frac{\alpha}{\omega_o}\ , \tag{B.38}$$

$$\alpha = R/2M\ , \tag{B.39}$$

$$\omega_o = \sqrt{(\text{undamped } \omega_o)^2 - \alpha^2}\ . \tag{B.40}$$

For the Helmholtz oscillation the (undamped ω_o)^2 is seen in Eq. (B.29) to be simply the reciprocal of the inertance and capacitance product. In a linear second-order lightly damped system, the overshoot ratio (O.R.) is also related to the damping:

$$\text{O.R.} = 1 - \pi\zeta \tag{B.41}$$

The failure of this relation to hold exactly in typical transients may be used as an indicator of their nonlinearity in practical test cases.

A number of comparisons have been made between noise and pressure perturbation transients on the FCTF. The conclusions are

1. The resonant frequencies for both standing wave and Helmholtz phenomena are in excellent agreement for the two test types.
2. Damping constants for these phenomena are only in approximate agreement with noise tests giving the smaller α's.

This last finding is not surprising because the large amplitudes in the transient tests lead to larger effective average resistances over a cycle than in the small amplitudes encountered in noise tests.

From the above equations, it is apparent that from a measured α and f_o any two of the three parameters R, M, and C may be determined if one is known a priori. Because of their association with system design features and specifications, perhaps the most meaningful and accepted pair of system characteristics would be the RC time constant of Eq. (B.11) and the effective capacitance C. These may be obtained as follows from α, f_o, and M:

$$RC = \frac{2\alpha}{\omega_o^2 + \alpha^2} \quad (B.42)$$

$$C = \frac{1}{M(\omega_o^2 + \alpha^2)} \quad (B.43)$$

These two results may be corrected to values that would exist in the absence of the contribution of chamber C merely by subtracting the chamber's contribution. (Thus, to minimize or avoid this condition, it could be advantageous to use a small or even no chamber volume.) Also, R may be reduced if the contribution from any added solenoid test value is known (e.g., as deduced from special tests).

A useful feature of noise and pressure perturbation tests is their ability to detect increases in R due to blockages. Two cases should be discussed. The simplest is for systems in which the terminating chamber and loop capacitances both well exceed other capacitances. Then each blockage at any location affects the single series of resistances equally. In the second case, the line's capacitance and other intermediate capacitances are not negligible. Then a contribution of a particular resistance, (i.e., blockage) to the effective R is determined by solving the complete network of Fig. B.1.

Finally, another useful feature of these tests in combination with model interpretation is their ability to detect anomalous changes in capacitance, whether at a sensor diaphragm or at an anomalous bubble in the sensing line. The ability of the model to interpret correctly the latter phenomenon was checked by comparing its calculations with transient tests in the 1000-psig UTK loop where a 35-cc bubble was deliberately introduced into the sensing line. Applying the model consisted of solving the network of Fig. B.1 for the Helmholtz frequency with and

without C_A. Calculations predicted a 0.56 lowering factor on the frequency due to the bubble; tests, not quite reproducible, gave 0.5 and 0.7 as the lowering factor.

From the discussion in this and prior sections of Appendix B it can be seen that the model presented here is useful in interpreting test data. The benefits become particularly evident in designing sensitive pressure perturbation tests and in helping to explain data that have changed due to a sensing system abnormality.

GLOSSARY
LIST OF SYMBOLS USED IN APPENDIX B

A	area
a, b,	any constants
B	bulk modulus
c	velocity of sound
C	capacitance (with dimensions, length^{4} time^{2} mass^{-1})
C_H	specific heat
d	diameter
f	frequency
h	impulse response
K	friction proportionality factor
K_H	heat conductivity
ℓ	line length
M	inertance (with dimensions, mass length^{-4})
O.R.	overshoot ratio
	$\frac{\text{1st pressure amplitude}}{\text{gauge pressure source}}$
p	pressure
r	radius
r_p	reflection coefficient for pressure
R	resistance (with dimensions, mass time^{-1} length^{-4})
s	Laplace variable
t	time
T	oscillation period
T_F	chamber initial fill time
μ	displaced volume(s)
ν	displaced volume
V	volume
χ	displacement
X	impedance of a component
Z	impedance total
α	damping constant [in a transient's envelope, $\exp(-\alpha t)$]
β	"angular velocity" when overdamped
γ	specific heat ratio if dimensional; propagation factor if dimensioned as reciprocal length
ζ	damping ratio = α/ω
ϵ	small number
λ	wave length
ρ	density
τ	time delay and time constant
ϕ	phase
ω	angular velocity = $2\pi f$

INTERNAL DISTRIBUTION

1. R. L. Anderson
2-6. M. E. Buchanan
7. B. G. Eads
8. D. M. Eissenberg
9-13. D. N. Fry
14. R. C. Kryter
15. A. P. Malinauskas
16-17. J. March-Leuba
18-21. L. F. Miller
22. J. A. Mullens
23. F. R. Mynatt
24. L. C. Oakes
25-26. G. E. Ragan
27. F. J. Sweeney
28. R. L. Shepard
29-30. J. A. Thie
31. B. R. Upadhyaya
32. R. S. Wiltshire
33. M. J. Kopp (Advisor)
34. P. F. McCrea (Advisor)
35. P. W. Murrill (Advisor)
36. H. M. Paynter (Advisor)
37. Central Research Library
38. Y-12 Document Reference Section
39. I&C Publications Office
40. Laboratory Records Department
41. Laboratory Records Department, RC
42. ORNL Patent Section

EXTERNAL DISTRIBUTION

43-45. T. W. Kerlin, The University of Tennessee, Knoxville, TN 37916
46. E. A. Salazar, System Safety Information Division, Sandia National Laboratories, Albuquerque, NM 87185
47. L. D. Goodrich, Jr., LOFT, Measurement Systems TSA, EG&G Idaho, Inc., Idaho Falls, ID 83401
48. J. R. Maner, Tennessee Valley Authority, Room 740, Chestnut Street Towers II, Chattanooga, TN 37401
49. A. S. Hintze, Electrical Engineering Instrumentation and Control Branch, MS 5650NL, Division of Engineering Technology, Office of Nuclear Regulatory Research, U.S. Nuclear Regulatory Commission, Washington, DC 20555
50-51. Office of Scientific and Technical Information, Oak Ridge, TN 37831
52. Office of Assistant Manager for Energy Research and Development, U.S. Department of Energy, Oak Ridge Operations, Oak Ridge, TN 37831
53-327. Given distribution as shown in NRC distribution R1.

NRC FORM 335 (2.84) NRCM 1102, 3201, 3202

U.S. NUCLEAR REGULATORY COMMISSION

BIBLIOGRAPHIC DATA SHEET

SEE INSTRUCTIONS ON THE REVERSE

1 REPORT NUMBER (Assigned by TIDC and Vol. No., if any)
NUREG/CR-4256
ORNL/TM-9574

2 TITLE AND SUBTITLE
Measurement of Response Time and Detection of Degradation In Pressure Sensor/Sensing Line Systems

3 LEAVE BLANK

4 DATE REPORT COMPLETED
MONTH: August
YEAR: 1985

5 AUTHOR(S)
M. E. Buchanan, L. F. Miller, J. A. Thie, T. W. Kerlin, G. E. Ragan, J. March-Leuba

6 DATE REPORT ISSUED
MONTH:
YEAR:

7 PERFORMING ORGANIZATION NAME AND MAILING ADDRESS (Include Zip Code)
Oak Ridge National Laboratory
P. O. Box X
Oak Ridge, Tennessee 37831

8 PROJECT/TASK/WORK UNIT NUMBER

9 FIN OR GRANT NUMBER
B0481

10 SPONSORING ORGANIZATION NAME AND MAILING ADDRESS (Include Zip Code)
U.S. Nuclear Regulatory Commission
Office of Nuclear Regulatory Research
Washington, DC 20555

11a TYPE OF REPORT
NUREG/CR-4256
ORNL/TM-9574

b PERIOD COVERED (Inclusive dates)

12 SUPPLEMENTARY NOTES

13 ABSTRACT (200 words or less)

A team evaluated several methods for remote measurement of the response time and detection of degradation (blockage or air in lines) of pressure sensor/sensing line systems typical of nuclear power plants. A method was developed for obtaining the response time of force-balance pressure transmitters by briefly interrupting the power supply to the transmitter. The data thus generated are then analyzed in conjunction with a model to predict transmitter response to an actual pressure perturbation. The research team also evaluated a pressure perturbation method for determining the asymptotic delay time of a pressure-sensing line and found that this method yields accurate results for essentially unblocked sensing lines. However, these pressure perturbation tests are not recommended for use in nuclear power plants because they are difficult to implement on-line. A third method for remote measurement applied noise analysis methods that yielded accurate estimates of asymptotic delay times for blockage or air in sensing lines. Even though noise analysis methods worked well in the laboratory, it is recommended that further evaluation be performed in operating nuclear plants.

14 DOCUMENT ANALYSIS - a KEYWORDS/DESCRIPTORS

b IDENTIFIERS/OPEN-ENDED TERMS

15 AVAILABILITY STATEMENT

16 SECURITY CLASSIFICATION
(This page)
(This report)
Unclassified

17 NUMBER OF PAGES

18 PRICE

120555078877 1 1AN1R1
US NRC
ADM-DIV OF TIDC
POLICY & PUB MGT BR-PDR NUREG
W-501
WASHINGTON DC 20555